Republic of Iraq

Ministry of Higher Education

And Scientific Research

University of Babylon

College of Materials Engineering

Department of Metallurgical Engineering

Preparation and Characterization of Additively Manufactured SS309L Stainless Steel Using Aluminium Alloy

A Dissertation

Submitted to the Council of the College of Materials Engineering/ University of Babylon in Partial Fulfillment of The Requirements for the Master Degree in Materials Engineering/Metallurgical

By

Rania Ali Hamoody Abdulkareem

Supervised by

Asst.Prof. Basem Mohysen Al-Zubaidy (Ph.D.)

2023 A.D **1445 A.H**

بسم الله الرحمن الرحيم

({وَأَن لَّيْسَ لِلإنسَانِ إلاَّ مَا سَعَى }

(39)

صدق الله العلي العظيم

(سورة النجم اية 39)

Dedication

To the one who taught me to be proud

Respected father

To the source of giving and generosity

Revered mother

For someone who is closer to my soul

My loving husband

To my pulse and the secret of my joy

My dear daughter

To all those I received advice, support and assistance

I present to you the epitome of effort and exhaustion

Acknowledgements

Foremost, praise be to ALLAH for the blessings of age, mind and health He bestowed upon me and the determination and patience with which I challenged the difficulties I encountered during the completion of this research.

My sincere appreciation and deepest gratitude are due to the Department of Metallurgical Engineering, I would like to thank **Prof.Dr. Basem Mohysen Al-Zubaidy** whom I had the honour of being under their guidance and supervision, their constructive suggestion, patience and continuous encouragement are highly acknowledged through this study.

Finally, I extend my thanks and appreciation to my family, my parents, and my husband and all the friends for their financial and moral support throughout the study period and my beloved daughter, Narjis who was my inspiration pursue this quest.

ABSTRACT

Computer Aided Design Double Wire Deposition Machine (CADDWDM). There are three internal samples of SS309 base alloy manufactured by CADDWDM. The CADDWDM process was used to deposit these walls with different percentages of added aluminum (0, 2.5%, and 5% Al, respectively). These samples (walls) of various types were examined, and their microstructure and mechanical properties were measured and compared. The parameters selected for the double arc additive manufacturing process in this study produce thin-walled components with few defects. Tests indicated that the components showed a high degree of thickness and had few cracks or porosity between the grains.

On the other hand, the grain size steadily decreased and became more uniformly distributed with increasing aluminum content (from 2.5% to 5% Al). The addition of aluminum enhanced the microhardness of the deposited wall. The difference in microstructure between these three sites is believed to be the reason for the difference in hardness. However, discrepancies in hardness between these sites are reduced by the addition of alumina particles until the hardness levels become nearly identical. The tensile strength of the samples increased while the ductility decreased significantly. Adding aluminum to SS309 improved its surface properties such as corrosion and oxidation resistance Computer Aided Design Double Wire Deposition Machine (CADDWDM). There are three internal samples of SS309 base alloy manufactured by CADDWDM. The CADDWDM process was used to deposit these walls with different percentages of added aluminum (0, 2.5%, and 5% Al, respectively). These samples (walls) of various types were examined, and their microstructure and mechanical properties were measured and compared. The parameters selected for the double arc additive manufacturing process in this study produce thin-walled components with few defects. Tests indicated that

the components showed a high degree of thickness and had few cracks or porosity between the grains. SS309 deposited without Al is characterized by two unique regions of microstructure: coarse grains as a matrix with fine grains shown as islands in the structure.

The addition of Al significantly changed the microstructure of the deposited layer by promoting the transition of columnar grains to the more complex structure by converting SS309 from austenitic stainless steel to duplex stainless steel. On the other hand, the grain size steadily decreased and became more uniformly distributed with increasing aluminum content (from 2.5% to 5% Al). The addition of aluminum enhanced the microhardness of the deposited wall. The microstructure transformed from single phase (Austinit) to double phase structure (Austinit+Ferrite) ,The difference in microstructure between these three sites is believed to be the reason for the difference in hardness. However, discrepancies in hardness between these sites are reduced by the addition of alumina particles until the hardness levels become nearly identical. The tensile strength of the samples increased. Adding aluminum to SS309 improved its surface properties such as corrosion and oxidation resistance ,The hardness rate increased before the heat treatment, as the hardness rate in the first wall without adding aluminum was 237, and when aluminum was added at a rate of 5%, the hardness rate became 277, and after thermal treatments, the hardness rate in the first wall was 221, and after adding aluminum in the third wall, the hardness rate became 268.

The addition of Al alloy to SS309L increased the ultimate tensile strength, for example, the ultimate tensile strength was about 610 MPa for the vertical specimens without any addition of aluminum. However, it became about 754 MPa for SS309L with the addition of 5% Al.

List of contents

List of tables

List of figures

List of Abbreviations

Code	Words
AC	Alternating Current
AM	Additive Manufacturing
ASRC	Alloy Steel Research Commission
ASTM	American Society for Testing Materials
AWS	American Welding Society
BM	Base Metal
BTF	Buy-To-Fly ratio
CAD	Computer-Aided Design
CE	Carbon Equivalent
CGHAZ	Coarse Grained Heat Affected zone
DC	Direct Current
DMLS	Direct Metal Laser Sintering
DED	Directed Energy Deposition
DCSP	Direct Current Straight Polarity
DCEN	Direct Current Electrode Negative
DCRP	Direct Current Reverse Polarity
DCEP	Direct Current Electrode Positive
DLF	Direct Laser Fabrication
FGHAZ	Fine Grained Heat Affected zone
GMAW	Gas Metal Arc Welding
GTAW	Gas Tungsten Arc Welding
HAZ	Heat Affected Zone
ICHAZ	Intercortical Heat Affected zone
LMD	Laser Metal Deposition
MIG	Metal Inert Gas
PAW	Plasma Arc Welding
PBF	Powder Bed Fusion
RP	Rapid Prototyping
SLM	Selective Laser Melting

SM	Shape Melting
SW	Shape Welding
SMD	Shape Metal Deposition
SFF	Solid Freeform Fabrication
SMAW	Shielded Metal Arc Welding
SCHAZ	Subcritical Heat Affected zone
WAAM	Wire Arc Additive Manufacturing

CHAPTER ONE

INTRODUCTION

INTRODUCTION

1.1 Introduction

Aluminum alloys mix aluminum and other elements to create new qualities that combine their benefits. Since aluminum is a precious metal due to its lightweight, durability, recyclability, rust resistance, ease of handling, formability, and electrical conductivity, its uses have multiplied and become essential to our lives. It is utilized in aircraft, railroads, fast automobiles, and thermal and electrical sectors. This is in addition to preserving food and medication and making computer parts. Aluminum resembles iron, copper, zinc, lead, and titanium physically, chemically, and mechanically. The melting point is 660.37 degrees Celsius, the boiling point is 2467.0 degrees Celsius, and the density is 2.702 g/cm3.

Aluminum has the symbol Al and the atomic number 13. The periodic table ranks it second in group thirteen, the third group according to the numbering of the significant groups. Aluminum is light, silvery-white, and low-density. It retracts and bends. It is the most common metal as the third most prevalent chemical element in the Earth's crust after oxygen and silicon. Global solid surface mass is 8% aluminum. Aluminum-27Al is its lone stable isotope.

Austenitic stainless steel Alloy 309 (UNS S30900) was created for high-temperature corrosion resistance. Under non-cyclic circumstances, the alloy resists oxidation to 1900°F (1038°C). Frequent heat cycling lowers oxidation resistance to 1850°F (1010°C).

Wire arc additive manufacturing (WAAM), or DED-arc, is being developed to increase engineered structure production efficiency. Local, on-demand production of very near-net-shape preforms without complicated tooling, molds, or dies can minimize cost, lead time, material efficiency, component performance, inventory, and logistics expenses.

1.2 General View

In contrast to subtractive manufacturing techniques, additive manufacturing (AM) is described by ASTM as "a process of combining materials to produce items from 3D model data, generally layer by layer." The terms "additive fabrication," "additive procedures," "additive methods," "additive layer manufacturing," and "freeform fabrication" are synonymous [1]. All sorts of materials, including metals, ceramics, polymers, composites, and biological systems, may be generically categorized under this description. While additive manufacturing (AM) has probably been used to treat materials for more than two decades, it has only lately started to become a significant commercial manufacturing technique.

Three-dimensional (3D) components are directly printed using the revolutionary technology of additive manufacturing, layer by layer, from digital models [2]. The process of near-net form fabrication is known as additive manufacturing, which is entirely distinct from traditional fabrication techniques like casting, forming, and machining. It may significantly increase design flexibility and shorten the lead time of production. As a result, The potential for additive manufacturing to enable intelligent production in the upcoming Industry is enormous [3]. Additionally, Metals, ceramics, and polymers can all be produced using a range of flexible, adaptive, and highly adjustable production techniques known as additive manufacturing [4].

Although additive manufacturing uses a wide range of technologies, this study focuses on Directed energy deposition additive manufacturing, as shown in Figure 1, which generates heat from high-energy-density beams, such as laser, electron, or electric arcs.

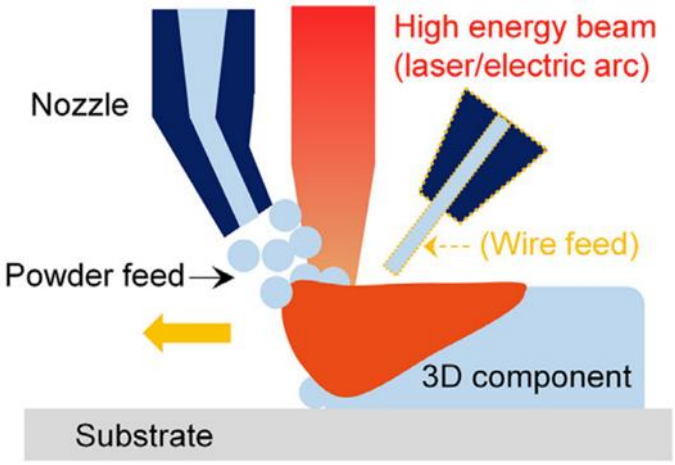

Figure 1.1 Directed energy deposition additive manufacturing [5]

Even though there are many different additive manufacturing approaches, when it comes to solid-state and indirect metal additive manufacturing, a comparison of the processes of binder jetting, fused filament fabrication, cold spray additive manufacturing, and ultrasonic additive manufacturing is needed. [6], Directed energy deposition additive manufacturing can create an intricate thermal history, and as a result, it can produce components with significantly improved performance [7].

The myriad process variables unique to each method of additive manufacturing provide enormous possibilities for modifying the physical characteristics of the manufactured metallic materials. Processing parameters alter the melt pool's flow dynamics, heat transport, and solidification characteristics, which in turn causes microstructural diversity in grain size, morphology, and texture [8], as shown in Figure [1.2]

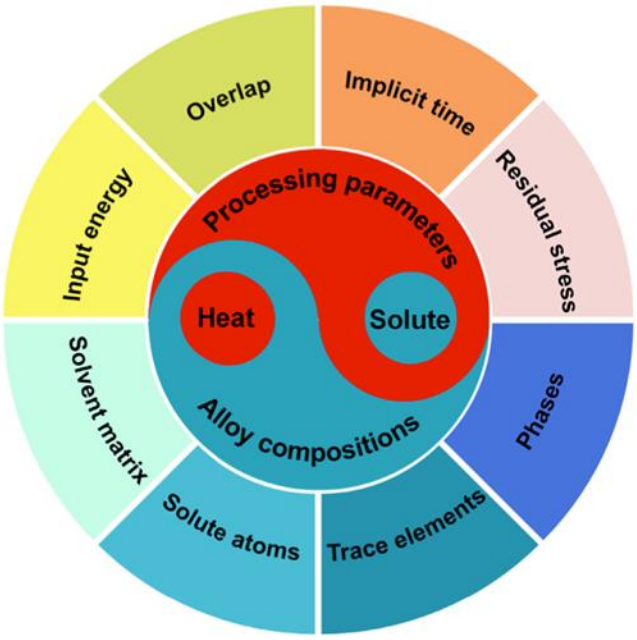

Figure1.2. Processing variables and alloy compositions are the metal microstructures' primary determinants produced additively [6].

1.3 Additive Manufacturing's Advantages and Challenges

1.3.1 Advantages [9]

Smaller batches of individualized products have a greater economic appeal when compared to standard methods of producing large quantities of identical goods.

No start-up costs are associated with direct production from 3D CAD models because the process does not need any tools or molds.

Because digital files of designs can be freely shared, it is much simpler to change and personalize not only the goods themselves but also the component elements.

The additive properties of the technology and the potential to recycle residual materials (such as powder and resin) from the production process both result

in material savings (estimated to be between 95 and 98 percent for the possibility of recovering metal powders).

Lattices, free-form enclosed buildings, and channels are some examples of brand-new and complicated architectural forms that are within reach of human ingenuity. All of these are possible to create.

Because the items are paid for in advance of their production, making things according to the client's requirements not only minimizes the danger of having finished goods in inventory that are unsold but also enhances the revenue flow because the items are paid for in advance of their production.

The distribution process makes it possible for local consumers and the end users of their products to engage in direct conversation with one another.

1.3.2 Challenges

Both the cost of manufacturing and its efficiency need to be considered. They are modifying the designers' ways of thinking about additive manufacturing and how it may be used by shifting their viewpoints. This ends the notion that additive manufacturing (AM), also known as 3D printing, can only be used for quick prototyping and cannot be utilized to manufacture direct components or finished things. The stage of post-processing is required a lot of the time. This might be because of the impact of stair-stepping that takes place due to adding layers one at a time, or it could be because it is necessary to add finishing layers to complete the process. Because the components that make up support structures cannot be recycled, it is required to validate the mechanical and thermal properties of the materials currently used in conjunction with AM processes. Development of systems utilizing a wide variety of colors and materials. Increasing the amount of planning that goes into industrial operations will lead to greater efficiency. to get the most excellent possible build-up orientation. Issues about intellectual property, most notably copyright issues.

Insufficient numbers of designers and engineers with knowledge of additive manufacturing. A relationship that is not linear and is localized, with ambiguous duties and obligations and a field of constantly moving opponents.

1.4 Additive manufacturing and sustainability

AM allows sustainability advantages to be attained in four main categories: product and process redesign, material input processing, manufacturing make-to-order components and products, and closing the loop. This has allowed for the identification of AM's sustainability benefits across the development and material life cycles and the obstacles that must be removed to realize these advantages [14], as shown in Figure [1.3].

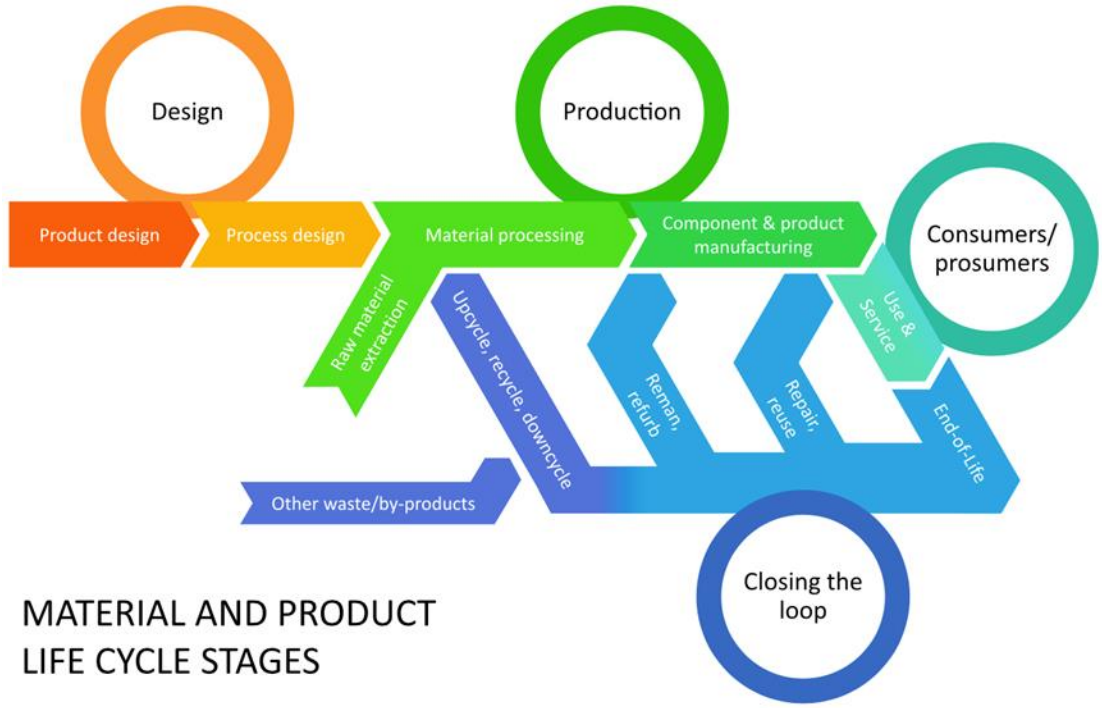

Figure 1.3. Life cycle perspective for identifying sustainability benefits of AM [14].

Given the benefits of AM shown in instances, it is evident that AM will aid in the shift to a more environmentally friendly industrial system since using AM technologies opens up possibilities for more environmentally friendly production and consumption. Lessons learned from previous research on organizational behavior and entrepreneurship suggest that established businesses will prioritize serving their current clientele and redesigning components and goods using additive manufacturing (AM) technology [15]. At the same time, entrepreneurial endeavors will investigate and grow the niches that arise in the AM business ecosystem. Additionally, AM gives organizations the chance to test new business strategies. Since digital designs can be duplicated as spare parts for repair and remanufacturing, the move to direct digital manufacturing will result in the storage of digital formats [16]. This will enable product life extension and provide incentives for business models that combine product and service offerings. By taking advantage of these possibilities, value chains will be rearranged, and manufacturing distribution will alter. Significant improvements, however, do not seem to be on the horizon since organizations must rethink their goods and components to have fewer subcomponents before supply chains may also be streamlined [17].

1.5 Problem Statement

Additive manufacturing, often known as AM, is a well-known technique that can be used in the modern world to generate actual three-dimensional objects. These objects can be made of metal, ceramic, plastic, or a mix of these materials and can be employed in various settings. These things have a wide range of potential uses, including those in the medical, aerospace, and automotive industries. The additive manufacturing method is characterized by many rapid heating and cooling cycles, in addition to

considerable temperature gradients. This is done to create three-dimensional objects. This results in the production of complex thermal histories, which directly impact the microstructures produced as a direct consequence of the manufacturing process .

The nature of this dynamic and far-from-equilibrium process causes different microstructural features to arise, and it is envisaged that these features will induce changes in the corrosion properties of additively made stainless steels in the future. This is because the process in and of itself is dynamic and not at all like a state of equilibrium.

1.6 The Objectives of this Study

This project aims to investigate whether or not it is possible to improve the mechanical and metallurgical qualities of components made from additively created stainless steel (SS309L) by including aluminum in the manufacturing process and doing so using a double wire-arc additive manufacturing method.

CHAPTER TWO

THEORETICAL PART

2.1 Introduction

There have been several earlier studies and investigations into the subject matter of the present dissertation. This chapter presents a review of the literature on the topic of the preparation and characterization of stainless steel produced additively manufacturing in the production process. In addition, highlight any improvements in the quality of the deposited component and materials used in the preparation and characterization of the deposited parts, as well as any changes in the microstructure and mechanical characteristics of the deposited amounts.

2.2 The Stainless Steel

Stainless steels are iron-base alloys that contain a minimum of about 12 % Cr, which is the quantity required to prevent the development of rust in unpolluted environments (i.e., in the presence of water). Few stainless steels include more than 30 % Cr, and a few contain less than 50 % iron [18]. The production of an invisible and adherent chromium-rich oxide coating is responsible for developing their stainless properties. In the presence of oxygen, this oxide develops and self-heals, restoring its original state. Nickel, manganese, molybdenum, copper, titanium, silicon, niobium, aluminum, sulfur, and selenium are some of the other elements used to enhance certain features of Stainless Steel. Carbon is generally found in levels ranging from less than 0.03 % to more than 1.0 % in various grades. Figure (2.1) [19] gives a helpful description of some of the compositional and physical relationships within the stainless-steel family of metals.

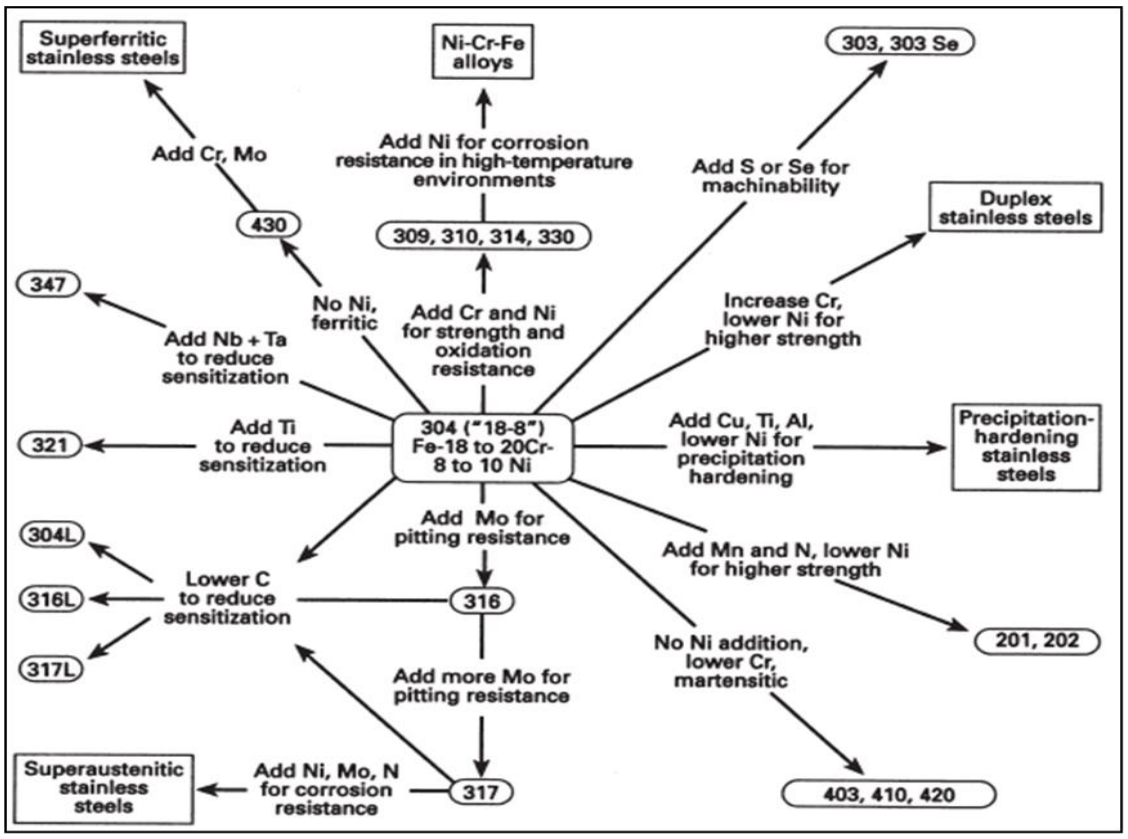

Figure (2.1) Composition and property linkages in the stainless-steel family of alloys [19]

2.3 Identifying the Different Types of Stainless Steels

Steels have historically been categorized based on their microstructure, with austenitic steels being the most frequent, martensitic steels being the second most common, and duplex steels (austenitic plus ferritic) being the most common (austenitic plus ferritic). The precipitation-hard enable (PH) stainless steels are a fifth family of stainless steels that can be differentiated from other stainless steels not by the microstructure but by the type of heat treatment applied. [20]

2.3.1 Austenitic stainless steels

The most common stainless steel in alloys and applications. They are divided into the following grades:

The iron, chromium, and nickel grades correspond to typical alloys in the AISI 300-series and specialized variations of these alloys. These alloys,

which are based on type 304 (18-8) stainless steel, typically consist of 16 to 26% Cr, 10 to 22% Ni, and trace quantities of additional alloying elements such as molybdenum, titanium, niobium, and nitrogen. The composition of these alloys may be seen in Figure (2.2) [21]

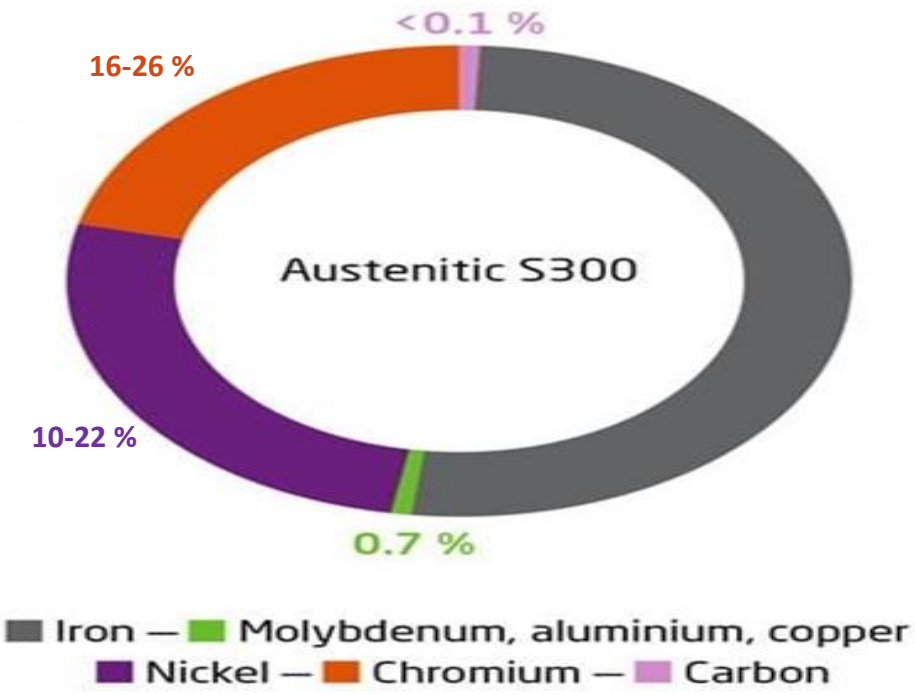

Figure (2.2) Composition of the Austenitic stainless steels S300 [22]

Different iron, chromium, manganese, and nickel grades can be purchased. These grades relate to both standard alloys in the AISI 200 series and specialized variants of these alloys. Some alloys can replace a portion of the nickel with manganese, ranging from 5% to 18%. When it comes to these alloys, it is typical to use nitrogen alloying techniques.[21]

Stainless steels composed of iron, nickel, and chromium are highly alloyed metals that can withstand higher levels of corrosion. The nickel content of these alloys could reach as high as 35% by weight. In addition to that, molybdenum and copper are frequently utilized as additives.[23]

For better corrosion resistance, super austenitic grades (as seen in Figure. 2.3) are readily available and contain 6% molybdenum in addition to high quantities of chromium, nickel, and nitrogen [19]

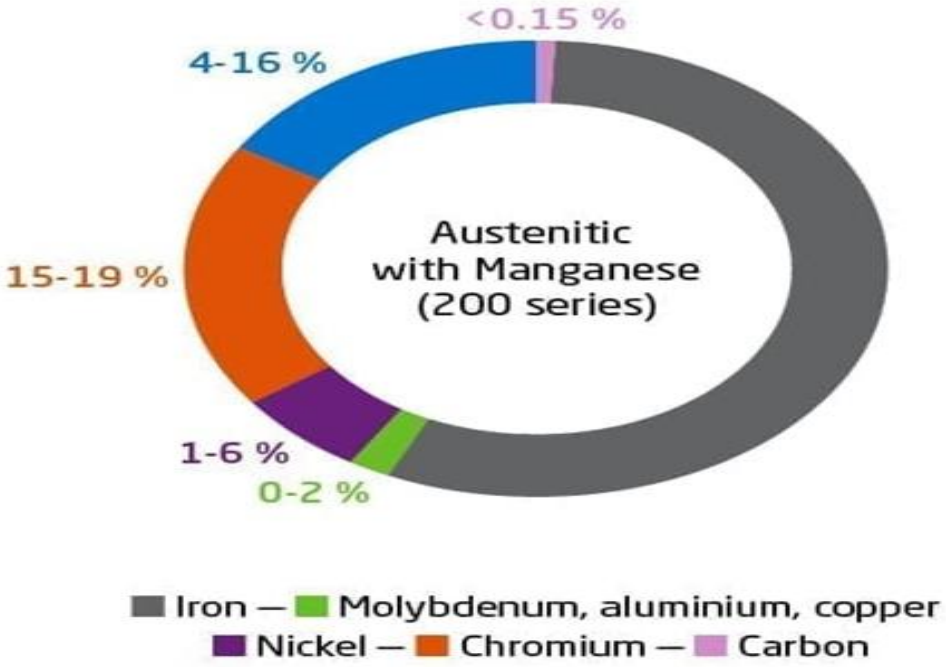

Figure (2.3) Composition of the austenitic stainless steels S200 [22]

2.3.2 Ferritic Stainless Steel.

Lack the ability to be toughened, such as iron-chromium alloys. The following [24] are included in this list:

A wide range of standard 400-series alloys and modified variations of these alloys, ranging from 11 to 27 % Cr, 0.08 to 20 % C, and trace amounts of ferrite stabilizers such as aluminum, niobium, and titanium, have been developed and tested.

Increased levels of chromium (up to 30 percent), molybdenum (up to 4 percent), and nickel content have been added to low-interstitial content (low carbon/nitrogen) grades that have lately been created (up to 2 %). Superfruits are grades of steel that exhibit exceptional resistance to stress-corrosion cracking (SCC) and other corrosion-related problems (see Figure. 2.4).

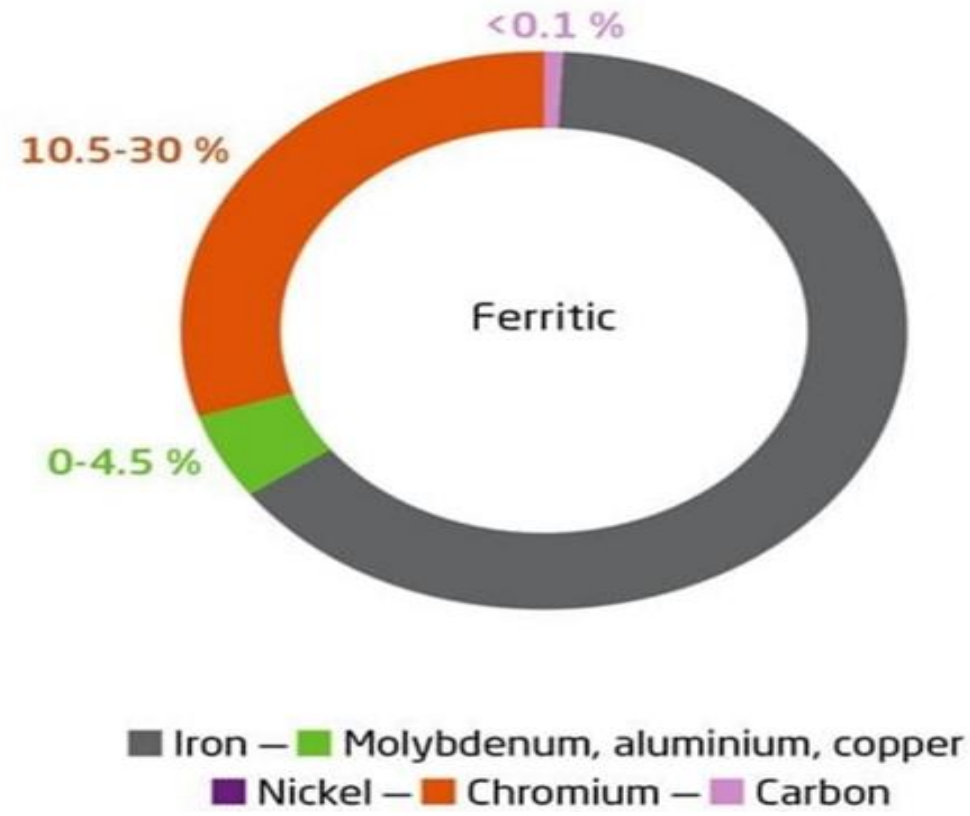

Figure (2.4) Composition of the ferritic stainless steels [22]

2.3.3 Martensitic Stainless Steels

The composition of the martensitic group is identical to that of the ferritic group, but it contains more carbon and less chromium to ease heat treatment hardening. This list includes the following items[23] :

In addition to trace amounts of manganese and nickel, standard 400-series alloys have between 11 and 18 percent chromium, up to 1 percent carbon, and additional elements.

Some grades, such as those that allow for free machining, those that are resistant to heat, and those that are suited for gears and bearings, are not typically employed.

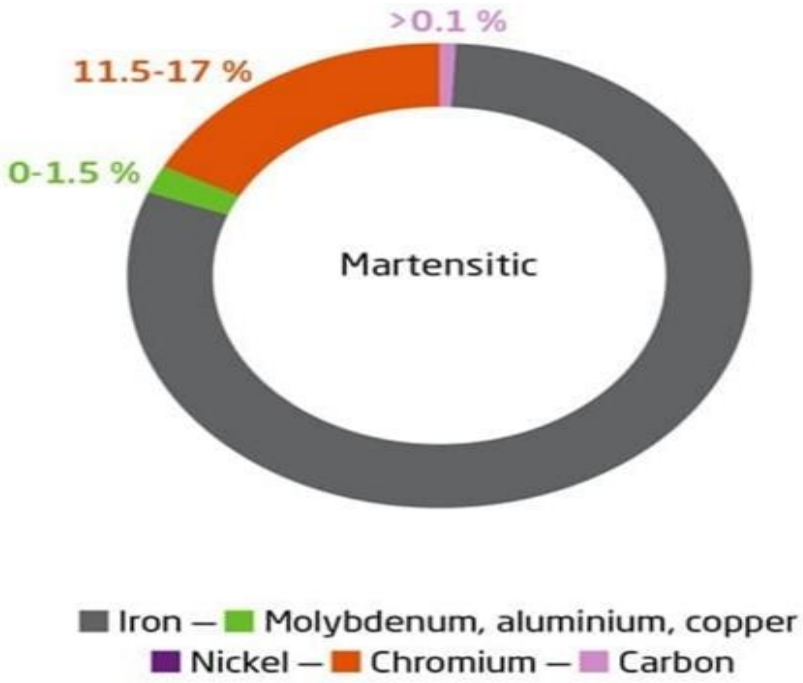

Figure (2.5) Composition of the Martensitic stainless steels [22]

2.3.4 Stainless Steels Made of Duplex

The get a microstructure consisting of austenite and ferrite in about equal amounts. They have anything from 22 to 25% Cr, 5 to 7% Ni, and up to 4% Mo in them, and small amounts of copper and nitrogen, among other elements and alloying constituents. Super duplex stainless steels are some of the most extensively alloyed and corrosion-resistant stainless steel varieties available [24]. Due to this property, duplex stainless steels are not considered part of the AISI 200, 300, or 400 groups. Most of them have UNS numbers, The term "United Nations Standard number" (UNS number) is not a standard term used by the United Nations (UN). It is possible that you may be referring to the United Nations Standard Products and Services Code (UNSPSC), which is a widely used classification system for goods and services.The UNSPSC is a hierarchical classification system that provides a standardized way of classifying products and services for the purpose of procurement and supply chain management. It covers a wide range of categories, including commodities, equipment, and services, and is used by

organizations around the world to streamline procurement processes and facilitate consistent data exchange. Each category in the UNSPSC is identified by a unique code consisting of four segments, separated by periods. For example, the code "43211503" represents "Computer printers," where "43" represents "Office machines and their supplies and accessories," "21" represents "Computer Equipment and Accessories," "15" represents "Printers and facsimile and photocopier and accessories," and "03" represents "Printers".It's important to note that if you are referring to a different type of standard number or code used by the United Nations, please provide more information so that I can assist you further. but the amounts of chromium and nickel also recognize some they contain. For instance, alloy 2205 has a weight distribution comprising 22% Cr and 5% Ni.

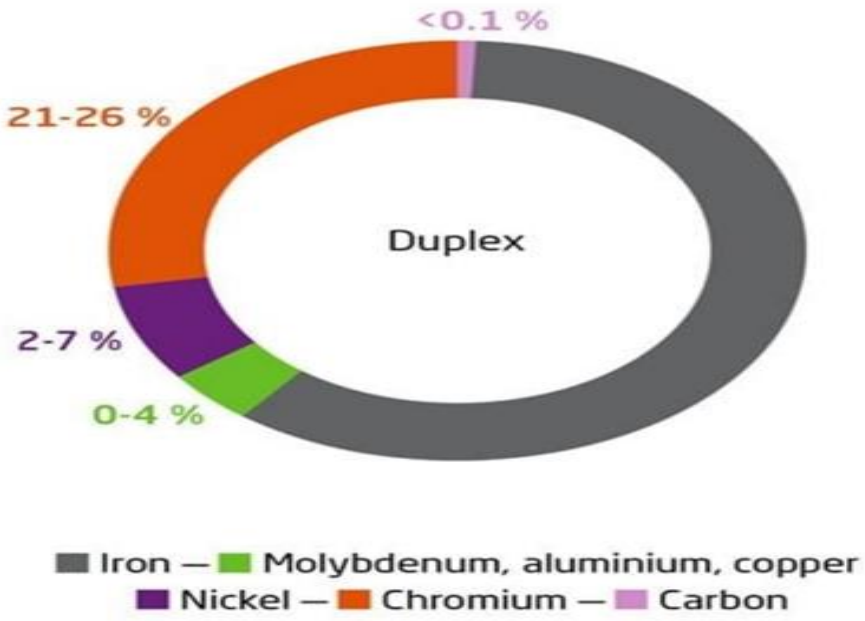

Figure (2.6) Composition of the duplex stainless steels [22]

2.3.5 Precipitation Hard Enable Stainless Steels

Alloy components such as aluminum, copper, or titanium are added to chromium-nickel alloys, allowing them to be toughened using a solution and aged heat treatment process. They are further subdivided into martensitic stainless steels, semi-austenitic stainless steels, and austenitic stainless steels. These steels are often referred to by their tradename or United Nations Standard number (UNS number).[24]

2.4 Effects of Alloying Elements on Stainless Steel

It is well known that the most important alloying elements in stainless steel are chromium and nickel. The content of these alloys (the equivalent of each of them) is highly affected by the structure of the resulting steel (as shown in Figure (2.7).[25]

As one of the main alloying elements in iron and steel, aluminum (Al) plays the role of deoxidation and grain refinement, which can improve the hardness of impact steel and aging[26]

Aluminum can strengthen the steel's resistance to corrosion, mainly when used with molybdenum, copper, silicon, chromium, and other elements, resulting in better results. The addition of Al in Cr-Mo steel or Cr steel can improve its corrosion resistance, and the presence of Al in high-carbon steels can cause brittleness, But Al will influence the Properties of hot working, welding, and cutting of the steel. It is widely used in special alloys, including nitrous steel, acid-resistant stainless steel, heat-resistant steel, ferroelectric alloy, soft magnetic and hard magnetic alloy, and so on [26].

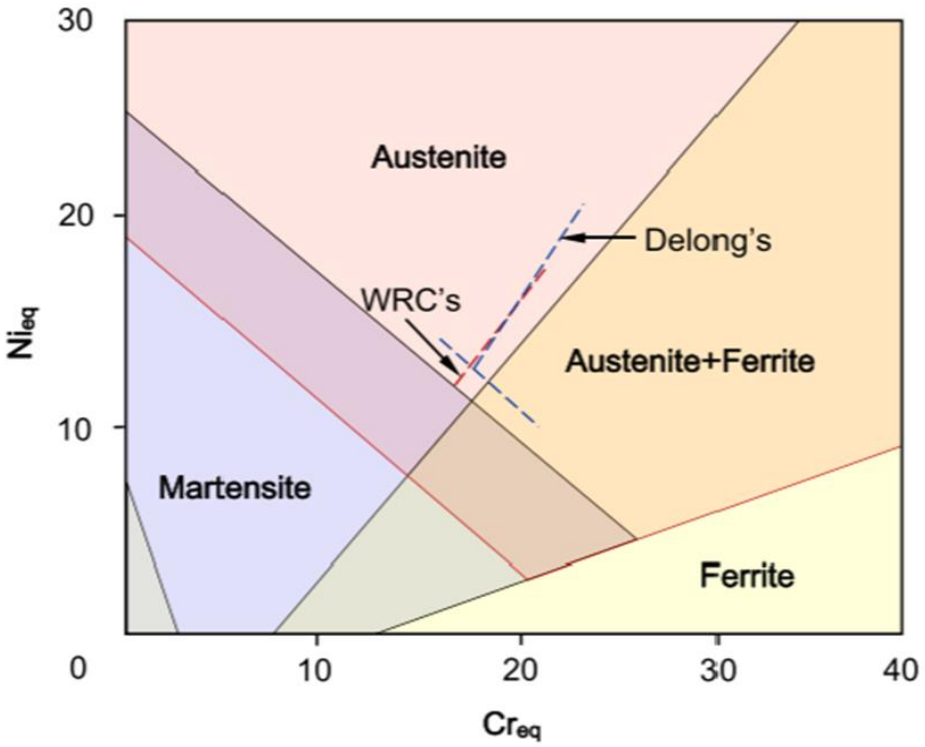

Figure (2.7) Effect of Nieq and Creq on the structure of stainless steels [25]

Nieq = Ni + 30C +0.5Mn , Creq = Cr +Mo + 1.5Si + 0.5Nb, where the contribution of each element to austenitic or ferritic stability .

2.4.1 Effect of Aluminum on the Mechanical Properties of Steel

Incorporating aluminum into steel as an extra alloying element results in the following modifications to the material's mechanical characteristics .[29]

Al lessens the sensitivity of steel to the gap, reduces or eliminates the aging phenomena of steel, and, in particular, lessens steel's brittle transition temperature hardness. Additionally, Al enhances the hardness of steel while it is cold.

Aluminum has a more robust and significant influence on the solution-strengthening process. The martensitic stainless steel 410 has lower high-temperature strength and toughness than the ferrite Fe-Al alloy, which has higher high-temperature strength and toughness.

Hard austenitic Mn steel has superior overall performance to other types of Mn steel.

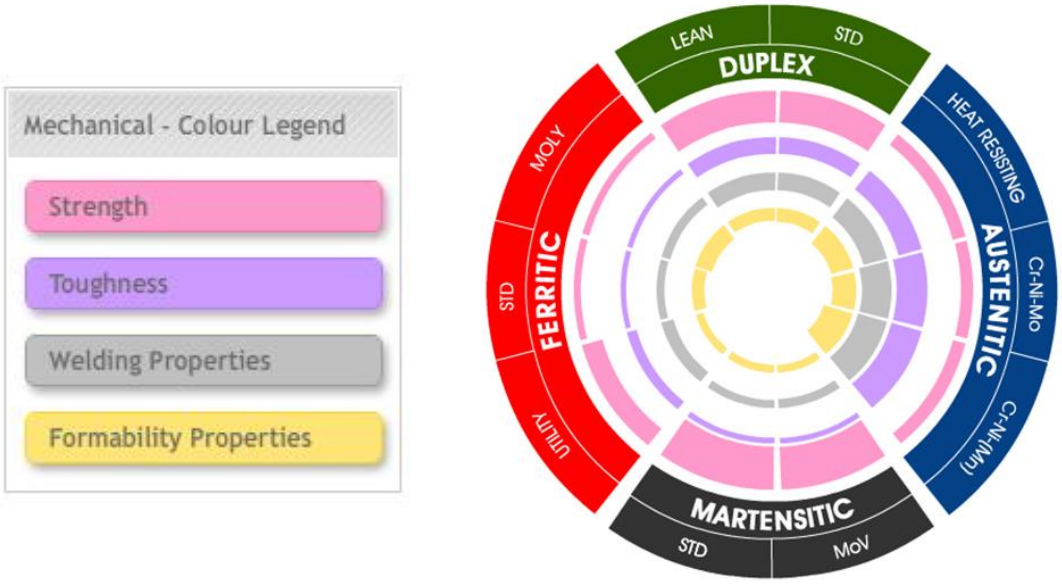

Figure (2.8): Mechanical properties of stainless-steel types [30]

2.4.2 Effect of Al on the Physical and Chemical Properties of Steel [31]

As a thermoelectric alloy material, Al-Fe alloy can lower the temperature coefficient of its resistance and may be employed in this capacity. In a manner analogous to that of the element Si, Al decreases the core loss of steel transformers. In sufficient amounts, aluminum can increase the resistance of hydrogen sulfide to acid oxidation corrosion and make the surface of passivation steel resistant to acid oxidation corrosion. In environments high in chloride and chlorine gas, aluminum's presence improves steel's resistance against corrosion; after forming an aluminum nitride layer, steel alloyed with aluminum creates a nitride surface. This can increase the material's hardness, fatigue strength, and resistance to wear. Aluminum can considerably increase steel's oxidation resistance when used as an alloying element. Applying an aluminum coating or coating made of

aluminum on the steel surface can increase the material's resistance to oxidation and corrosion.

The presence of Al negatively impacts the performance of hot welding and cutting activities.

2.5 Corrosion of Stainless Steel

The corrosion problem is one of the most frequent problems in several industries: chemical, petrochemical, mineral exploration, and mining industries, mines, as well as energy regeneration industries, due to the presence of compounds and chemical elements that interact with equipment and devices in industrial facilities, and phosphorus acid and the impurities in it have very severe corrosive features [32]

1- Stainless steel 310 has very high corrosion rates compared to the rest of the tested stainless steels, with its high chromium content.
2- Stainless steels type 316Ti and H18N10MT have high corrosion rates compared to the rest of the tested stainless steels, but they are lower than the corrosion rate of steel 310, and this can be attributed to the apparent difference in the %age of titanium.
3- 904L stainless steel has low corrosion rates in doped phosphoric acid and is distinguished from the tested types with a high percentage of chromium, nickel, and molybdenum, as well as copper.
4- The tested types of stainless steel 316, 321, Sw-01Ch19N9, and Sw-07Ch19-N10B have meager corrosion rates in doped phosphorous acid, which can be attributed to cooperation between the alloying elements.
5- Stainless steel alloys that contain traces of titanium have low corrosion rates and are lower than those with more enormous titanium proportions.
6- The types of stainless steel form a galvanic chain with each other in doped phosphorous acid, and they can be arranged from the noblest

mixture (321) to the least noble (310) as follows: (321, 904L, Sw-01Ch19N9, Sw-07Ch19-N10B, 316Ti, 320, H18N10MT, 316, 310) [33].

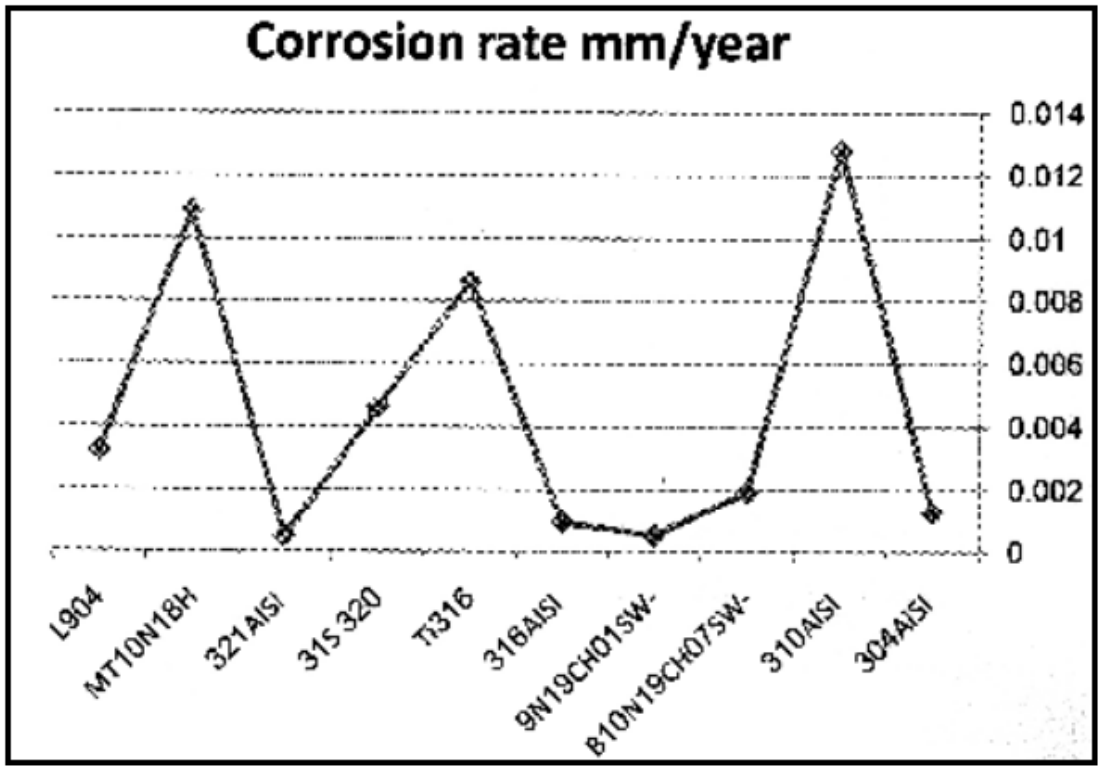

Figure (2.9) A graph showing the increase and decrease in corrosion rates in industrial phosphorous acid according to the type of stainless steel [34]

2.6 High-Temperature Applications of Stainless Steel

This type of steel is characterized by its resistance to creep, oxidation, and scaling because it contains elements such as chromium, aluminum, and silicon, as the oxides of these elements are in the form of a protective film. The structure of this type must be stable (unchanged) at high temperatures to prevent carbon deposits in granular border areas or their balling [29].

Its ability to operate with machines and weld is also one of the characteristics of this type of steel and its fatigue resistance.

This type is used in steam power generation stations. It is the Millenium container with a 5.0 %, which helps the formation of tuberculosis cabins. It is also used in the valve industry when it contains the two races of 8 %and

the silicon with a 5.3 %range and is used in the manufacture of feathers and the dust of the gas—18% [35].

2.7 Oxidation of Stainless Steels

The resistance of stainless steel to oxidation is the quality that contributes to the desirability of this group of metals for a wide variety of applications. After the early phase of rapidly forming a protective oxide covering, the oxidation rate eventually falls to zero in most everyday situations.

The chemisorption of an active species comes first in the oxidation process. This is the initial stage. After that, dissociation of the adsorbed molecule takes place, followed by a combination of the adsorbed atoms with the bits on the substrate material's surface [36].

There has yet to be any quantitative research conducted on the first oxidation of stainless steel; moreover, several studies of this type have been published for iron,25-35 chromium, and nickel. 36-42 These investigations should indicate the initial oxidation of stainless steels because these metals are the primary ingredients in most stainless steels. In general, a process involving multiple stages of oxidation has been discovered. The first step is fast dissociative chemisorption, which occurs on the surface of the metal. After that, the oxygen that has been adsorbed combines with the metal atoms on the surface. When this stage is reached, a surface reconstruction may or may not occur. This is determined by the lattice plane exposed to the oxidation and the type of metal used. For test pIe, just the Cr (1(0) face is reconstructed, whereas the Ni (I(0) face has not been touched. This second step moves along quickly until a few oxide monolayers are produced (usually between two and four). There is evidence that impurity atoms on the surface of a material alter the oxidation kinetics of that material. The third stage of the process is the gradual oxidation of the bulk metal oxide [37]. According to Driscoll 5, a sulfur monolayer prevents iron oxidation at temperatures between 200 and

300 degrees Celsius. The oxidation kinetics were unaffected by quantities of less than half a monolayer. Windway 43 investigated the transition on a nickel surface between chemisorption and oxidation and the effect that surface contaminants play in the change. A sulfur-nickel place exchange occurs when there is sulfur on the surface of the metal, which lends confidence to the place exchange mechanism as the initial step in the metal oxidation process [38].

2.8 Classification of Additive Manufacturing Processes

Based on the adhesion and bonding methods used, ASTM International [41] categorizes additive manufacturing technologies into seven major groups. There are a few different types of photopolymerization in a vat, including vat photopolymerization, binder jetting, material extrusion, material jetting, and sheet lamination. VAT polymerization and material jetting are among the many options for liquid additive manufacturing. At the same time, filament processes can use material extrusion as an alternative when binding powder particles together; powder fusion, binder jetting, or direct energy deposition are all viable options. As depicted in Figure.(2.10), the bonding procedures are categorized based on the raw materials "feedstock." With Charles W. Hull's invention of additive manufacturing in 1986 [42]. It is still a young manufacturing process. Since then, several new procedures have been put into practice. Figurer. (2.10) shows a classification of several additive manufacturing processes based on the state of the raw material.

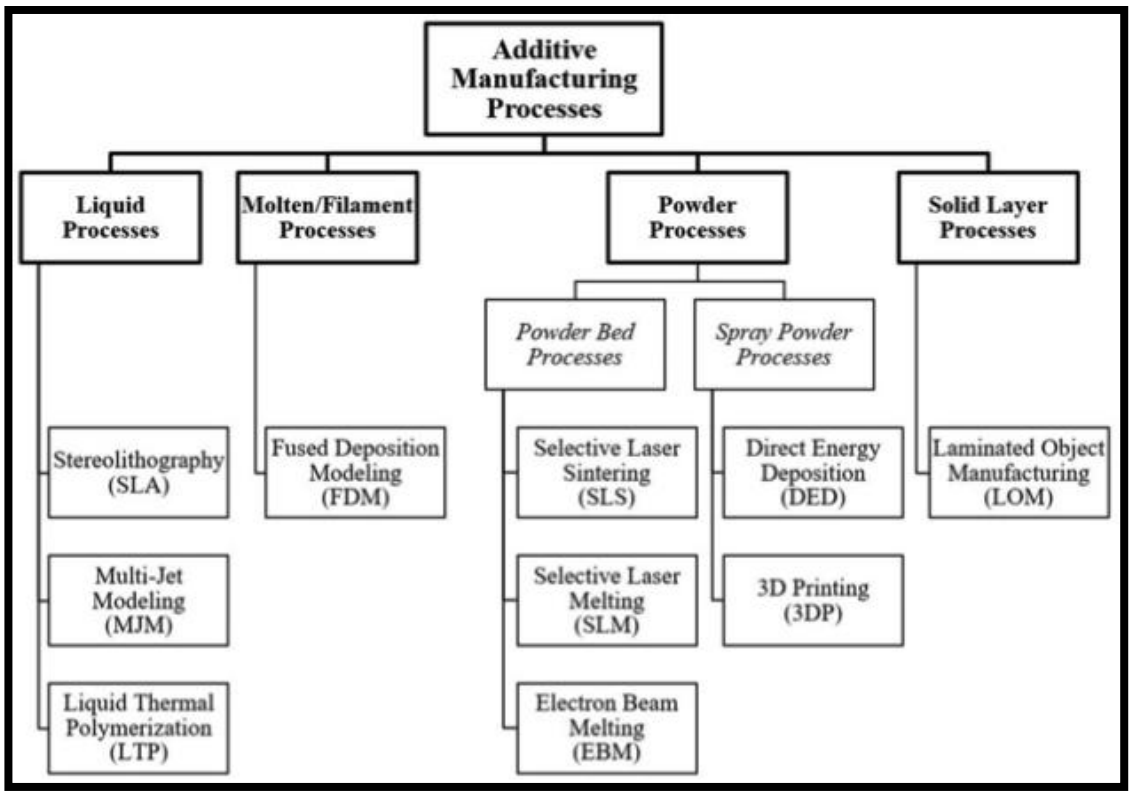

Figure (2.10) Processes for additive manufacturing [43].

2.9 Fusion Zone Microstructure Evolution

There are four solidification and solid-state transformation possibilities for austenitic stainless steel weld metals. These reactions are listed in Table 6.5 and related to the Fe-Cr-Ni phase diagram in as seen (Figure 2.11). Note that A and AF solidification modes are associated with primary austenite solidification, whereby austenite is the first phase to form upon solidification. Types FA and F solidification have delta ferrite as the primary phase. Following solidification, additional microstructural modification .

Table 2.1 Solidification Types Reaction , and Resultant Microstructures .

Solidification Type	Reaction	Microstructure
A	$L \rightarrow L + A \rightarrow$	Fully austenitic,well-defined solidification structure
AF	$L \rightarrow L + A \rightarrow L+A+(A+F)_{eut} \rightarrow A+F_{eut}$	Ferrite at cell and dendrite boundaries
FA	$L \rightarrow L+F \rightarrow L+F+(F+A)per/eut \rightarrow F + A$	Skeleatal and/ or lathy ferrite resulting from ferrite – to-austenite transformation
F	$F \rightarrow F + A$	Acicular ferrite or ferrite matrix with grain boundary austenite and Widmanstatten side plates

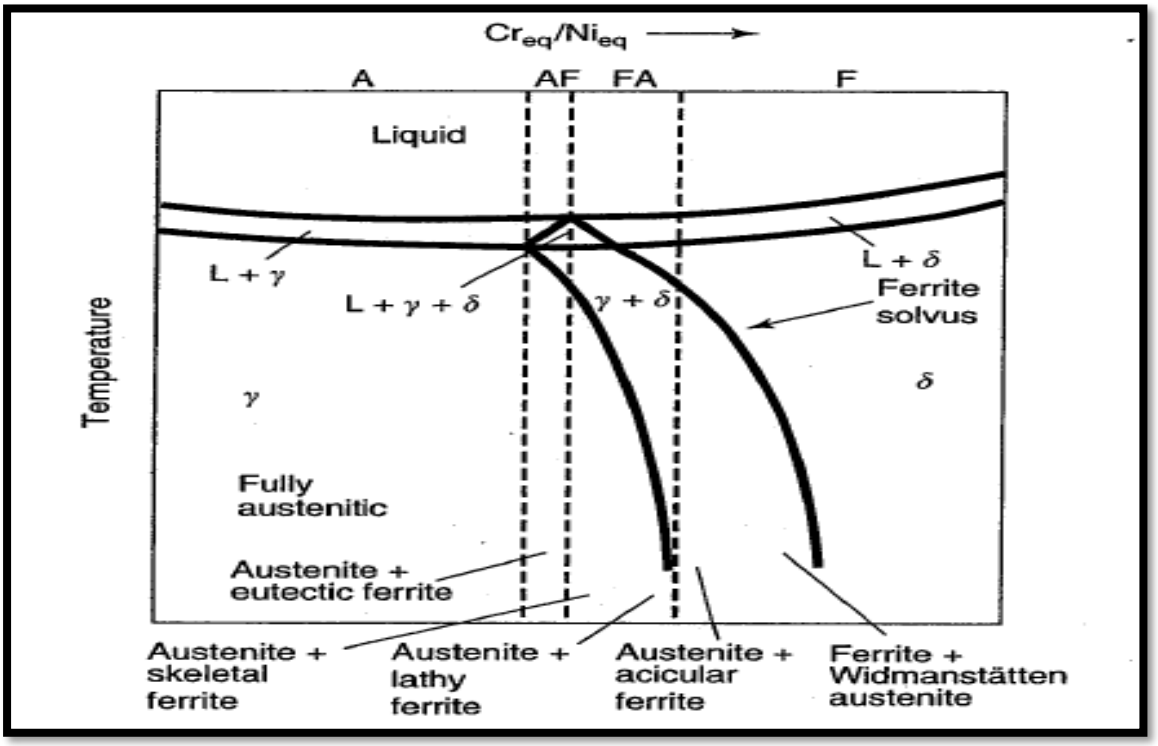

Figure (2.11) Relationship of solidification type to the pseudo binary phase diagram .

2.9.1 Type AF Solidification

Type AF solidification occurs when a eutectic reaction generates ferrite after primary austenite solidification. If enough ferrite-promoting components (mostly Cr and Mo) partition to the solidification subgrain boundaries during solidification, ferrite forms as a terminal product. The three-phase triangle section in Figures (2.12) and 6.6's phase diagram suggests a eutectic reaction. Since it is rich in ferrite-promoting components, the border ferrite resists austenite transition during weld cooling. Figure (2.12). AF solidification schematic. A microstructure with femte along solidification subgrain boundaries is depicted in Figure (2.12). As this is primary austenite solidification, the substructure is easily visible.

2.9.2 Type FA Solidification

Two options exist for primary ferrite solidification. Type FA has austenite after solidification. After solidification, peritectic-eutectic reactions generate this austenite near the ferrite solidification borders. David et al. [8,9], Lippold and Savage [1,10,11], Brooks [12], Arata [13], Katayama [14], Leone and Kerr [15], and others [16,17] have thoroughly examined this response. These experiments show that FA solidification produces ferrite morphologies by the following solidification and transformation procedure (Figures 2.12 and 2.13).

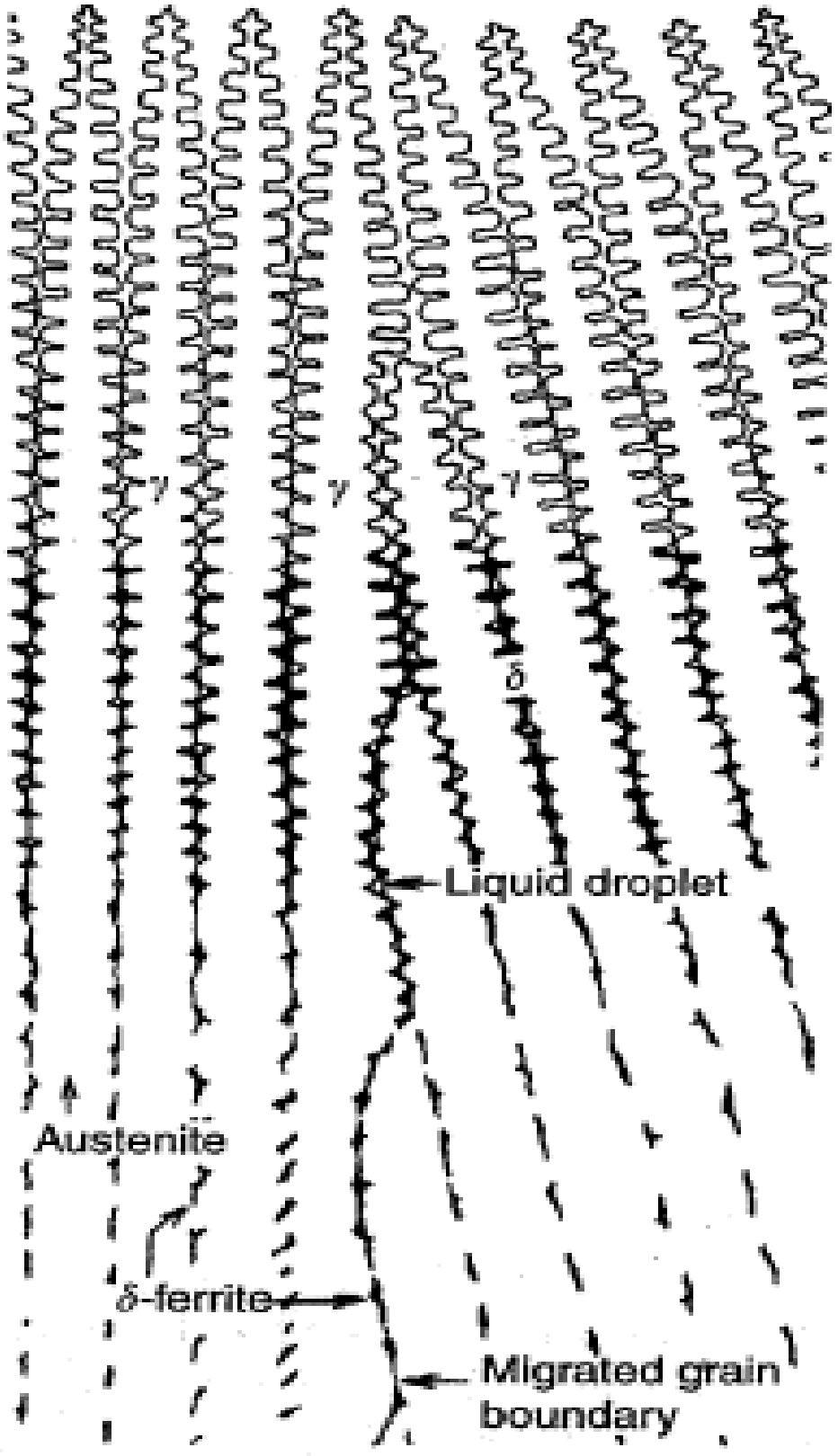

Figure (2.12) Fusion zone microstructure from Type AF solidification (From Katayama et al) . [14] .

1. After primary ferrite solidification, a peritectic-eutectic reaction forms austenite at the cell and dendrite borders. The triangular three-phase area in Figures (2.13) and 6.6 hosts this reaction. It's dubbed a peritectic-eutectic reaction since it's composition-dependent and results from a Fe-Ni system peritectic reaction to a Fe-Cr-Ni system eutectic reaction (Figure 2.13).
2. The microstructure is primary ferrite dendrites with an austenite interdimeric layer after solidification. The Cr/Ni ratio and solidification circumstances determine austenite content. ep As Cr/Ni rises, austenite declines until ferritic solidification. The solidification type changes from FA to F.
3. The two-phase delta ferrite + austenite field cools the weld metal, making the ferrite unstable and allowing the austenite to devour it via diffusion. This response was formerly debated [1,8,9,11,15], but it is now commonly accepted.

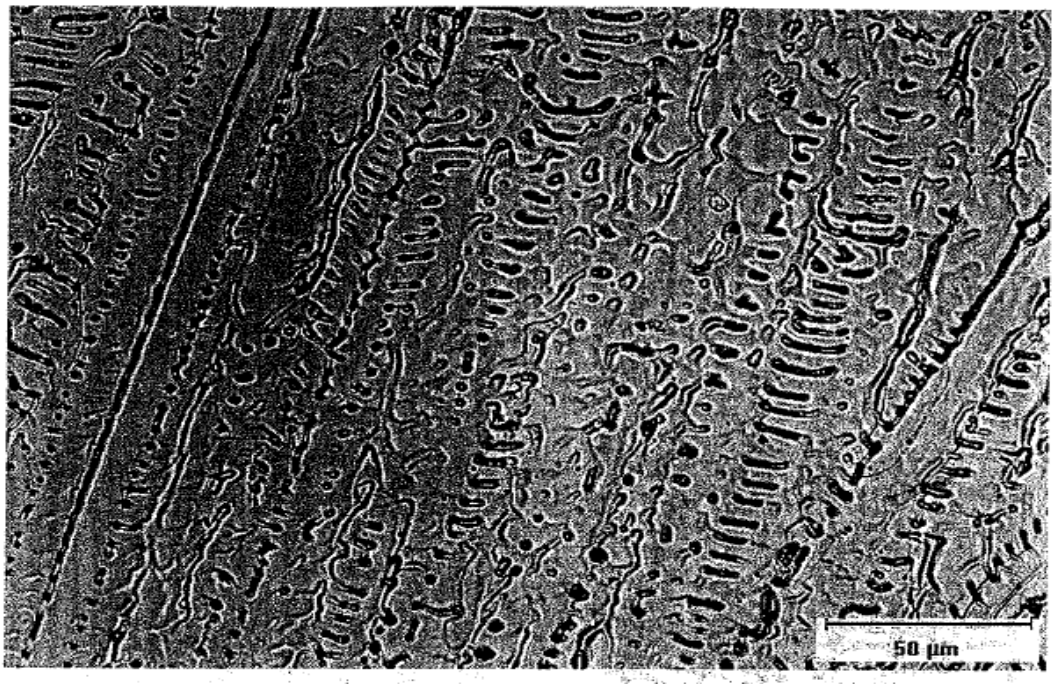

Figure (2.13) Fusion zone microstructure resulting Frome Type AF solidification

4. Vermicular, or skeleton, ferrite shape emerges from moderate weld cooling rates and low Cr/Ni within the FA range (Figure 6.13). The austenite consumes the ferrite until it is enriched in ferrite-promoting elements (chromium and molybdenum) and depleted in austenite-promoting elements (nickel, carbon, and nitrogen) enough to be stable at lower temperatures where diffusion is limited. Figure (2.14) la and Figure 6 depict the skeletal microstructure schematically and micrographically.
5. Lathy ferrite morphology results from high cooling rates and Cr,,/Nii increases within the FA range in Figure (2.14). Lathy morphology replaces skeletal morphology during the femte-austenite metamorphosis due to constrained diffusion. When diffusion distances are shortened, the transformation proceeds more efficiently as densely spaced laths, leaving a residual ferrite pattern that crosses the dendritic or cell development direction. Figures (2.14b) and (2.14b) depict this schematically and micrographically.
6. Due to a diffusionless, "massive" transition, ferrite can become austenite during laser or electron beam welding at high solidification and cooling rates. High solidification rates can also change main solidification mode from ferrite to austenite. Section 6.5.1.5 details this behaviour.

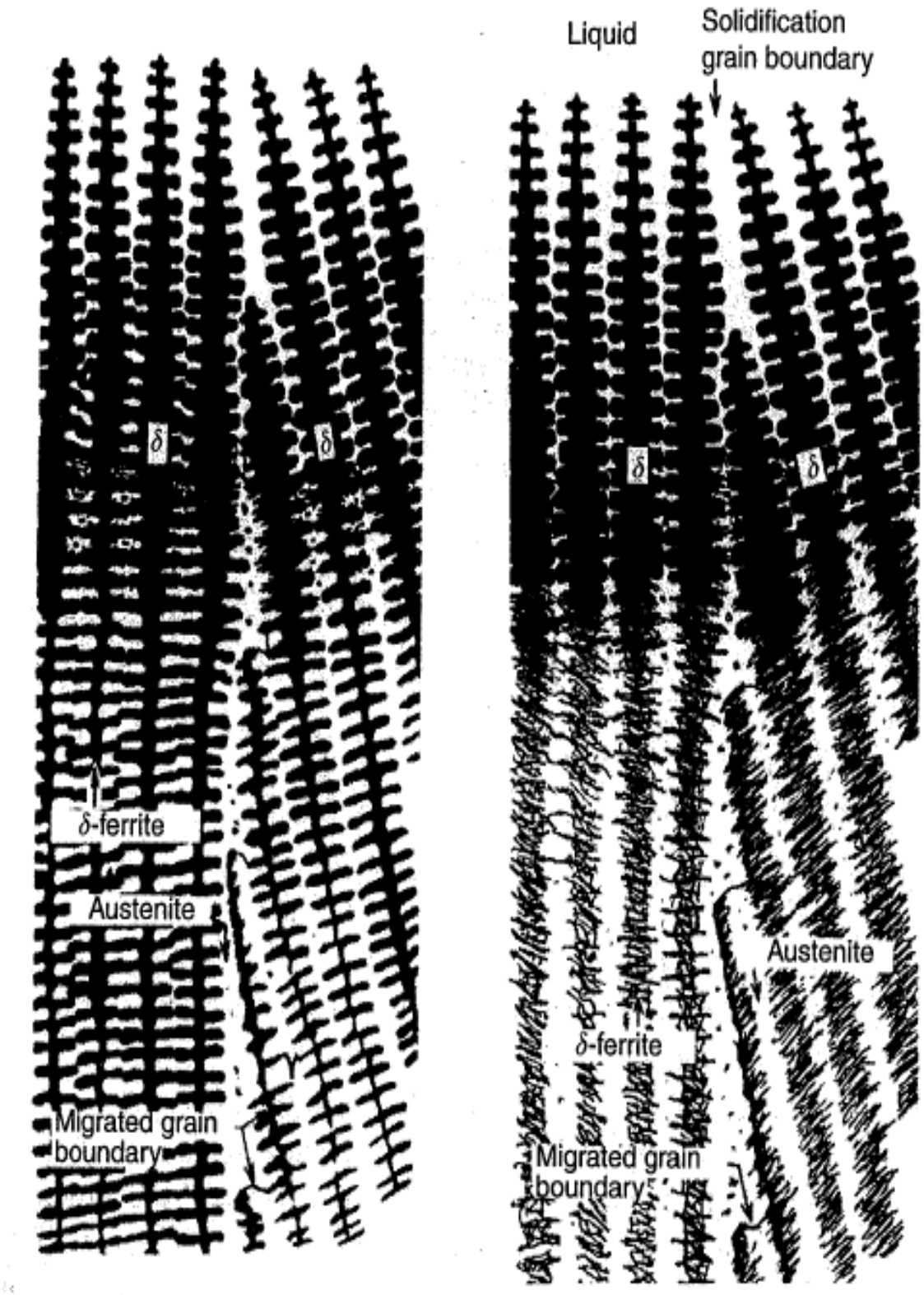

Figure (2.14) Type FA solidification : (a) skeletal ferrite ; (b) lathy morphology . (From Katayama et . al) [14].

2.9.3 Type F Solidification

Type E refers to full solidification as ferrite. In this example, the microstructure is totally fenitic after solidification, as seen in Figure (2.15). As weld metal cools below the ferrite solvus, austenite first forms at the ferrite grain boundaries.

The ferritic structure between the solidus and ferrite solvus prevents composition gradients during solidification, resulting in a microstructure during transition.

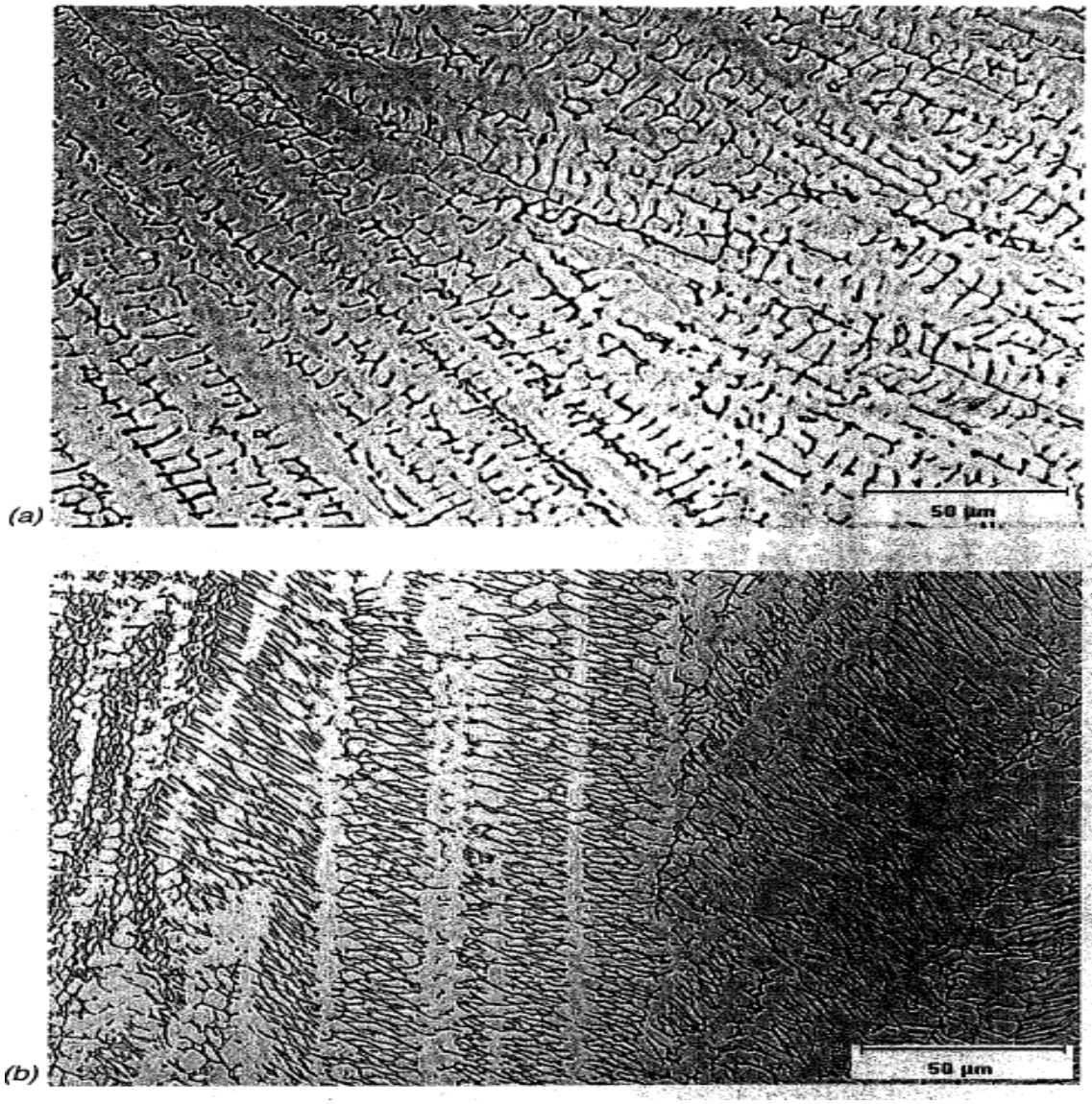

Figure (2.15) Fusion zone microstructure resulting FA solidification (a) skeletal ferrite morphology ; (b) lathy morphology .

2.9.4 Solidification Modes .

Metals are capable of solidifying in a variety of different ways. These modes are used to characterize the many morphological shapes that may be present at the S–L interface, and in many instances, these forms are still visible after the system has been cooled to ambient temperature.

Plane front solidification is possible when the conditions are right, whether those requirements include low solidification rates, steep temperature gradients, or both. In the vast majority of real-world situations, the planar front may be decomposed into various modes that are either cellular or dendritic in their morphologies. The interaction of composition, temperature gradient, and rate of solidification has a combined impact that determines which solidification mode will be the most stable. Figure (2.16) [6] is an illustration of the wide variety of solidification modes that may be seen in metals. A planar front of solidification initially disassembles into a cellular front and then into smaller fronts.

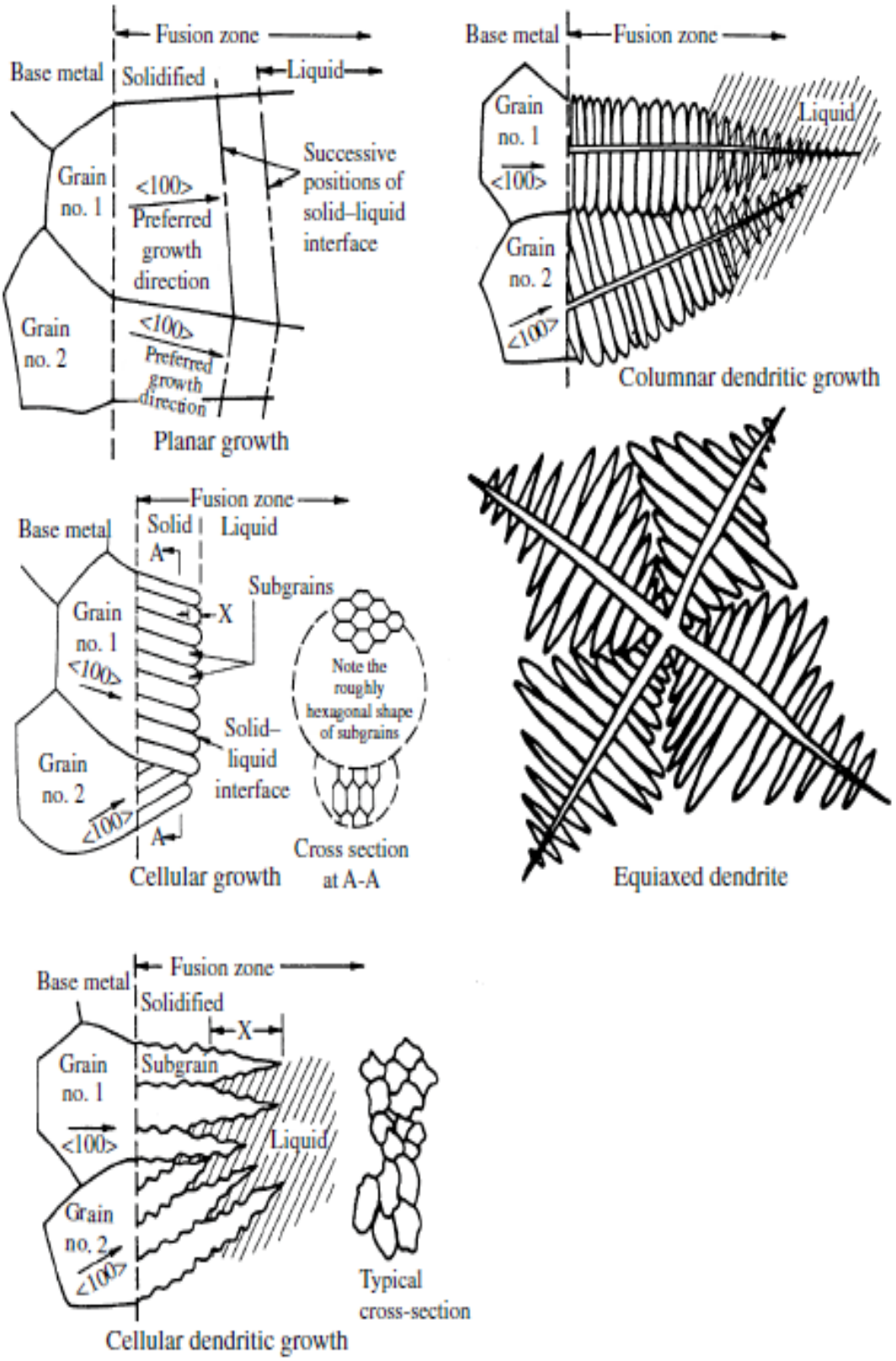

Figure (2.16) . Solidification modes that occur in metals . [6]

2.10 Review of WAAM of Stainless-Steel Composites

Feng relied on a novel approach known as dual-wire feed plasma arc additive manufacturing (DWF-PAM) when fabricating components out of stainless steel. Compared to the SWF-PAM methodology, the DWF-PAM method produced beads with a superior look and improved microstructure and mechanical qualities in the end product. At the same settings for the operation, the DWF-PAM technique likewise increases the deposition rate, that is, on average, 1.06 times higher.[61] Due to wholly grown equiaxed ferrite (CGEF) grains, the DWF-PAM-processed materials have a fine-grained microstructure and higher mechanical characteristics, including a considerable increase in ultimate tensile strength and elongation rate. This is because of the presence of CGEF grains. When fabricating components out of stainless steel, the DWF-PAM process is a more effective and efficient method.

Ahsan et al., 2020 [62] examined the possibility of replacing traditionally constructed functionally graded components with bimetallic additively produced structures (BAMSs) to reduce post-processing-induced regional mechanical degradation. BAMSs were made using a wire + arc additive manufacturing (WAAM) approach based on gas metal arc welding, layering Inconel625, and austenitic stainless steel. The prepared samples showed a seamless compositional transition with similar hardness values at the interface between the two materials. The controlled thermal history of WAAM resulted in BAMSs with suitable properties with a tensile strength of stainless steel as high as 600 MPa and elongation of 40%.**[71]** produce thin-walled parts of 316L stainless steel using Wire Arc Additive Manufacturing (WAAM) technology. The study dealt with three process parameters, scanning speed, bottom current mode, and cooling time, to determine their effects on the stability of the deposition process, macro morphology, structure, and mechanical qualities of the finished product. The

investigation found that a gradual decrease of current, layer-by-layer, improved the bottom molding, performance, deposition efficiency, and process stability. Reducing cooling time or increasing scanning speed destabilized the end formation and reduced the effective deposition rate. The deposition in speed cold welding mode, with a rapidly decreasing bottom current, a scanning speed of 30 cm/min, and a cooling time of 10 seconds, showed excellent stability and produced anisotropic but industry-compliant samples.

The study by **Chaudhari et al., 2022 [72]** used gas metal arc welding (GMAW) for additive manufacturing of significant metallic components. One of the main issues in the items produced by this process is the quality loss on the side face. The study proposed a laser vision system-based approach for evaluating surface roughness and examined the effects of wire feed speed and travel speed on thin-walled items. They found that the increased surface quality of thin-walled components is associated with decreased inter-layer temperature. Moreover, surface roughness can be reduced using a slower wire feed speed and travel speed.

The study conducted by **Hosseini et al., 2019 [60]** explored the effect of heat cycles on the microstructures of duplex stainless-steel blocks prepared by wire-arc additive manufacturing. Different heat inputs and interlayer temperatures were used to prepare samples. They found that high and low heat input methods could build similar shapes. Nevertheless, the intense heat input method resulted in a more austenite fraction due to faster cooling rates. Samples that were heated multiple times showed identical austenite fractions; however, longer reheating at high temperatures resulted in higher secondary phases. Most samples had an acceptable austenite fraction with a small percentage of secondary phases at high peak temperatures.

The article by **Rumman and Ali, 2019** [61] investigated the use of wire with arc additive manufacturing (WAAM) to produce metal products in nearly net

shape. The study involved fusing low-carbon steel and AISI 316L stainless steel using gas metal arc welding (GMAW) and building a new M2WAAM system utilizing commercial resources. The samples' compositional, microstructural, and mechanical properties were compared, and no welding defects were found at the joint between the two components. The diffusion of chromium from the SS side into the LCS side increased the interfacial hardness. However, the failure occurred on the LCS side, away from the contact. The WAAM technique can properly combine LCS and SS, and it has welding strength equivalent to steel but with less ductility.

Table 2.2 Those aspects of the manufacturing process that have an impact on the macro morphology of WAAM stainless steel components

WAAM Techniques	Material	Process Parameters	Macroscopic Characteristics	References
MIG	316L (austenitic) stainless steel	Welding current mode Increasing scanning speed Gradual reduction of bottom current	Improves bottom formation Unevenness of both ends	(Feng,Y, et al, 2018)
PAM **PAM:SWF-PAM,DWF-PAM**	H00Cr21Ni10 (austenitic) stainless steel	SWF-PAM: single-wire feed and plasma additive manufacturing DWF-PAM: double-wire feed and plasma additive manufacturing Increasing scanning speed	Slightly better surface quality than that of Double-wire feed and plasma additive manufacturing //// Better surface quality	(Hosseini, V, et al, 2019)
MIG	Type-2209 (duplex) stainless steel	Deposition path Alternating direction deposition path One-direction deposition path	Uniform layer height Uneven sides: the start side was higher than the end side.	(Md. Rumman , et al, 2019)
MIG	H08Mn2Si low-carbon steel	Decreasing interlay temperature Increasing scanning speed Increasing wire feeding speed	Surface roughness decreases Surface roughness increases Surface roughness increases	(Md. R.U, et al, 2020)

2.11Survey of Studies of Preparation and Characterization of Additively Manufactured Stainless Steel

investigated the sub-grain structure of 316L stainless steel produced by additive manufacturing (AM) methods, such as electron beam melting (EBM) and selective laser melting (SLM). **[58]** The AM 316L is noted for its heterogeneous and hierarchical structure, including micro-sized melt pools, grain structure, nano-sized sub-grain structure, and nano-sized inclusions. The study explores the connection between these structures and their effect on mechanical characteristics. The AM process parameters were modified to produce tailored mechanical properties, resulting in SLM SS316L with higher strength and EBM SS316L with high ductility. The study showed that rotating 45 degrees between each layer improves cell communication across melt pools. The study also created YZ0, which added oxide dispersed strengthening steel (ODSS) to improve its performance at elevated temperatures. Large AM specimens, including complex inner pipe structures, were successfully tested for use in the nuclear industry.

In the research carried out by **G.T. Gray III et al. (2017)** [73], cylindrical samples of 316L stainless steel were produced using a LENS MR-7 laser additive manufacturing system from Optomec (Albuquerque, New Mexico). This system was outfitted with a 1kW Yb-fiber laser. In the investigation, the material's behavior was analyzed and compared to the conduct of annealed wrought 316L stainless steel plate material. Using flyer-plate impact-driven spallation tests, we studied the dynamic shock-loading-induced damage development and failure response of all three 316L stainless steel materials. The spall strength of AM-produced 316L SS and recrystallized AM-316L SS declined with increasing peak shock stress, but the spall strength of annealed wrought 316L SS remained virtually constant with growing peak shock stress. AM stands for additive manufacturing. The evolution of the damage, as evaluated by optical metallography and electron

backscatter diffraction, was considerably different for each of the three microstructures of 316L stainless steel.

In their study, **Md. Rumman & Ali Newaz (2018) [61]** focused on wire with arc additive manufacturing (WAAM) as a way to produce almost net-shaped metal products by sequentially welding two materials together. Gas metal arc welding Low carbon steel and AISI 316L stainless steel were employed in constructing bimetallic additively manufactured structures (BAMS) using the GMAW welding technique. The newly designed M2WAAM system was used to demonstrate the practicality of the method, and the mechanical qualities, microstructure, and composition of the specimens were investigated. The results showed that WAAM can properly fuse the two materials without any defects. The hardness rating increased significantly at the interface, on the other hand, and the failure occurred on the weaker LCS side away from the contact. The study also found that WAAM has a welding strength equivalent to that of steel but lower ductility, which could be improved by heat treatment.

Gu, C. et al., 2020 [75] With HK40 steel as the foundation, a heat-resistant steel with the formula ZG40Cr20Ni20Alxy (x = 0, 1.76, 3.45, and 5.34) was developed. At high temperatures, they discovered that the addition of Al greatly improves the oxidation resistance of ZG40Cr20Ni20 steel. Under high oxygen partial pressure conditions, the spinel oxide scales formed by $FeCr_2O_4$ are more stable than those formed by ZG40Cr20Ni20, and a continuous film of Cr_2O_3 forms between the matrix and the spinel oxide. After 480 hours of oxidation at 1100 degrees Celsius, steel that contains 5.34 weight percent aluminum accumulates just 1.1 mg/cm2 of mass gain, while steel that does not include aluminum accumulates 103.6 mg/cm2 of mass gain. The oxide scale is made up of one continuous layer of Al_2O_3, and its matrix has an appearance that is comparable to that of austenite and ferrite.

The research of **Suvi Santa-aho et al. (2020) [76]** investigated the impact of shot peening post-processing on the microstructure, surface, and subsurface residual stress distribution of additive manufactured (AM) samples. The post-processing resulted in compressive residual stresses of over 400 MPa, extending to a depth of over 100 μm below the surface. Grain refinement and low-angle boundary creation were observed on the sample surface layer, as well as SiC residue adhesion, which should be considered in the final product. Furthermore, there was no significant difference between the AM and reference samples in terms of SCC resistance after 674 hours of testing in a hot magnesium chloride solution using four-point bending immersion testing.

B.P. Eftink, et al, (2020) [77] examined the effects of irradiation with 1.5 MeV protons at temperatures between 40-150 degrees Celsius on additively manufactured 304L stainless steel. The microstructure and mechanical behavior of the material were analyzed and compared to that of wrought stainless steel. Despite differences in the unirradiated samples, the results showed that both types of stainless steel developed toward a similar state after irradiation. The study used TEM and nanoindentation to analyze the changes in microstructure and hardness, and the results were interpreted in terms of dislocation content, structures, and chemical homogeneity.

The study by **Ahsan, et al (2020)** [78] demonstrates the successful creation of a bimetallic additively manufactured structure (BAMS) using a wire + arc additive manufacturing (WAAM) method. The BAMS is made up of austenitic stainless steel and Inconel625, which have a seamless compositional transition with smooth and cross-interface crystallographic development. The hardness values of both materials were consistent and the mechanical testing showed ultimate tensile strength and elongation of 600 MPa and 40%, respectively. The WAAM method is capable of creating BAMS with accurate properties, which can replace traditionally constructed

functionally graded components and eliminate regionally deteriorating mechanical qualities caused by post-processing.

In their work **[Reza Ghanavati, et al,2021][79]** discussed the use of Functionally Graded Materials (FGMs) in advanced applications and the potential benefits of using additive manufacturing (AM) technology to produce them. The purpose of this work is to investigate the behavior of solidification and the evolution of the microstructure of thin-walled stainless steel 316L-Inconel 718 graded materials that were manufactured by laser additive manufacturing. According to the findings of the research, morphological evolution commonly occurred between solidification modes as a result of the re-melting of layers. Additionally, dilution caused the mixing of neighboring layers, which resulted in a deviation from the intended composition distribution. In addition, the micro segregation of certain components during non-equilibrium solidification resulted in the creation of secondary phases, which may hurt the mechanical properties of the material. However, the variations in microhardness that were found along the cross-sections of the samples showed that grading the various thin-walled structures can effectively bring the characteristics and behavior of neighboring layers closer together. This can be beneficial in terms of extending the amount of time that the materials are useful for their intended purpose.

CHAPTER THREE

EXPERIMENTAL PART

Chapter Three

Experimental Part

3.1 Introduction

The experimental setup, materials, methods, and tools used to create stainless steel 309 specimens utilizing a computer-aided design double-wire deposition machine (CADDWDM). are discussed in this chapter. Additionally, the chapter describes the research study's primary materials, dimensions, welding consumables, and method. Additionally, it covers specifics regarding the operation environment, substrate preparation, and welding preparation, including welding rigs and power supply units. They were put through several tests to analyze the behavior of these materials and learn more about how they perform, including hardness testing, tensile testing, metallographic analysis using scanning electron microscopy (SEM), X-ray diffraction (XRD) analysis, and optical microscopy (OM).

3.2 Experimental Procedure (Materials and Methods)

Base materials, dimensions, and welding consumables are listed below. Substrate preparation operating conditions, including power supply and welding apparatuses, are all covered. All study activities are summarized in (Figure 3.1).

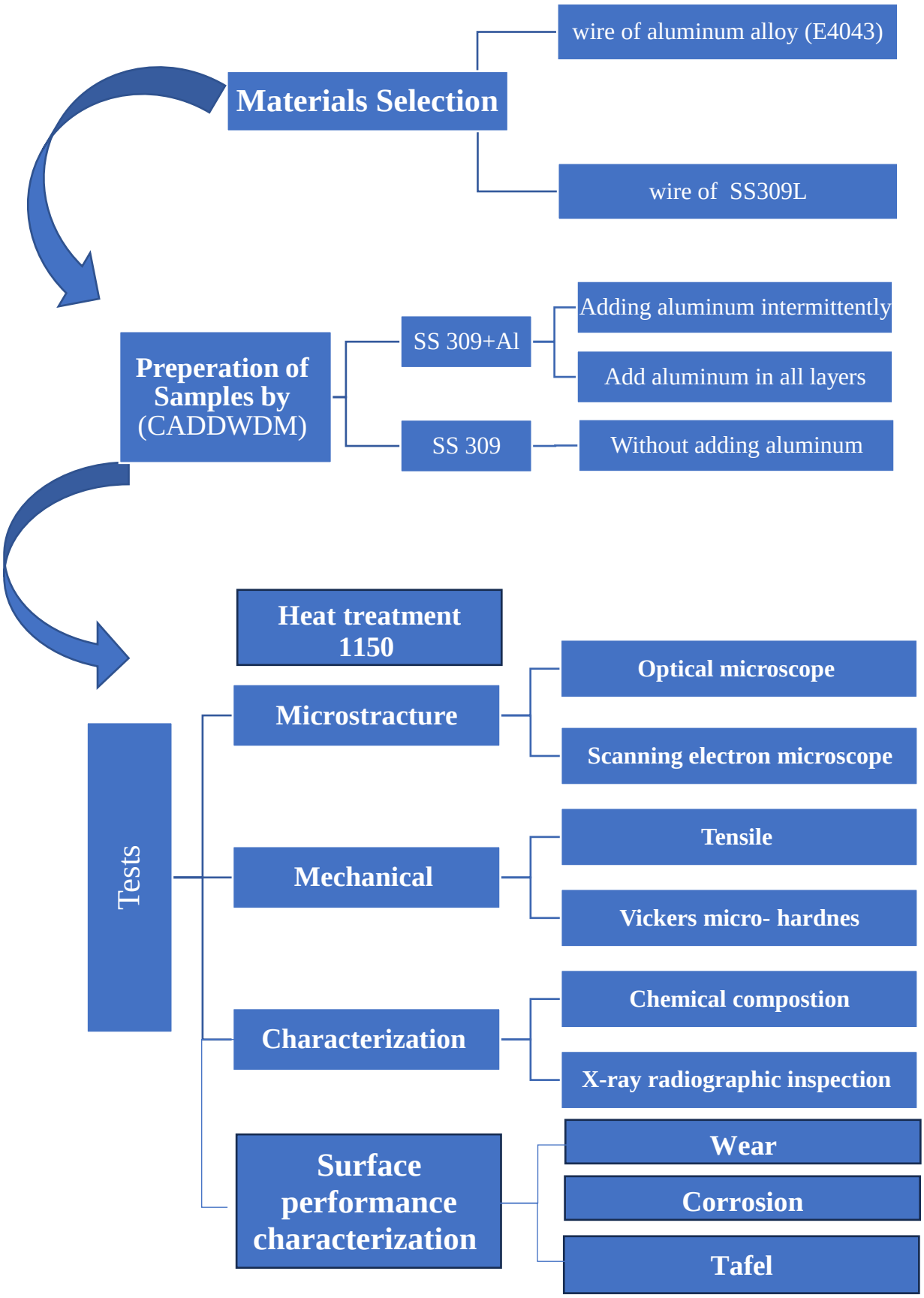

Figure (3.1): Flow chart of the present work

3.3 Materials Used in the Current Research

The chosen material for (CADDWDM) was the stainless steel 309 in the form of a welding wire with a diameter of 1.2mm. Its grade was selected according to AWS A5.22 specification, so the wire grade is "E309L" FLUX-CORE austenitic stainless steels have good strength and high corrosion resistance. In addition, they are weldable and have less embrittlement in the welded structure. They are widely used in thermal power plants, pressure vessels, and the medical industry. So, this group of stainless steel is considered suitable for additive manufacturing.

Mild steel "St. 3," according to DIN standard having dimensions of 200mm × 200mm × 8 mm, was employed as a substrate to deposit the weld beads. It was mechanically cleaned utilizing a stainless steel wire brush to remove the top surface rust, grease, etc., from the base plate before the deposition process.

The chemical composition in wt.% of the deposition metal wire and substrate is shown in Table (3.1).

Table (3.1) Chemical composition of the deposited material and the substrate.

Materials	C	Si	Mn	S	P	Mo	Ni	Cr	Cu	Fe
Wire	0.03%	0.9%	1.3%	----	----	0.1%	12.5%	24%	0.1%	Rem.
Substrate	0.1 max	0.03-0.15	0.2-0.45	0.04	0.04	----	----	----	----	Rem.

All the chemical composition analysis was done using the chemical composition analyzer shown in Figure (3.2), located at the laboratories of the Ministry of Science and Technology

Figure (3.2): The workplace is in the laboratories of the Ministry of Science and Technology.

The additive manufacturing process included adding another metal wire, aluminum alloy E4043 with a diameter of 1.2mm (E4043), which is often used to take advantage of the element's capability of promoting fluidity in aluminum and is less sensitive to weld cracking and defect. Table (3.2) shows the chemical composition of the E4043 wire used in this study.

Table (3.2): Chemical composition of E4043 wire (wt.%).

Alloy		Al	Si	Fe	Cu	Mn	Mg	Zn	Ti	Be
E4043	Standard	Remain	4.5-6.0	<0.80	<0.30	<0.05	<0.05	<0.10	<0.20	<0.0008
	Tested	94.7	5.04	0.134	0.0301	0.0011	0.0017	0.0010	0.0109	0.00033

3.4 Computer-Aided Design Double Wire Deposition Machine (CADDWDM).

The preparation of samples in the current study was carried out using a new SMD machine, designed, built, and developed for metal deposition processes using the double wire (DW-MIG) arc technique, as shown in Figure (3.4). A computer interface window controls the developed CADDWDM with three-axis positions operated and driven in

three directions by stepper motors. SMDM is utilized with several other parts of the CADDWDM cell to create an integrated work cell to produce the required components. The melting of deposited metal is done using a Lincoln MIG-MAG / FLUX / BRAZING welding machine, as shown in Figure (3.5a).

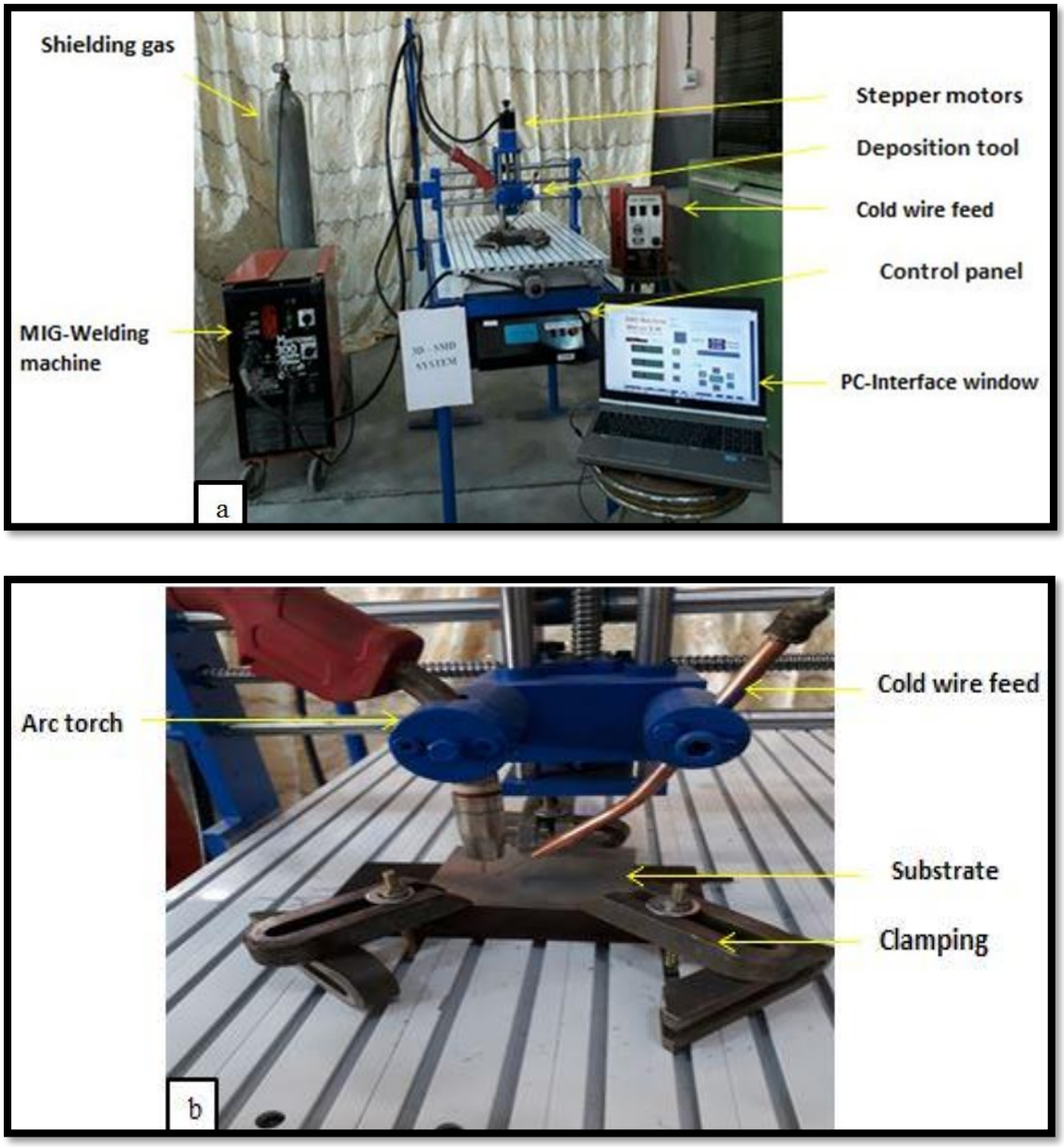

Figure. (3.3) Experimental setup: (a) overall view of the SMD system (b) close-up view of the deposition tool.

An external device provided the cold outer wire to insert the additional deposited wire into the deposition area and use the primary heat source of the electric arc of the MIG welding machine to melt the other cold metal

within the deposition area, as shown in Figure (3.4b). Table (3.3) shows the constant conditions of the machine's setup. The angle of the leading torch (MIG-torch) is 90 degrees, and the arc between the nozzle of the cold wire feed (CWF) and the workpiece material is 30 degrees.

(a) (b)

Figure. (3.4) MIG welding machine (a) Lincoln MIG welding machine; (b) Cold wire feeder machine.

Table (3.3) Nominal pre-set operating conditions used for conventional MIG- SMD.

Length of deposit wall samples	**160 mm**
Polarity	**DCRP**
Arc length (L)	**1mm**
Feeding angle (α)	**30°**
Torch angle	**90°**
Wire stick-out	**15 mm [50,119]**
Layer step height (hs)	**3mm**
Current value	**[160 Amp]**
Gas	**Argon**

3.4.1 Cooling System and Clamping Arrangements

The substrate is firmly installed to overcome the resulting distortion. A water-cooled copper backing plate (Figure 3.5) provided a large heat sink for the substrate plate. The cooling plate helps to improve the heat flow during the deposition process and reduces the waiting time between the subsequent layers.

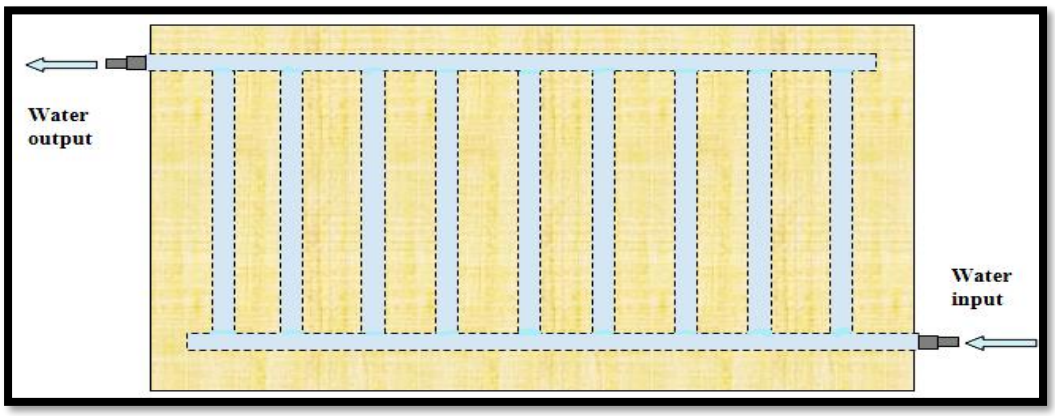

Figure (3.5) Water-cooled copper backing plate.

3.5 Methods

The Preliminary experiments for developing the process model. The CADWDM system can manufacture various fully dense parts using solid wire material layer by layer. However, before the deposition process, it is necessary to adjust the main process parameters carefully, such as arc current (I), arc length (L), travel speed (TS), and wire feed speed ratio (W.R), which represents the ratio of wire feed come from the welding machine (stainless steel 309) to cold wire feed come from an external nozzle device (E4043) .knowing that these parameters must be selected appropriately to stabilize the process. However, other essential conditions also affect the stability of the deposition process, such as the angle of wire feeding (α) and the end of the wire tip in the weld pool. In addition, these parameters controlled the amount of heat input, metal deposition rate, and bead geometry.

Several experiments have been conducted to adjust the operational parameters and other conditions. These preliminary experiments were carried out using filler wires of automatic protection FLUX-CORE-SS309L to identify the main parameters and limits of different shapes and their effects on the deposition process and bead geometry. The experiment method selected a combination of arc current and travel speed, depositing beads with different wire ratio speeds starting from 1 m/min and increasing it by 1 m/min until the deposition process showed an excess of wire. Then, the procedure was repeated for the other arc currents and traverse speed sets.

We chose aluminum as our material of choice due to its inherent ability to resist oxidation and corrosion at high temperatures thanks to a defensive layer called aluminum oxide.

Aluminum was added because aluminum near the surface may react with iron to produce new compounds, one of which is aluminum iron (ferro aluminate), which is resistant to oxidation even when exposed to high temperatures. This was the motivation behind adding aluminum.

There are three Bead-On-Plate experiments setup have been carried out in this study:

3.5.1 Single–Metal (without adding aluminum)

The substrates were prepared and restrained before performing the deposition process and installed on the water-cooled copper backing plate. Before depositing the first layer, the substrate was preheated using an electric arc. The other states were constant: arc length L= 1 mm, $\alpha = 30°$, torch angle 90^{o}, and forward feeding direction.

The filler materials and welding consumables produced single-metal deposits using a wire diameter of 1.2 mm SS309LSi. (Figure 3.6) shows the critical output parameters of the single deposited layer, such as the bead

height (H) and width (W). The width and size of the deposited beads were measured using calipers and a digital Vernier.

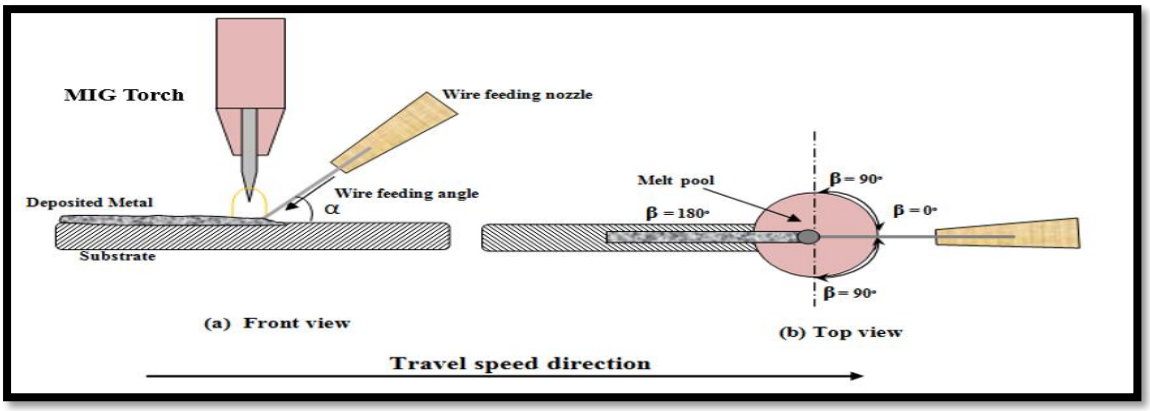

Figure (3.6) Single bead transverse cross-section.

3.5.2 Multi-Metal Deposition (intermittently)

These particular studies made use of SS309LSi FLUX-CORE welding wire that had a diameter of 1.2 millimeters. The process for preparing the substrates was the same as described in section 3.5.1. The length of the continuous welding beads was close to one hundred millimeters, and the diameter of the aluminum alloy (WF2) wire was 1.2 millimeters (E4043). They added aluminum in spurts, with each layer adding aluminum alloy before the feeder was turned off for the subsequent layer.

3.5.3 Multi-Metal Deposition (Al in all layers)

These particular studies made use of SS309LSi FLUX-CORE welding wire that had a diameter of 1.2 millimeters. The wire of aluminum alloy (WF2) measures 1.2 millimeters (E4043). Aluminum is added to all of the layers.

3.6 Effects of Main Process Parameters

The most important parameters used in the SMD process are welding current (I) and travel speed (TS). In this study, An additional parameter was introduced, namely, cold wire feeding (the ratio of wire feed speed of the main wires (W.F1) to the rate of cold wire feed coming from

an external device (W.F 2)) (W.R). To get a stable and reliable deposition process, these parameters should be accurately selected. This study uses the L9 orthogonal array with three welding process parameters. Therefore, only three experiments were required.

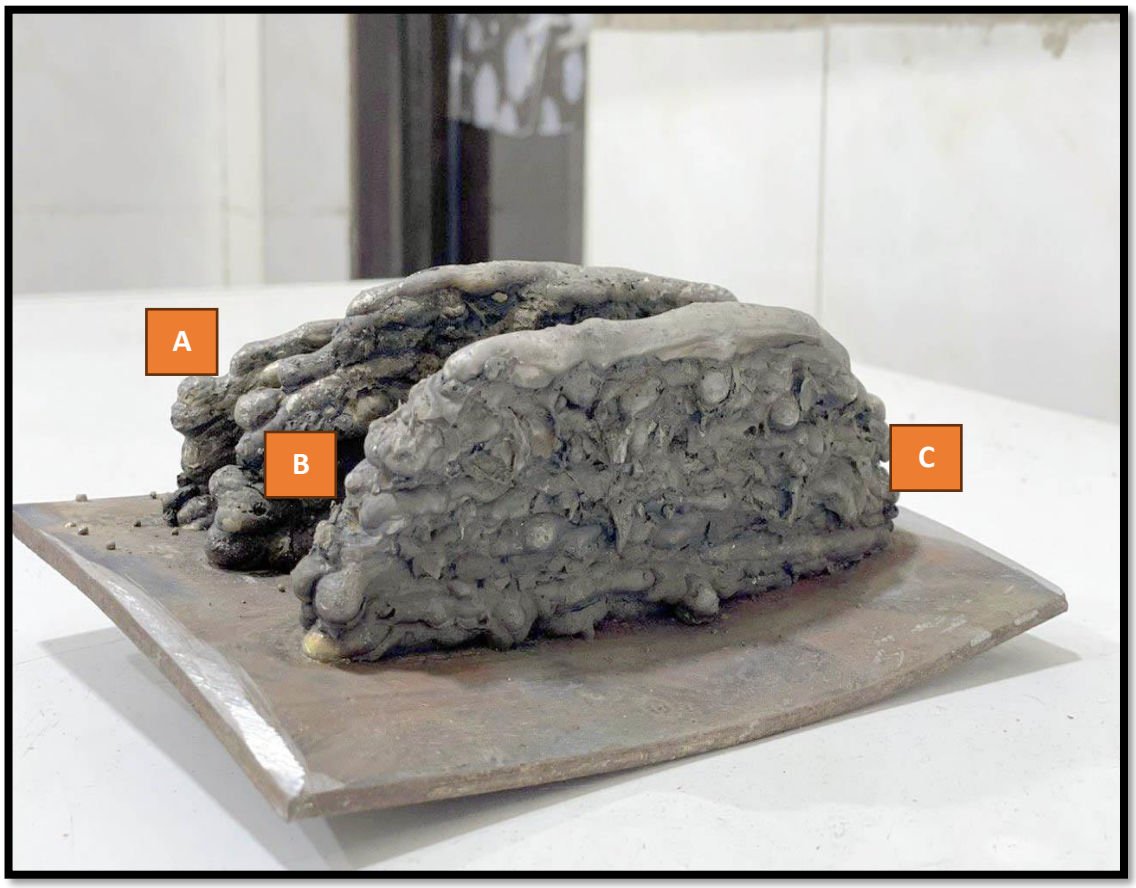

Figure. (3.7) Samples of deposited walls

The following step was of the three walls, A, B, and C, as shown in (Figure 3.7) (A) It represents the first wall, (B) it represents the second wall, and (C) it represents the third wall.

3.7 Preparation of Samples

To prepare the required samples for each experiment, the three walls (with three different compositions) were cut using the Vertical Milling Machine (VMC) shown in Figure (3.8) in the workshops of Al Atba Al Alawya to become three separate walls A, B, C, The work was done on a

Prison CNC machine called GSK a Chinese system GSK 3D Year of manufacture 2022 as shown in Figure (3.9)

Figure (3.8) Vertical Milling Machine (VMC).

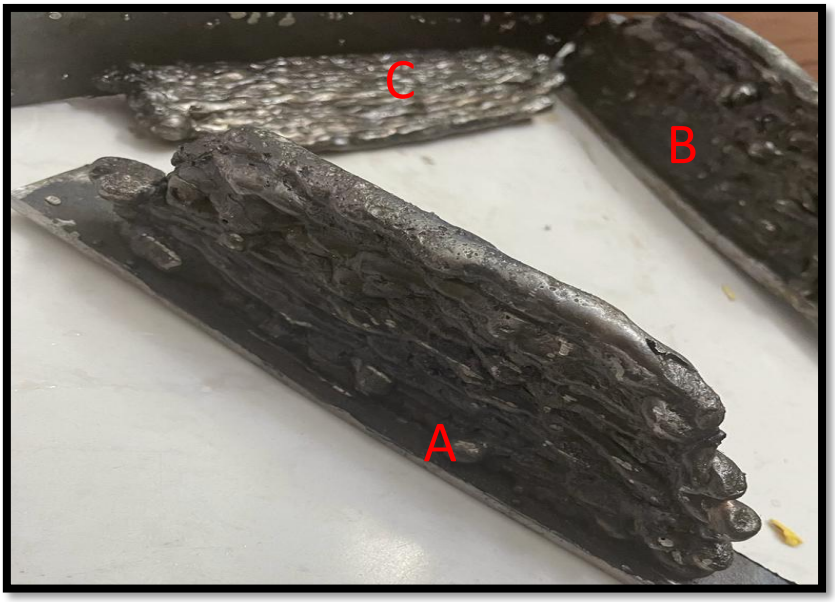

Figure (3.9) A, B, and C samples after separation.

The following step was the grinding of the three walls, A, B, and C, as shown in (Figure 3.9), which were then tested using x-ray radiography inspection to ensure the integrity of the walls.

(Figure3.10) shows a Computer-Aided Design (CAD) model of the WAAM deposit and indications of the reference coordinate system and tensile specimen orientations. The deposition direction is said to be parallel to the X-direction. The height of the wall is referred to as the Y-direction. This depicts the WAAM wall in its as-built state (3.12). After samples are deposited using the WAAM method, they are cut away from the substrate plate using wire EDM to provide specimens for tensile, microstructure, and microhardness tests.

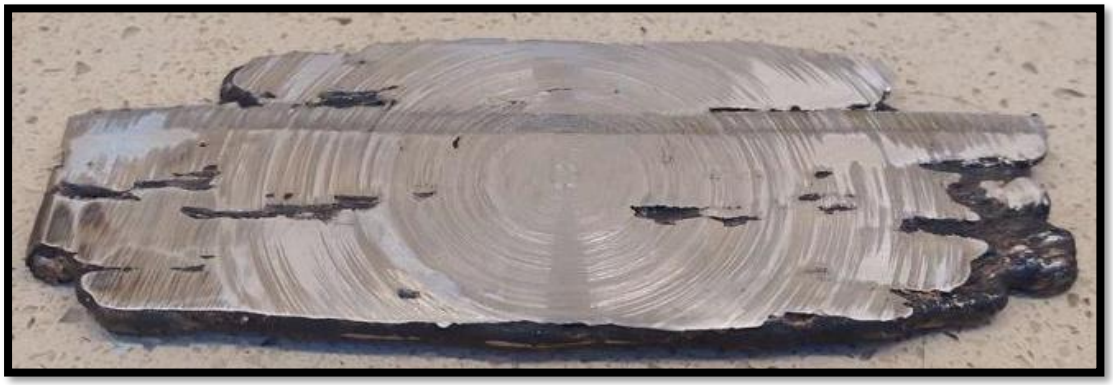

Figure (3.10) Sample side after milling

3.8 Homogenization Heat-treatment

To ensure the uniform distribution of alloying elements throughout the built samples, they were heat treated (homogenized) at 1150 °C for 4 hours. The treatment was carried out in the Metallurgical Eng. Dep. / Faculty of Materials Engineering labs at the University of Babylon using an electric furnace (LHT 02/16 - LHT 08\18), as shown in Figure (3.11).

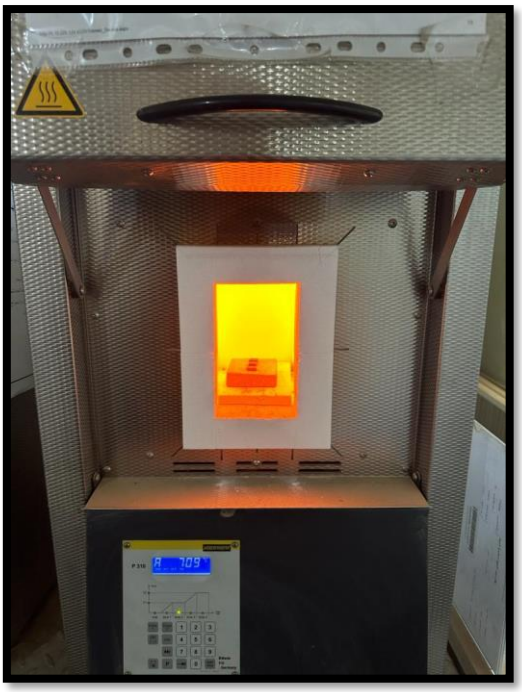

Figure (3.11) The electric furnace used in homogenization heat treatment and oxidation test

3.9 The Examinations

3.9.1 X-ray Radiography Inspection

This X-ray radiography inspection determines the kind, size, and position of internal defects (cracks, porosity, etc.). This test was conducted at the State Company of Heavy Engineering Equipment in Al Doura Baghdad. Before any processing or cutting into specimens, all of the wall samples were inspected. The XXG- 3005 X-ray device, shown in Figure (3.12), with (150 kV) was used for this test.

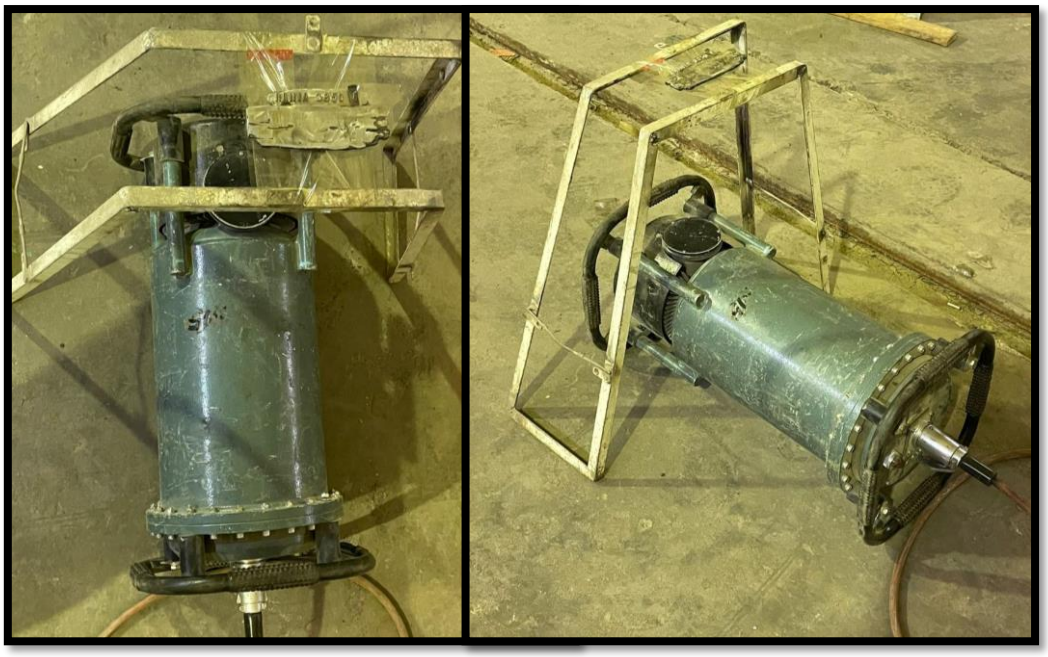

Figure (3.12) X-ray radiography inspection device

3.9.2 Wear Test

To study the tribological behavior of samples, dry sliding wear tests were carried out following ASTM G99-05 using a pin-on-disk wear tester made by the DUCOM instrument shown in Figure (3.14) Two independent variables were used in this investigation; the expected load and sliding distance (rotational speed, radius and time-dependent), to understand the effect of these variables on the responses of the alloys in terms of coefficient of friction and wear rate. In the tests, the radius of rotation was kept constant at 3.0 mm with a total testing time of 15 min. On the other hand, the samples were rotated at three different rates: 100,200 and 300 rpm (i.e., a total sliding distance of 28.27, 56.55, and 84.82 m, respectively), with loadings of 5,10 and 15 N.

$$\frac{\pi D * r\,.p\,.m * t}{1000}$$

$$\frac{6\,\pi * 100 * 15}{1000} = 28.27$$

Figure (3.13) Wear testing machine.

3.9.3 Corrosion Test

The samples were cut into rectangular pieces (10 * 10 mm) with a thickness of (1.5 mm), For the possibility of hanging them, they were pierced with a hole with a diameter of (2 mm) after that; they were washed with distilled water and then ground using grinding papers (180,400,800,1000). The following process was the polishing using a diamond paste. The samples were washed with distilled water and alcohol after each process. Corrosion was tested in a saline solution of sodium chloride with a concentration of 3% (by weight) and an acidic solution of 3% HCl (by volume).

The weight loss per unit area was used as a criterion to monitor and compare the effect of adding aluminum on the corrosion behavior of stainless steel. The samples were weighed before the immersion in the solutions and several times after the immersion. Then, the standard procedure was followed to find the relation between immersion time and the weight loss per unit area for each sample.

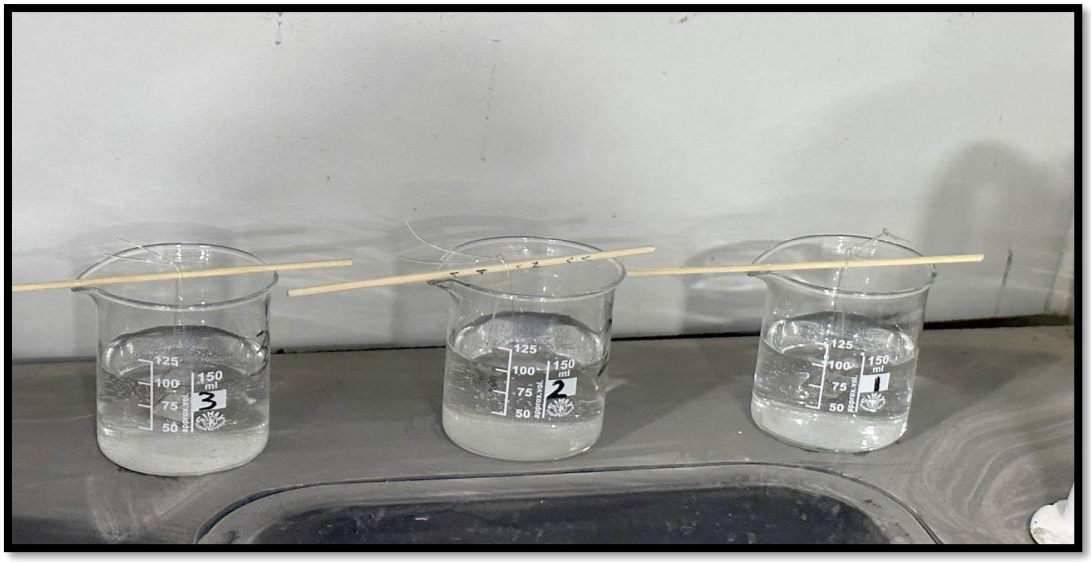

Figure (3.14) Corrosion test in 3 wt. % NaCl solution.

3.9.4 Tafel Extrapolation Method

The device used in this test (Figure 3.16) consists of the measuring cell and its electrodes. The enclosure is made of a non-corrosive material such as glass. The capacity of the cell is one liter. The cell includes three electrodes: the working electrode, the sample used, and the auxiliary electrode, which is made of platinum. The voltage of the working electrode is inserted into a third electrode, the reference electrode, which is made of saturated calomel. It is placed in a salt bridge containing the same electrolyte solution used in the cell, and the electrical circuit is connected to conduct the test.

The cell is filled with the test solution, and the auxiliary electrode and the reference electrode are placed in the cell solution. The working electrode is prepared with alcohol and placed in the measurement cell. In this system, a power supply of the type (PRT) is used, which also supplies a continuous current in the range of 0-500 mA. Use a digital voltmeter to measure the voltage difference between the working electrode and the reference electrode, and to measure the current passing between the working electrode and the auxiliary electrode, use a milliamp, where the

voltage difference is changed at a rate of (10 mV/min) and measure the value of the passing current corresponding to each value of the applied voltage and in the range (±250 mV) approximately at the point of open circuit potential.

The inhibition efficiency was calculated using the following equation:

$$IE\% = \frac{Ic(un) - Ic(in)}{Ic(un)} * 100\%$$

Where $I_{c(un)}$, $I_{c(in)}$: Corrosion current density in the presence and absence of the inhibitor, respectively.

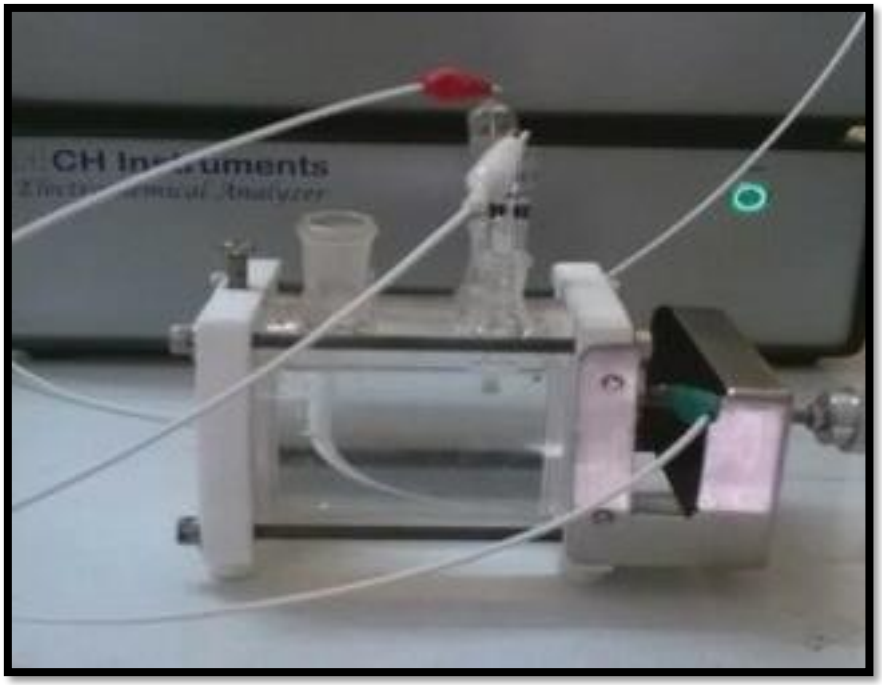

Figure (3.15) Tafel extrapolation test setup

3.9.5 Microstructure Examination

3.9.5.1 Electro-Chemical Etching

To prepare the samples for the microstructure examinations an electrochemical etching procedure was used. The electrolytes used consisted of acetic acid, perchloride acid, and ethanol. as seen in Figure (3.17). A distance of four centimeters separates the cathode and anode, and a potential difference of 5V was maintained for one minute.

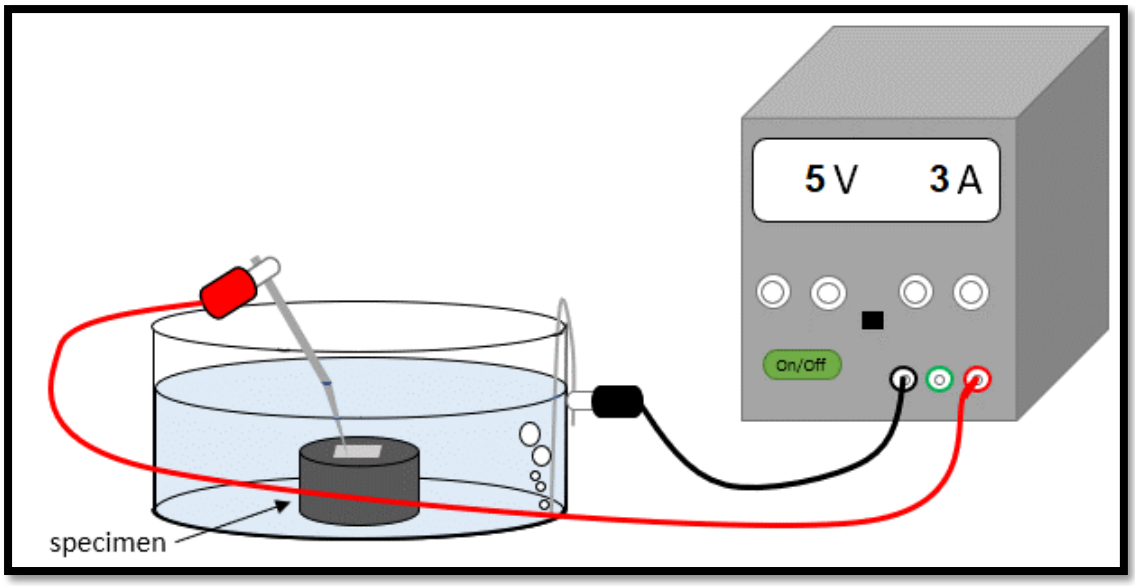

Figure (3.16): Electrochemical etching setup

3.9.5.2 Optical Microscopy (OM)

The specimens were prepared for microstructure investigation using conventional metallographic methods. First, the samples were polished for 20 minutes using a diamond paste of 1 μ m grit after being processed using SiC grinding sheets (180- 3000 grit). Then, the samples were subjected to the electrochemical etching procedure mentioned in section **3.9.5.1**. This inspection was conducted at the University of Babylon's Laboratory of the Metallurgical Engineering Department of the Faculty of Materials Engineering.

3.9.5.3 Scanning Electron Microscope (SEM)

The scanning electron microscope (SEM) and energy dispersive spectrometer detector (EDS) were conducted at the College of Pharmacy / University of Babylon and the laboratories of the Ceramic and Building Materials Dep. of the Faculty of Materials Engineering. Figure (3.18) shows one of the SEM devices used in this study. The same procedure used to prepare OM specimens was also used to prepare the samples for SEM.

3.9.6 The Mechanical Test

3.9.6.1 Hardness Test

A digital Vickers microhardness tester was used to conduct a microhardness test (HVS-1000). This test with a 500 g load and a 10-second dwell time. The vertical sections of all three specimens were ground and polished before the measurements. With several readings for each of the three regions (top, middle, and bottom) and (0.5 mm) between each adjacent lesson, the three areas were examined as lines of tested points. The Metallurgical Engineering Department, Faculty of Materials Engineering, and the University of Babylon laboratories were used for this test.

3.9.6.2 Tensile Test

1-Preparation of Tensile Test Specimens

According to the BS EN ISO 6892-1:2009 standard [80], the tensile specimens were prepared with a dog-bone shape. They have a gauge length of 38.3 mm and a cross-sectional area of (10 * 2.5) mm. Figure (3.19) shows the dimensions of the prepared specimens. Wire EDM was used to prepare each model. These specimens were taken from parallel and perpendicular directions to the deposition direction. Three specimens were extracted for each wall in each order using the arrangement previously demonstrated in Figure (3.20).

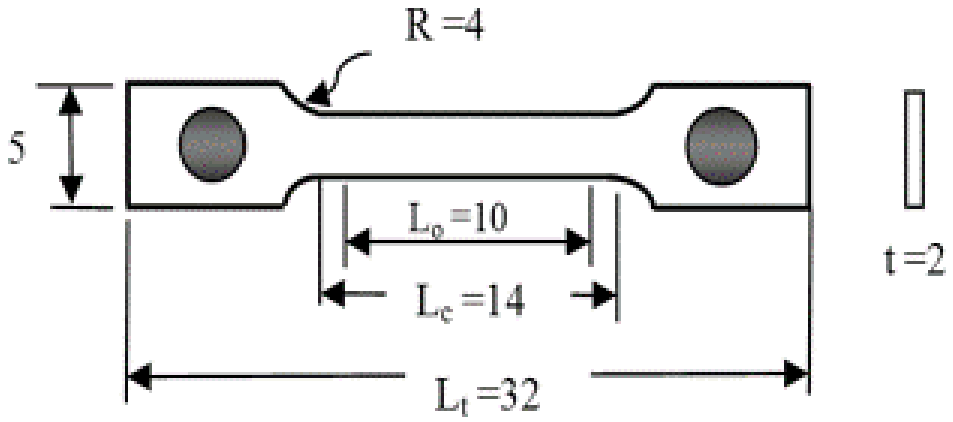

Figure (3.17): Tensile test specimens' dimensions

Figure (3.18): Tensile test specimens' dimensions

The tensile tests were done for all six specimens via a universal testing machine with a cross-head speed of 1 mm/min and carried out according to (ASTM A370-03a). Figure (3.21) shows the universal testing machine with a unique setup used due to the small size of the specimens.

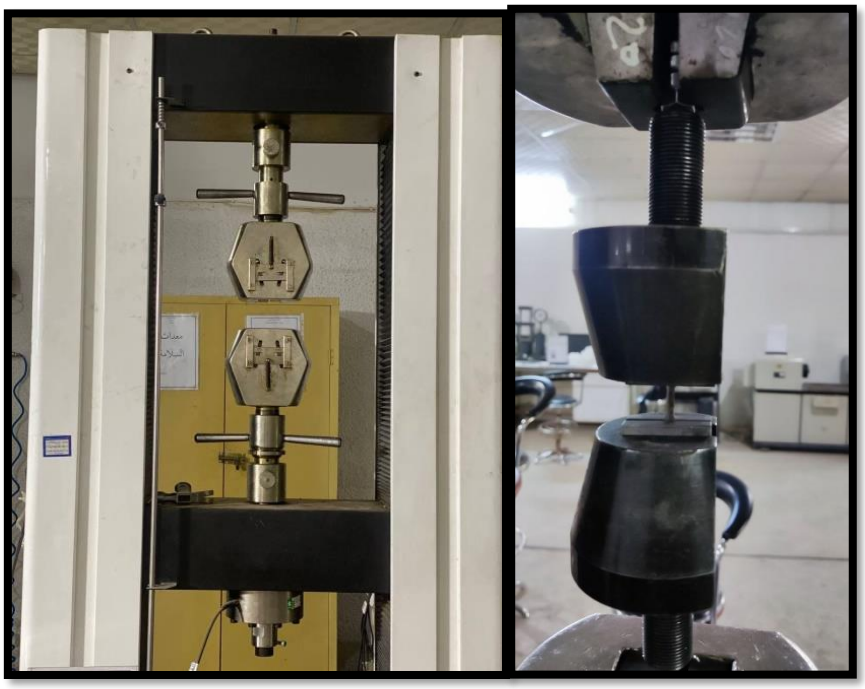

Figure (3.19): The universal testing machine

CHAPTER FOUR

RESULTS & DISCUSSION

CHAPTER FOUR

Results and Discussions

4.1 Introduction

Additive manufacturing, also known as 3D printing, is a rapidly developing technology that has the potential to revolutionize the manufacturing industry. by allowing the creation of complex metal parts with geometries that would be diffident to produce using traditional manufacturing methods. The findings of the experimental work of this research are shown and explained in this chapter, along with a discussion of them.

4.2 X-ray Inspection

X-ray inspection of metallic parts is one of the important techniques used in a variety of laboratory and industrial applications to detect flaws and ensure quality. This type of imaging is non-destructive, which means that it does not damage the part being inspected such as ultrasonic testing. To find internal flaws between and through the layers of the walls, an X-ray examination was done on the three walls right after the samples were built. As shown in Figure (4.1), the tests of all three walls' ((1, 2, 3) are the names of the fortifications) revealed no interior flaws, crakes, or impurities. This truth is demonstrated by the seven bright lines in each sample. However, some dark regions can be seen in these images but they do not represent internal inclusions or defects because they could be seen on the sides of the specimens by visual inspection. On the other hand, these surface inclusions could be removed by grinding the surfaces to prepare the specimens for later tests. The Quality Control Division of the Heavy Equipment Company provided a certificate demonstrating that these examples are free of any flaws.

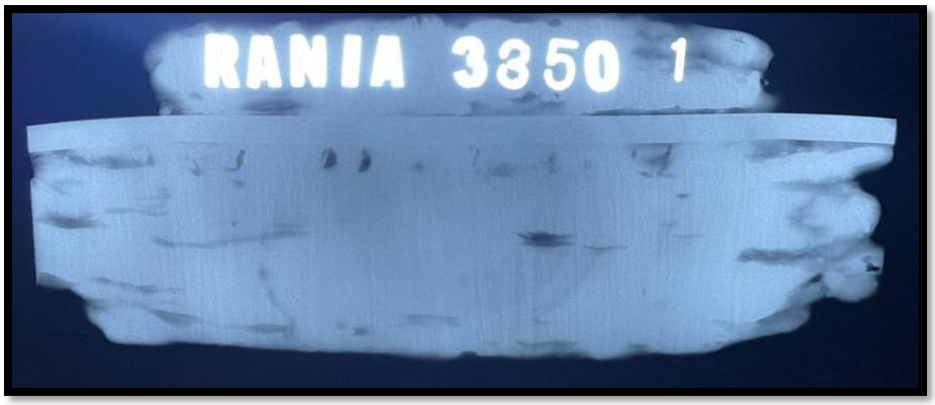

A :The first wall is 309L without addition

B: The second wall is 309 L, with a percentage of aluminum added 2.5

C:The third wall is 309 L, adding 5 % aluminum

Figure (4.1)(A-B-C) Stainless Steel (309) samples inspected by X-ray radiography.

4.3 Microstructure of Additively Manufactured SS309 (Without and With the Addition of Aluminum)

There are several challenges associated with AM of metals and alloys, one of which is that the microstructure of additively manufactured parts can be different from conventionally produced parts, and this can affect their properties.

When WAAM prepared SS 309, the microstructure typically consists of elongated grains in the building direction, as shown in Figure (4.2). This means that the grains in the metal part are oriented along the direction in which the part was built, rather than being randomly oriented as in conventionally produced parts. These elongated grains are formed due to the solidification process that takes place during the steps of AM. At the of these steps, a layer of material is deposited on a metallic build substrate. This process is repeated until the whole part is built. The deposition of each layer produces a temperature gradient in the part, with the hottest top surface (in the liquid state or just solidified) and the coolest bottom surface. This temperature gradient results in the growing of the grains in the part in the direction of heat flow, which is perpendicular to the building substrate

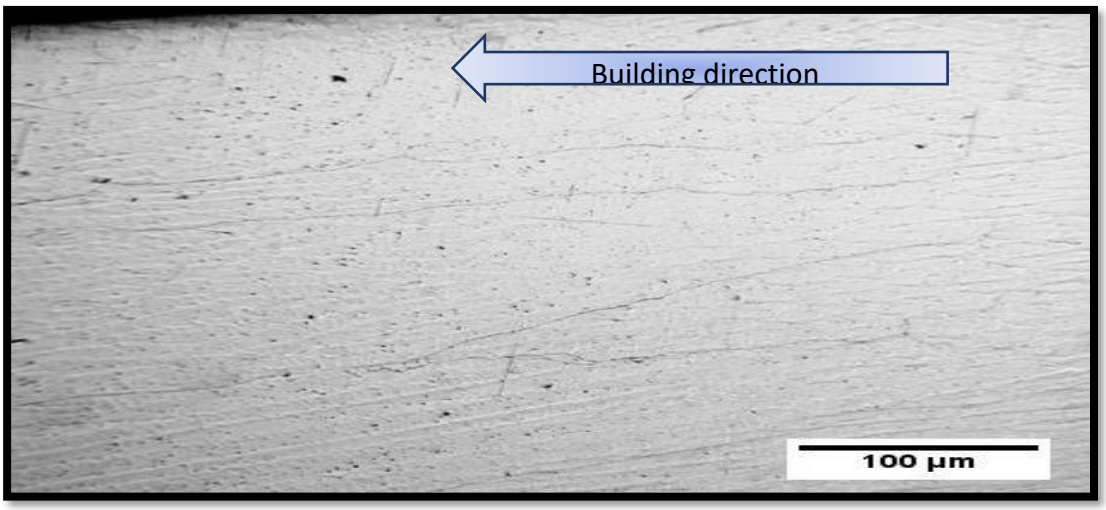

Figure (4.2): OM image for the microstructure of the SS 309 prepared by WAAM without adding aluminum (without heat treatment).

In general, the microstructure of WAAM-produced SS 309 is influenced by the cooling rate during solidification, which affects the formation of various microstructural features such as dendrites and grain boundaries. Without the addition of aluminum, the microstructure is not significantly altered, although the material exhibits some degree of porosity due to the nature of the WAAM process.

More details in the microstructure could be seen when using SEM for the same sample of SS 309 (as shown in Figure 4.3). The microstructure of WAAM-produced SS 309 shows some dendritic structure. These dendrites are formed during solidification and can be observed as elongated structures extending along the building direction.

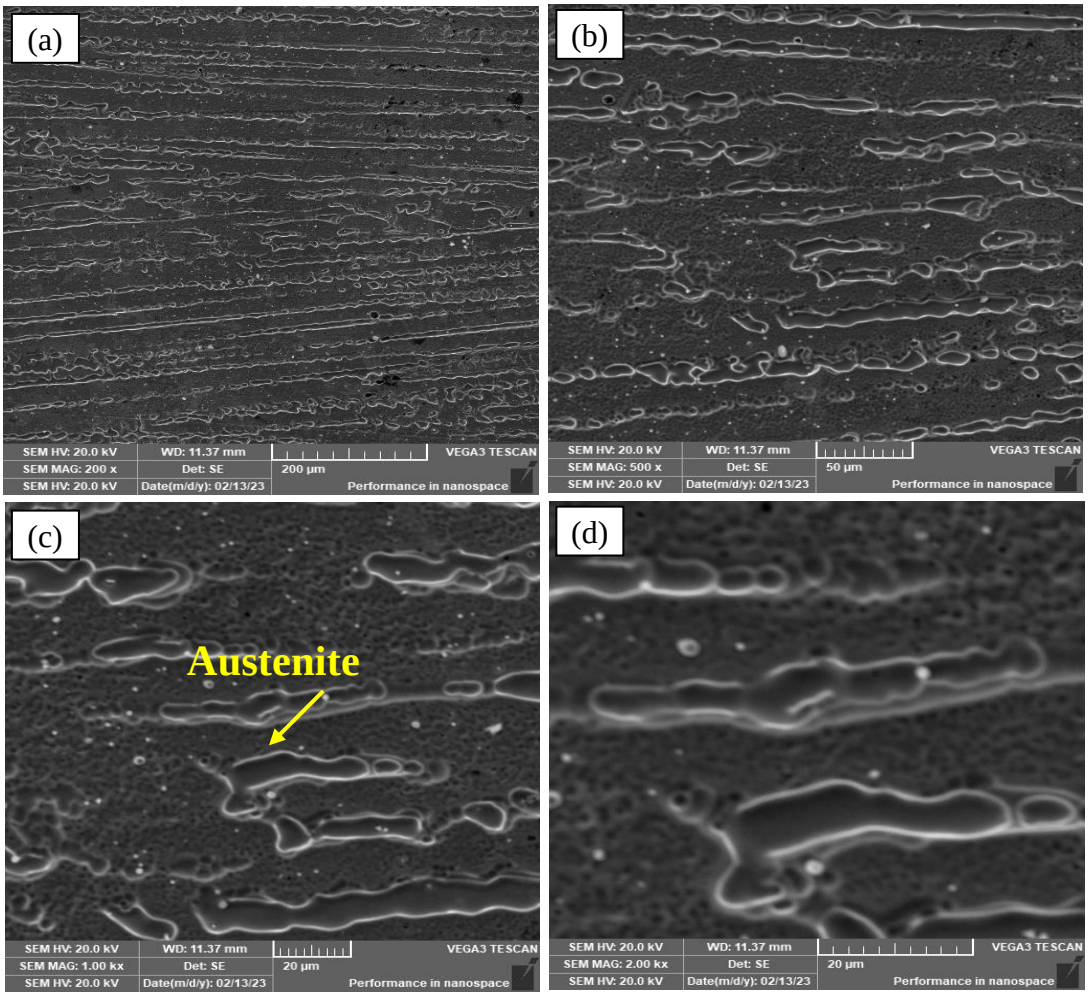

Figure (4.3): SEM with different magnifications for the microstructure of the SS 309 prepared by WAAM (without any heat treatment).

At higher magnifications (500x), as Show(4.5.b) the microstructure of WAAM-produced SS 309 shows more details of the dendritic structure and the grain boundaries. The dendrites comprise a primary phase rich in chromium and nickel and a secondary phase enriched in manganese, silicon, and carbon. The secondary phase is typically present as small precipitates within the dendrites and at the grain boundaries,[81] as shown in Figure 4.3. At even higher magnifications (1kx to 2kx), as Show(4.5.d) the microstructure of WAAM-produced SS 309 shows further details of the second-phase precipitates, which appear as small, discrete particles within the dendrites and at the grain boundaries.

According to [82], the solidification of some stainless steels (for example AISI 304, 304L, and 308L) produced by different AM processes (such as EBAM-fabricated specimens), starts by the formation of austenitic dendrites from the melt at the early stages (primarily austenitic structure) followed by the formation of ferrite in the interdimeric areas between austenite. Different morphology could be detected for the ferrite colonies including point-like, cellular, vermiculate, or lathy. A microstructure with two phases ($\gamma+\delta$) is predictable in AISI 304/308 steels produced using AM taking into consideration the Creq/Nieq ratio. Nevertheless, AM process parameters (such as heat input value) could affect the morphology of the phases and their ratio. [82].

A dramatic change in the microstructure could be seen when SS 309 is prepared by Wire Arc Additive Manufacturing (WAAM) with the addition of 2.5 wt., % Al. The resulting microstructure shows a mixture of austenitic and ferritic phases [83]. The addition of aluminum can promote ferrite formation in the microstructure, as shown in Figure 4.4. This Figure shows two distinct regions. The first one (light region) consists of large grains which are generally austinite surrounded by some particles around the grain boundary (4.5). This region represents the layer where no aluminum

was added. On the other hand, the second region (the darker region) consists of very fine grains with two phases (austinite and ferrite).

More detailed microstructure images can be seen in Figure 4.5. The SEM image shows an overview of the microstructure of the first region (light region), revealing the presence of large grains (austenite) surrounded by intermittent lamella of another phase. The second phase is supposed to be ferrite. The presence of ferrite at this region may be attributed to the diffusion of some aluminum during the AM process from the region with aluminum addition to the region without addition. However, the amount of diffused aluminum could not alter all the microstructure in this region. The addition of 2.5 wt. % Al promotes the formation of ferrite, leading to a more heterogeneous microstructure compared to SS 309 without any Al addition.

The nature and distribution of these phases will depend on the specific composition of the material and the processing conditions used during WAAM as shown in (Figure 4.4)

Overall, SEM imaging can provide valuable information about the microstructure of SS 309 prepared by WAAM with the addition of 2.5 wt. % Al without any heat treatment, which can help to understand its mechanical properties and performance.

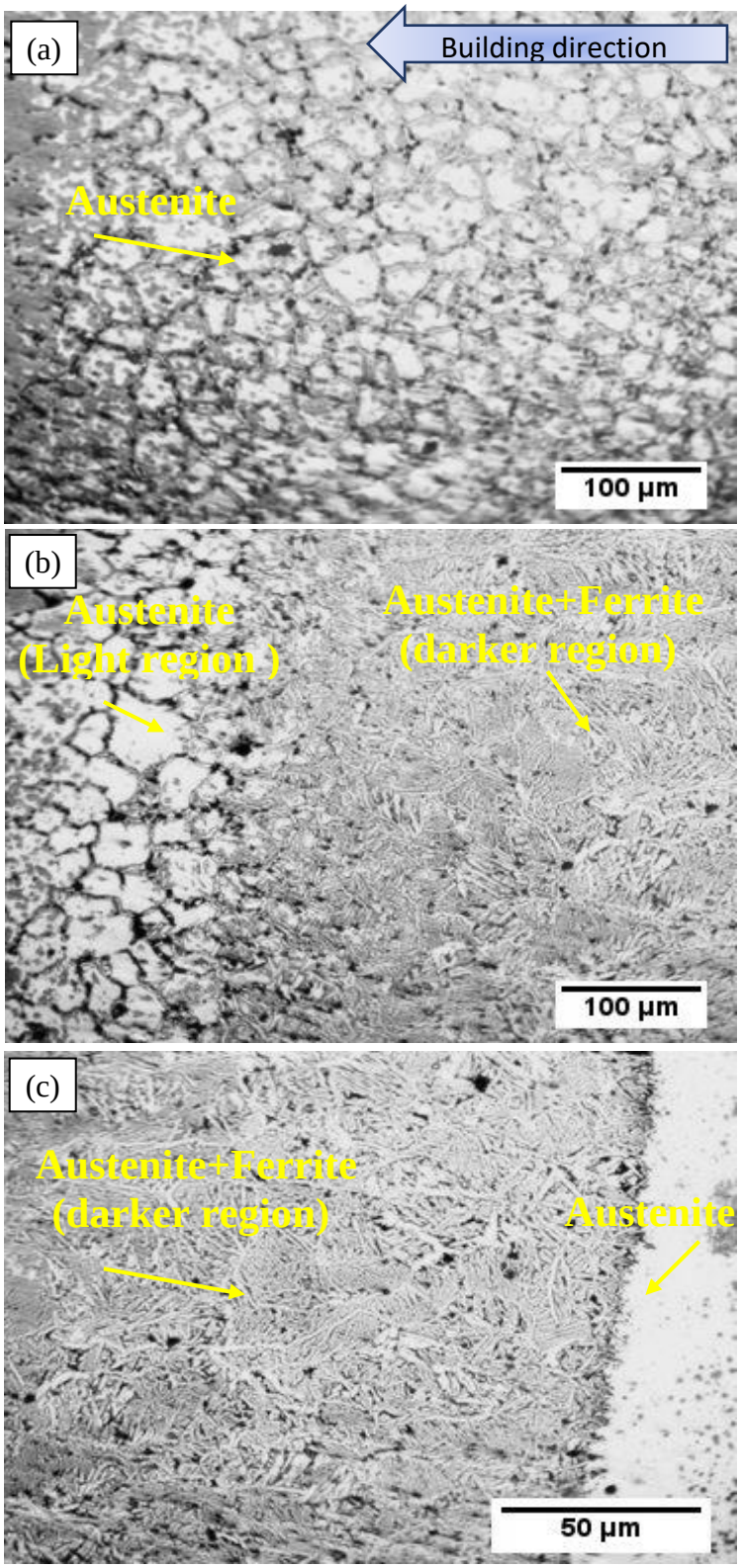

Figure (4.4): OM image for the microstructure of the SS 309 prepared by WAAM with the addition of 2.5 wt. % Al as a percent of the overall weight of SS 309. (without any heat treatment).

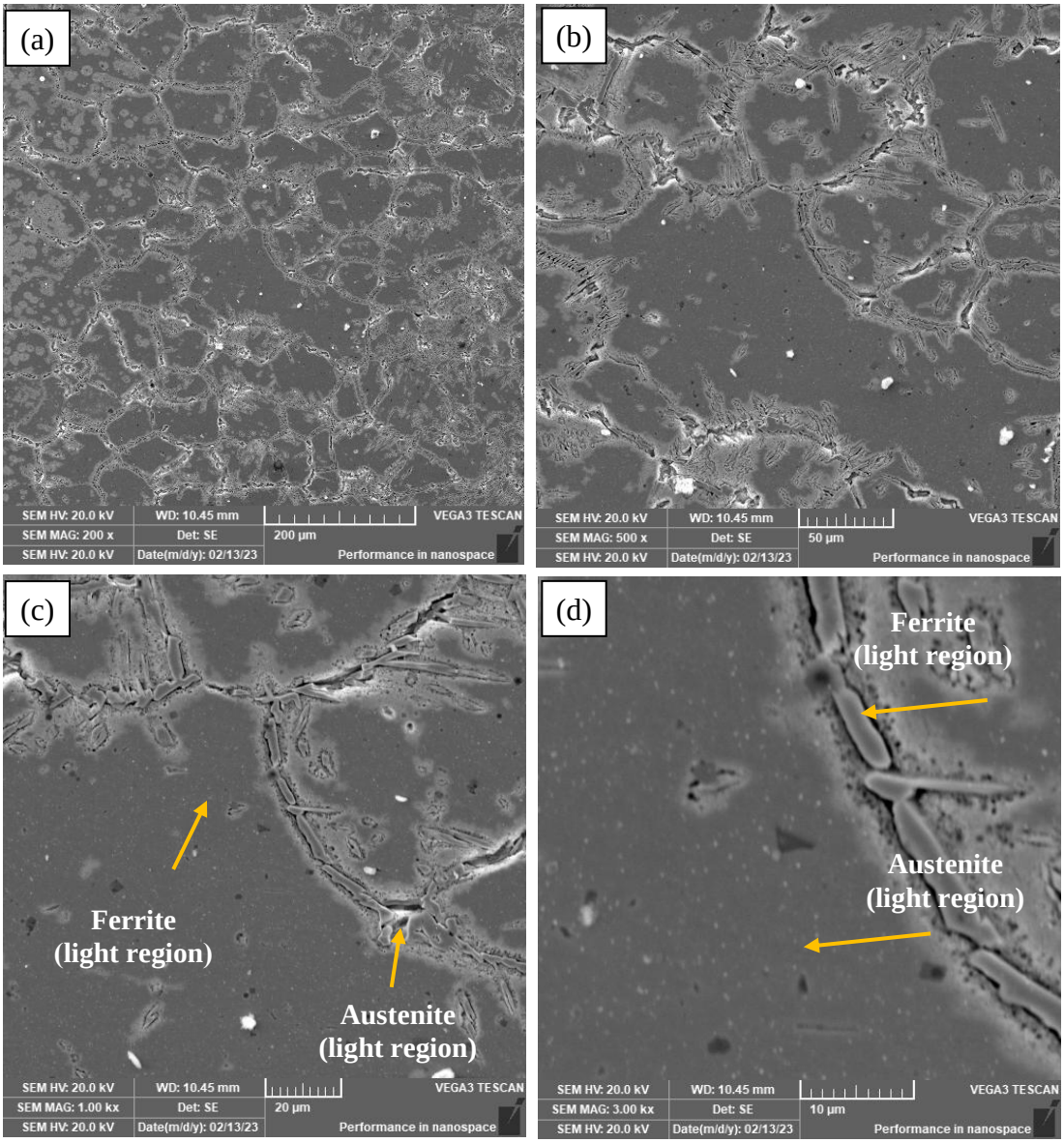

Figure (4.5): SEM with different magnifications for the microstructure of the SS 309 prepared by WAAM with the addition of 2.5 wt. % Al as a per cent of the overall weight of SS 309. (without any heat treatment).

The addition of 5 wt. % Al (adding aluminum to all layers) can significantly affect the microstructure of SS 309, promoting the formation of ferrite. The resulting microstructure is more heterogeneous and complex than that of SS 309 without any al addition as shown in (Figure 4.6).

In OM images, the microstructure shows more refining effect when adding 5 % Al compared to the same material with 2.5 % Al addition (as shown in Figure 4.6).

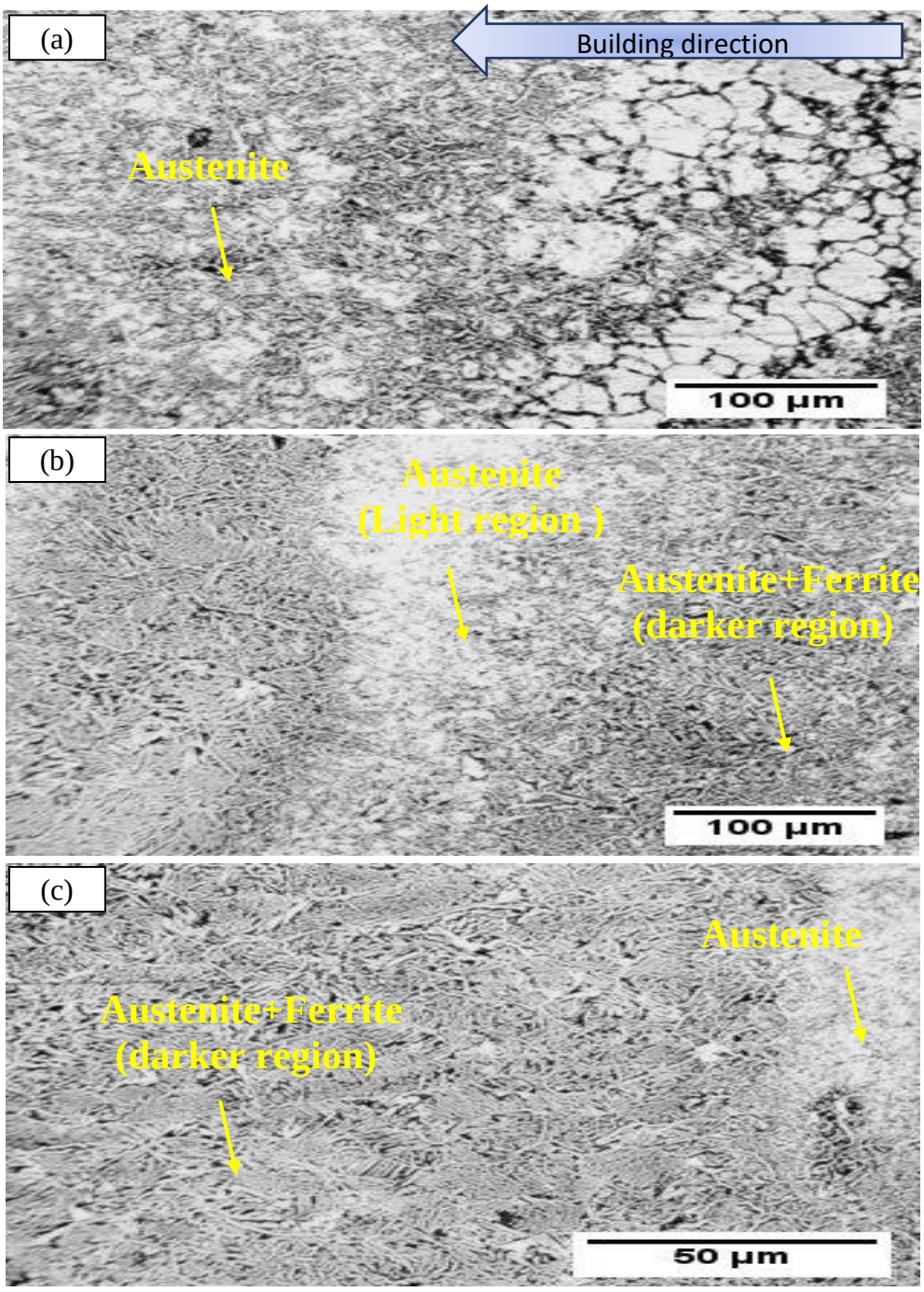

Figure (4.6): OM image for the microstructure of the SS 309 prepared by WAAM with the addition of 5 wt. % Al as a per cent of the overall weight of SS 309. (without any heat treatment).

The refining effect resulted from the addition of aluminum, which shifted the structure of the SS alloy from a single austenitic phase to a austenite + ferrite austenitic-ferritic alloy, which can be seen by comparing the SEM images with the same magnification in as Show in Figures (4.7 and 4.8). However, some large austinite grains still appear in some regions in the form of separated islands. This means that the content of aluminum in these regions is low.

In general, the microstructure of this alloy is likely to be more complex and heterogeneous and finer compared to SS 309 without any Al addition due to the change of the alloy from a single-phase alloy (austenitic stainless steel) to double phase alloy (austenite + ferrite SS) associated with the presence of Al.

Overall, SEM imaging can provide valuable information about the microstructure of SS 309 prepared by WAAM with the addition of 5 wt. % Al without any heat treatment, which can help to understand its mechanical properties and performance. However, additional analytical techniques are needed to fully characterize the microstructure and identify the presence of specific phases and intermetallic compounds.

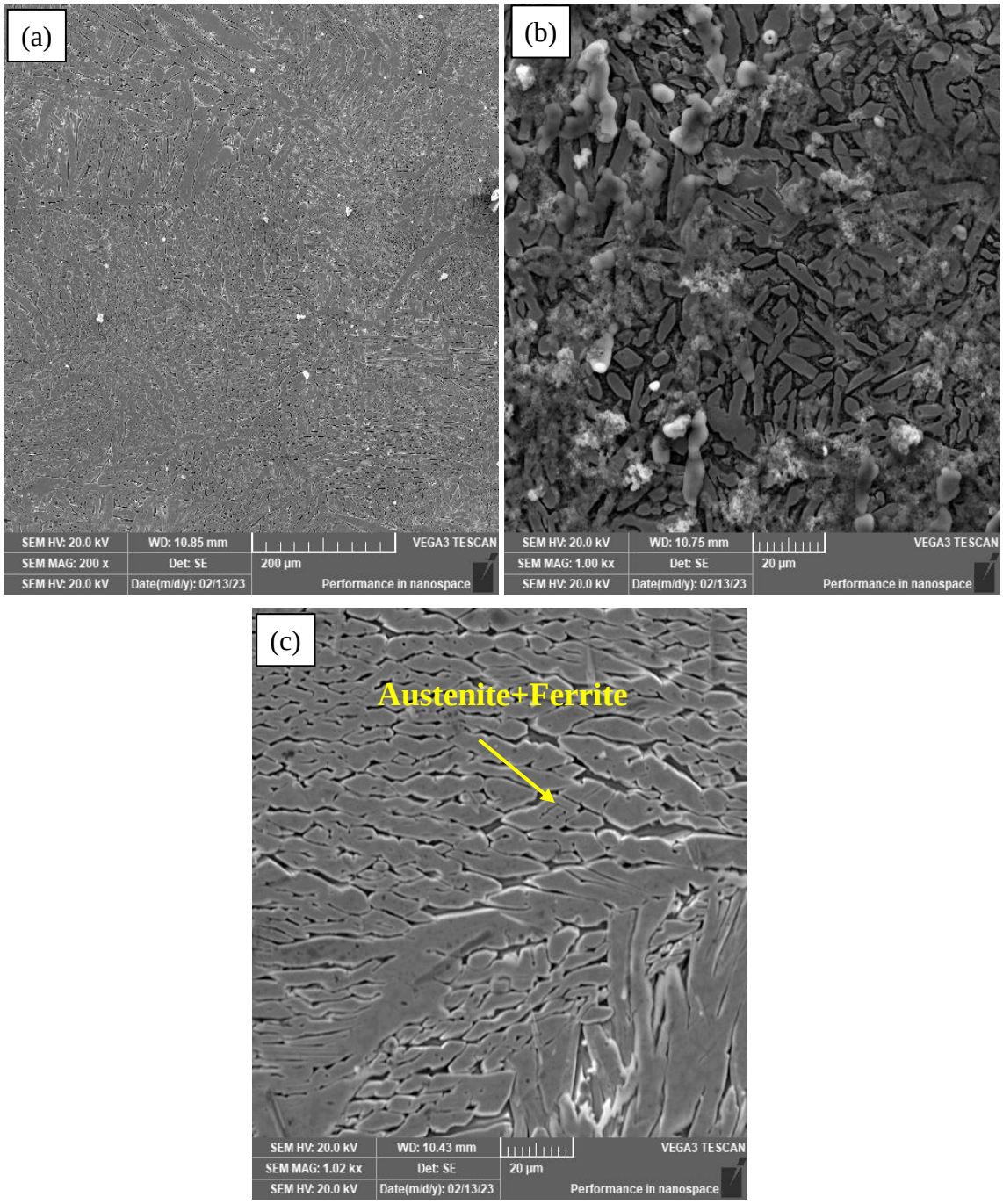

Figure(4.7): SEM with different magnifications for the microstructure of the SS 309 prepared by WAAM with the addition of 5 wt. % Al as a per cent of the overall weight of SS 309. (Without any heat treatment).

After heat treatment of SS 309 prepared by WAAM specimens at 1150 °C for 4 hours followed by water quenching, they showed clear changes. (Figure 4.8) shows an optical microscope image of SS 309 prepared by

WAAM, the microstructure appears homogenous with fine grain size and consists of two distinct regions. A clear phase with a nearly net shape elongated in the building direction can be seen. These dark regions in the structure may be attributed to the presence of the ferrite phase. Whereas, a brighter region (matrix) is mostly expected to be of austenite. Grain boundaries also are visible, appearing as thin lines separating the different grains. These structures could not be seen in the OM image of the specimens before heat treatment (as shown in Figure 4.8). However, this structure seems to be slightly similar to that seen in SEM images in (Figure 4.9) with clear links between the grains of the second phase (dark phase) (as shown in Figure 4.9). The microstructure present in such alloy depends on the specific heat treatment conditions used and other factors such as the cooling rate during heat treatment, the initial grain size and distribution, and any residual stresses in the material.

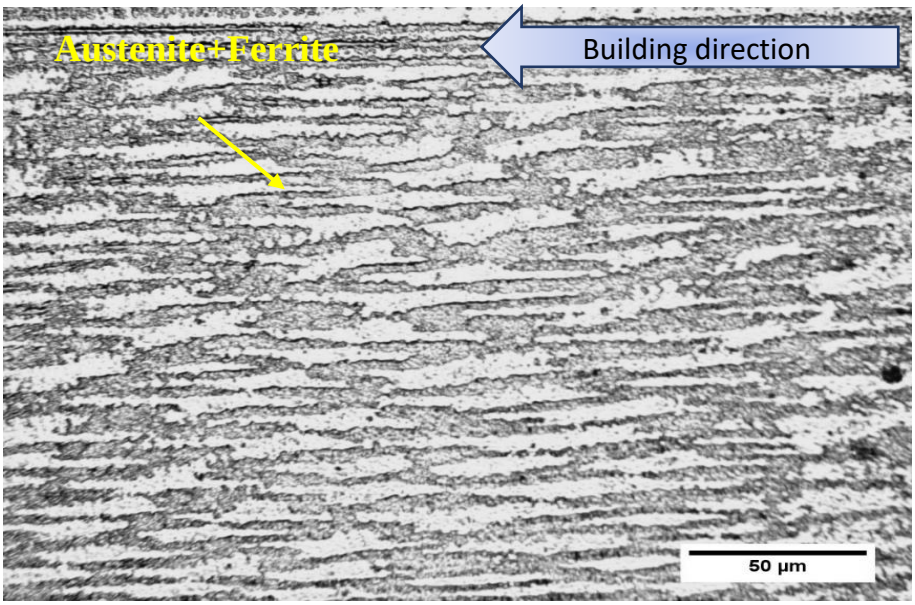

Figure (4.8): OM image for the microstructure of the SS 309 prepared by WAAM without the addition of aluminum (heat treated).

The higher magnification for the sample in (as shown in Figure 4.9) using SEM revealed different microstructures. The morphology of the grains of the secondary phase present in (as shown in Figure 4.9), seems to be uncourteous islands instead of a net-shaped structure. The grains appear as distinct regions of different brightness or contrast elongated in the building direction.

Overall, SEM can provide valuable information about the microstructure of SS 309 prepared by WAAM without adding aluminum. Most of the grain's stile have directional structure (depending on the process procedure or in other words the building direction) even after the heat treatment of the specimens. This conclusion allows for a better understanding of the material properties and potential applications of this process.

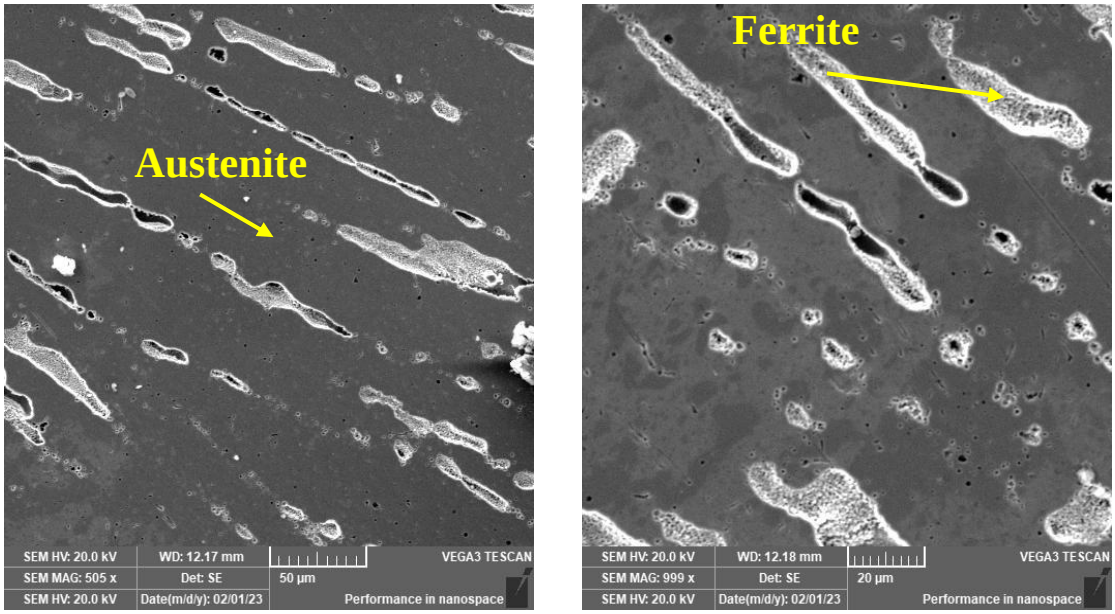

Figure (4.9): SEM with different magnifications for the microstructure of the SS 309 prepared by WAAM without the addition of aluminum (heat treated).

The OM image of the microstructure of SS 309 with 2.5 wt. % Al after heat treatment shows a typical austenite + ferrite structure consisting of austenitic and ferritic phases. Adding Al can promote the formation of

second phases which can influence the microstructure and properties of the alloy as shown in Figure (4.10).

The effect of heat treatment can be seen on the microstructure when comparing as shown in Figure (4.10) with Figure 4.4c. The size of the single bright region (the austenite) was reduced dramatically offset by an increase in the two phases region. This change in the microstructure may be attributed to the diffusion of aluminum from the high aluminum concentration layers (two-phase layers) to the layers without aluminum (single-phase layer). The interesting thing about the Figure is that the penetration of the second phase to the single-phase region extended in the grain boundaries which are the preferred path for the diffusion of aluminum atoms.[6]

The overall morphology of the microstructure, with the austenitic and ferritic phases appearing as distinct regions with different shades or colors. The grain size and shape of the double-phase region remain without visible changes compared to that of the same alloy before heat treatment. The SEM image (as shown in Figure 4.11) shows the overall morphology of the microstructure, with the austenitic and ferritic phases. In this region, a fine-grain structure can be seen. These grains have complex branched shapes completely different to that seen in the equiaxed austinite grains of the original material (without the addition of aluminum).

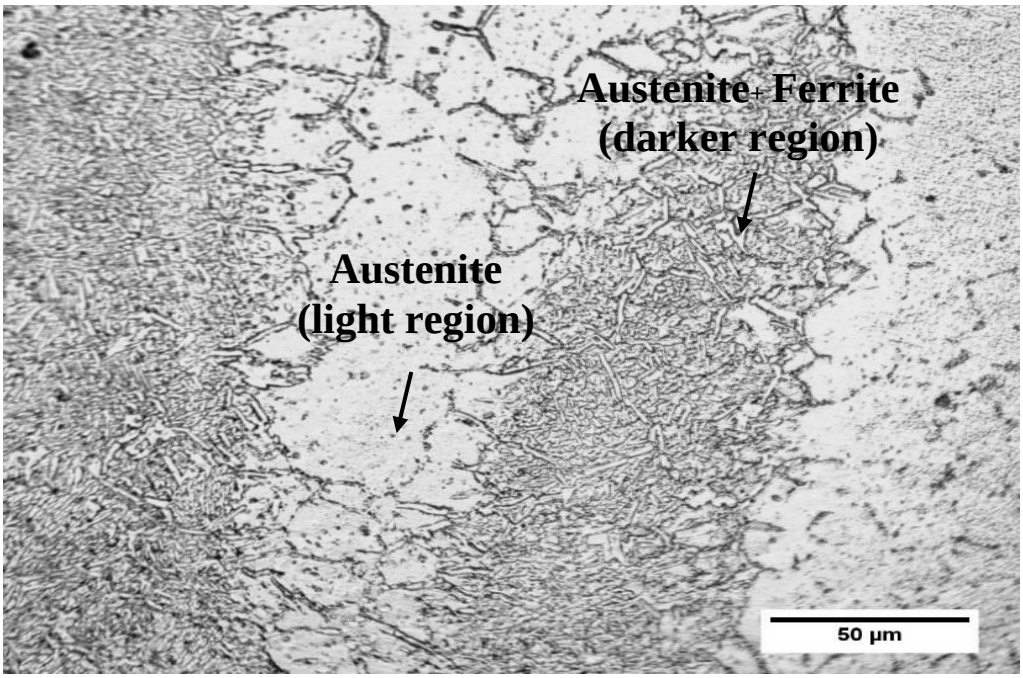

Figure (4.10): OM image for the microstructure of the SS 309 prepared by WAAM with the addition of 2.5 wt. % Al as a per cent of the overall weight of SS 309. (heat treated).

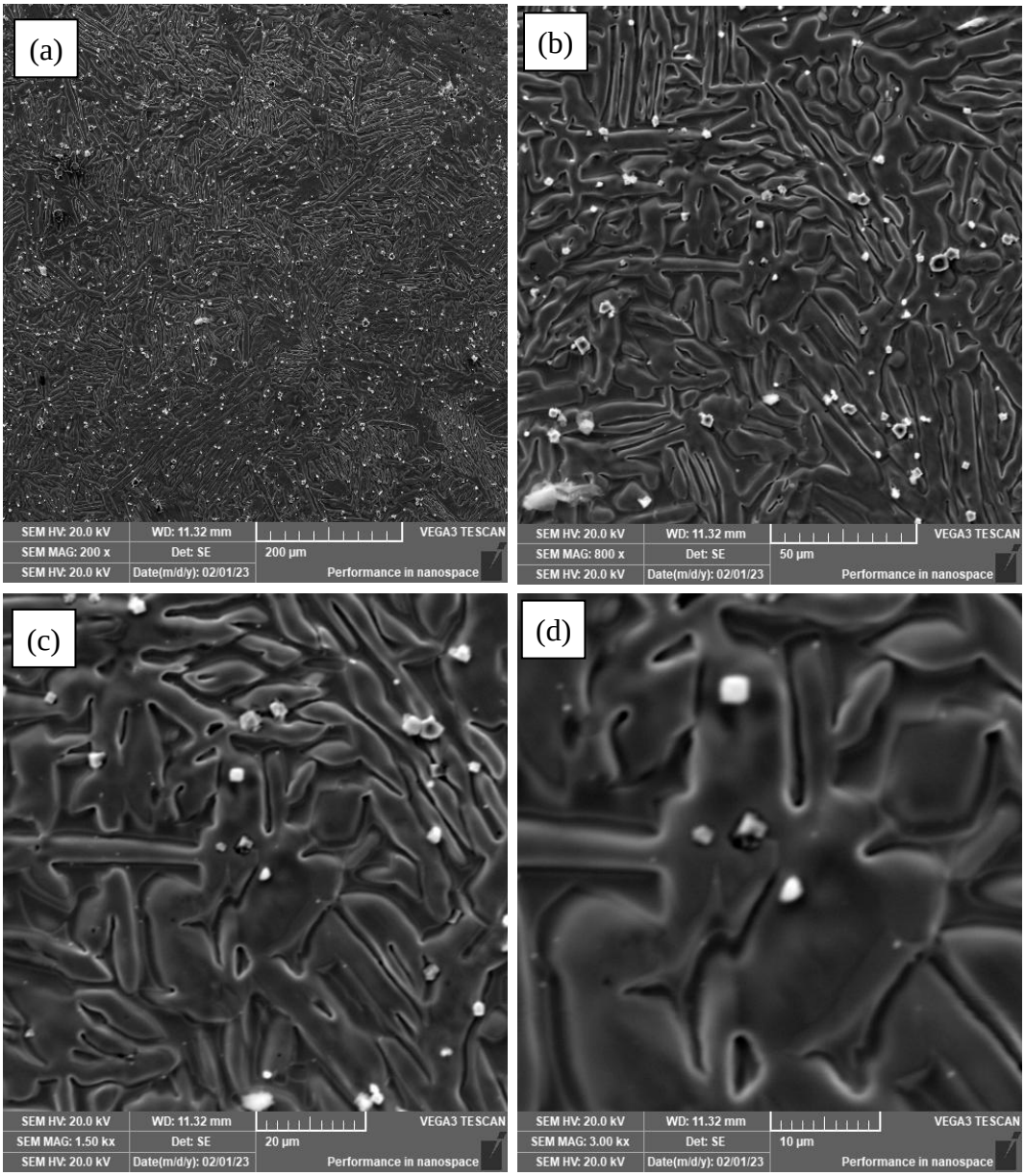

Figure (4.11): SEM with different magnifications for the microstructure of the SS 309 prepared by WAAM with the addition of 2.5 wt. % Al as a per cent of the overall weight of SS 309. (heat treated).

With further increase in the addition of aluminum to 5 wt. % Al and heat treatment, the microstructure of SS 309 became significantly different from the alloy without any aluminum addition. After heat treatment, the microstructure tends to show a more homogeneous distribution of these phases throughout the material. The microstructure is to consist of a fine-

grained matrix with a uniformly dispersed second phase resulting in a structure similar to the eutectic structure as shown in Figure 4.12. However, the general view of the distribution of the different phases provided by the SEM image (as shown in Figure 4.13) shows details for the microstructure similar to that seen in Figure 4.11 with grains having different sizes and morphologies.

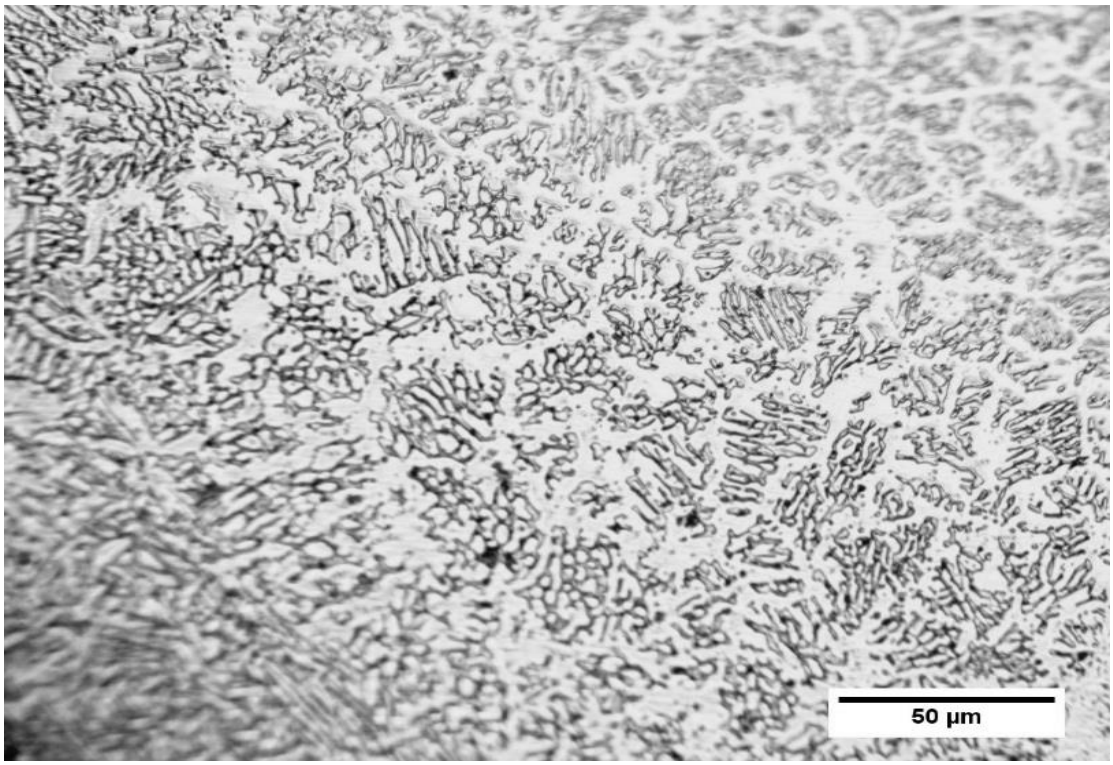

Figure (4.12): OM image for the microstructure of the SS 309 prepared by WAAM with the addition of 5 wt. % Al as a per cent of the overall weight of SS 309. (heat treated).

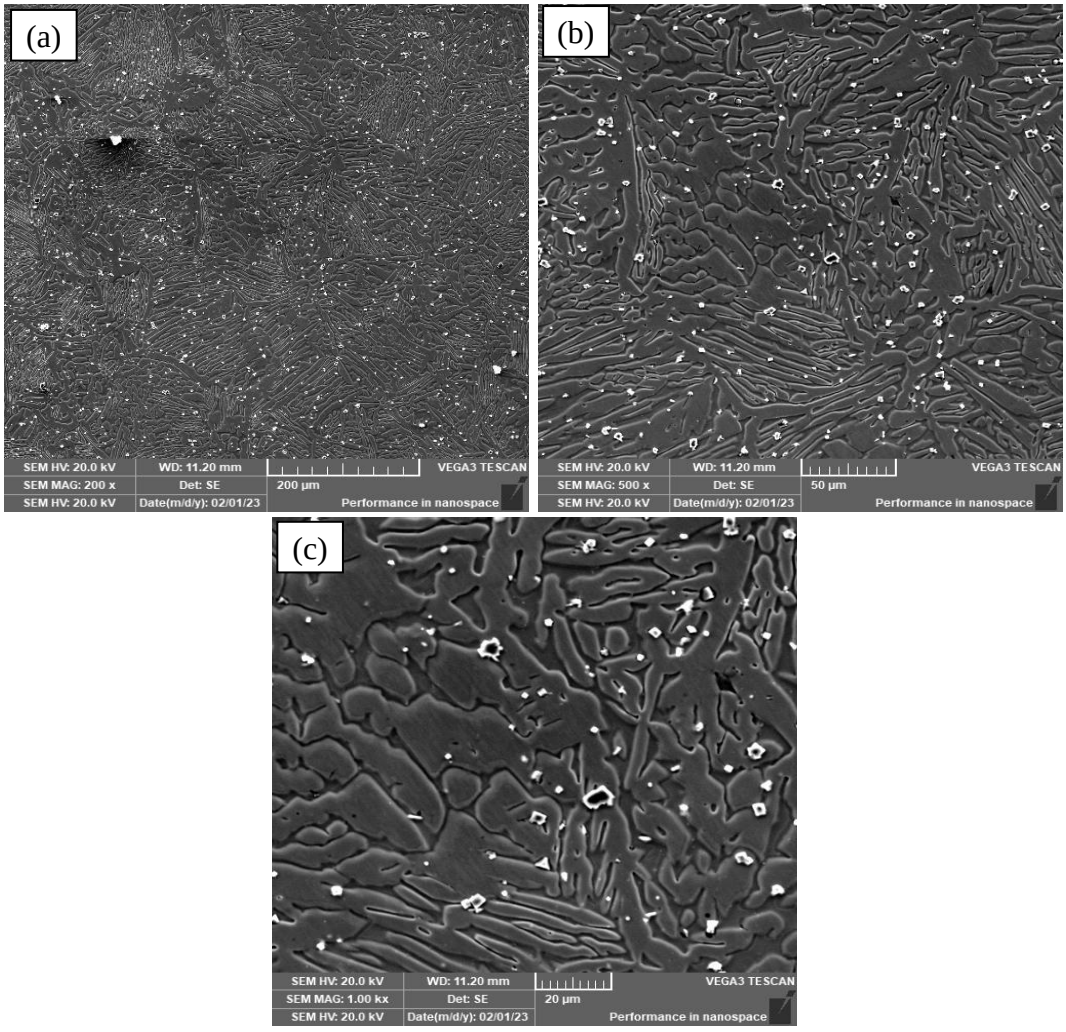

Figure (4.13): SEM with different magnifications for the microstructure of the SS 309 prepared by WAAM with the addition of 5 wt. % Al as a per cent of the overall weight of SS 309. (heat treated).

4.4 Hardness Test

The microhardness measurements were made along the vertical section for all the deposited walls to demonstrate the variations in the hardness values across the entire sample. The average of at least three measurements obtained in the same area was the basis for all hardness values.

In the as-deposited wall without Al, the microhardness measurement finds location-dependent reading variations. (Figure 4.14) At the zero line (the

interface between the substrate and the built-up walls), the hardness increased rapidly due to the transfer from the material of the substrate (carbon steel) to the wall's material (stainless steel). The hardness on both sides of the interface shows a clear change in its level. It is increased in the side of the carbon steel and decreased in the side of stainless steel due to the inter-diffusion of carbon and other alloying elements which changes the chemical composition in these regions and as a result the structure and local properties. However, because the change in hardness level extended only one millimeter or less through the wall material, therefore, this region is not very important in terms of the overall microstructure and mechanical properties of the walls especially when considering that this region will be removed during the finishing of any component. After the base region, the hardness continued at almost the same level and shows very slight fluctuations. This stability in hardness level may be attributed to the little variation in the microstructures.

Adding Al to the wall material greatly influenced the hardness values. However, the hardness homogeneity was significantly affected by the addition of Al (layer by layer). The hardness shows a very high level in the layers with Al addition and lower hardness in the layers without additions. This fluctuation can be seen in the samples with overall additions of 2.5 % Al. The main reason behind the increase in hardness is the shifting of the microstructure of the regions with aluminum additions to a microstructure consisting of two very fine phases (see section 4.3). Due to transfer from carbon steel substrate to stainless steel wall, hardness rose fast. Both sides of the interaction have changed hardness. It is higher in carbon steel and lower in stainless steel due to the inter-diffusion of carbon and other alloying elements, which modifies the chemical composition and structure and local characteristics.

On the other hand, the specimens with full aluminum additions of 5 % Al (in all layers) show much less fluctuation in hardness level due to the change of the microstructure of the alloy to almost completely two fine grains phases in all regions.

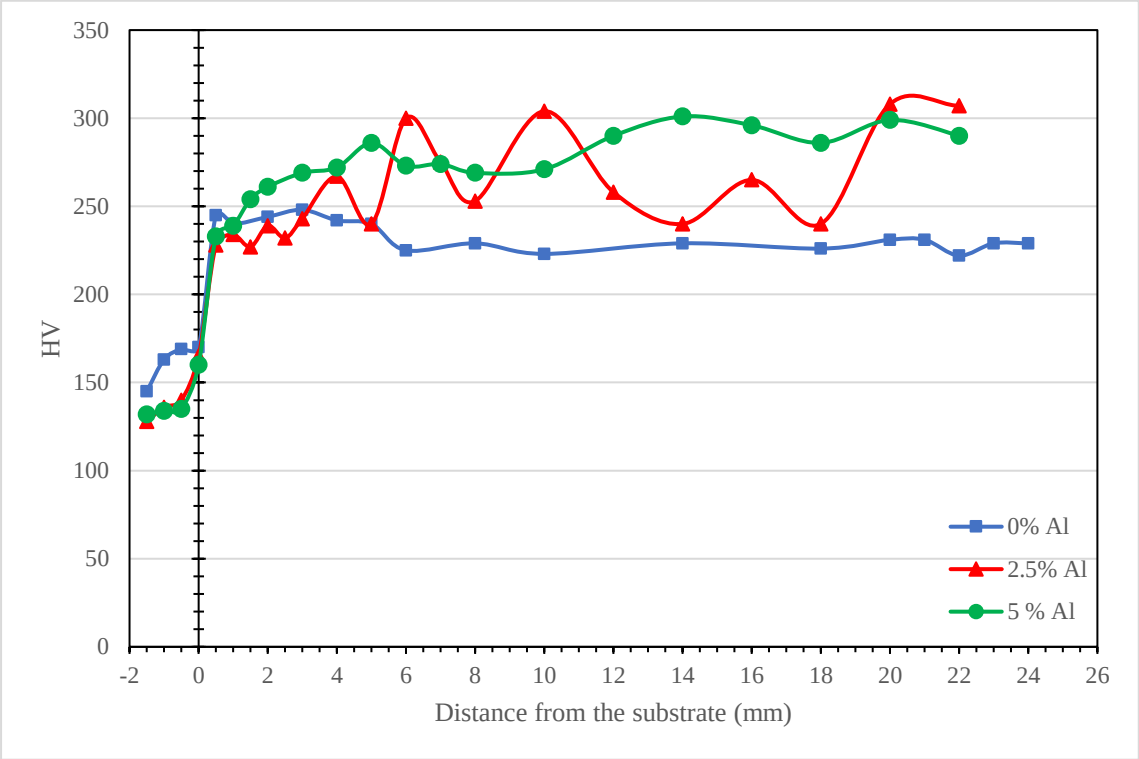

Figure (4.14) Microhardness distribution along the vertical section of the deposited walls before Heat-Treatment.

It could be possible to bring the amount of hardness variation down to a more manageable level by subjecting all of the samples to heat treatment. This heat treatment nearly homogenized the microstructure, which led to the formation of more uniform characteristics as compared to the structure that existed before the treatment was applied. The hardness profile of the longitudinal section of the three walls, with varying amounts of aluminum added (0, 2.5, and 5%) may be seen in (as shown in Figure 4.15) As can be seen by comparing this to (Figure 4.15), there has been a significant alteration to the levels and contour of the curve. However, the behavior of the wall was where the most noticeable difference could be detected with

the addition of 2.5% aluminum. Following the application of heat treatment, virtually all of the oscillations in the level of hardness that can be seen in Figure 4.20 were eliminated. The heat treatment brought about this alteration in the alloy's microstructure, which brought about the modification we see here. Where the microstructure started to become more uniform is where the majority of the material is (see Figures 4.14 and 4.15).

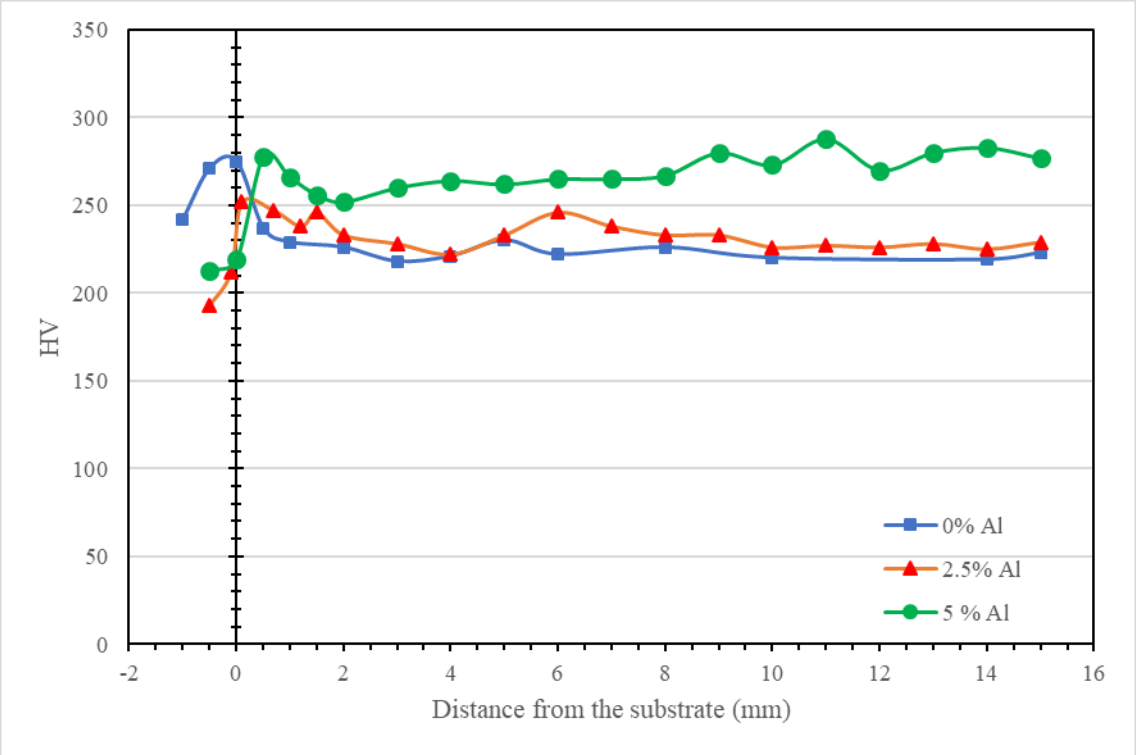

Figure (4.14) Microhardness distribution along the vertical section of the deposited walls after Heat-Treatment.

Another interesting change that can be noticed after heat treatment is the hardness level at and near the interface between the substrate (carbon steel) and the built walls. For example, in the sample of SS without the addition of aluminum, the hardness increased at this region from almost 170 HV to about 270 HV. This change can be attributed to the interdiffusion of carbon, chromium and other alloying elements at the high temperature of the heat treatment which promoted the production of carbides and other

hardening compounds. However, this region extends almost one millimeter through the wall material and does not affect the properties (the hardness) far away from the interface.

4.5Tensile Strength

The addition of aluminum to stainless steel 309 could modify the tensile behavior of the material. However, the specific effects on the tensile curve depend on various factors such as the percentage of aluminum added and the resulting microstructure of the material. In general, the addition of aluminum enhanced the strength of stainless steel due to the change in the microstructure of the resulting alloy (see section 4.3). The change of the microstructure of the alloy from austenitic (with some ferrite) to austenite + ferrite due to the addition of aluminum which also refined the grain structure led to improving the tensile strength and reducing the ductility (as shown in Figure 4.15).

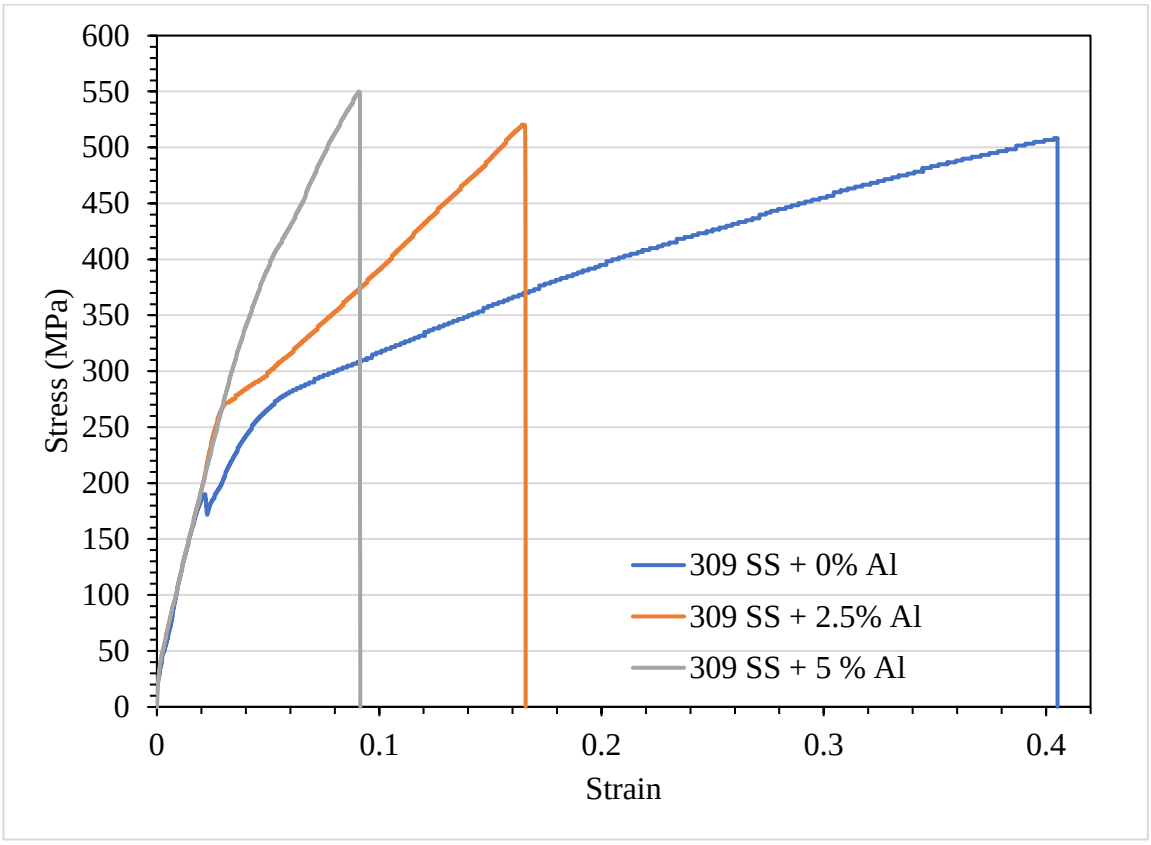

Figure (4.15) Stress-strain curves of horizontal samples with and without the addition of aluminum.

The stress-strain behaviors of vertical specimens of SS309 with and without aluminum (Al) addition (as shown in Figure 4.16) are also different due to the changes in the microstructure of the alloy. Overall, adding Al to SS309 increased the yield strength and ultimate tensile strength but also decreased its ductility. Therefore, the stress-strain curve of the vertical sample of SS309 with Al addition shows a higher yield point and more significant strain hardening than the vertical sample of SS309 without Al addition and this effect increases with increasing the Al additions from 2.5 % to 5 %. Generally, by comparing (as shown in Figures 4.16 and 4.17) the ultimate tensile strength shows much higher levels in the vertical specimens compared to the horizontal specimens. This can be attributed to the directional nature of the microstructure of the built material (see section 4.3).

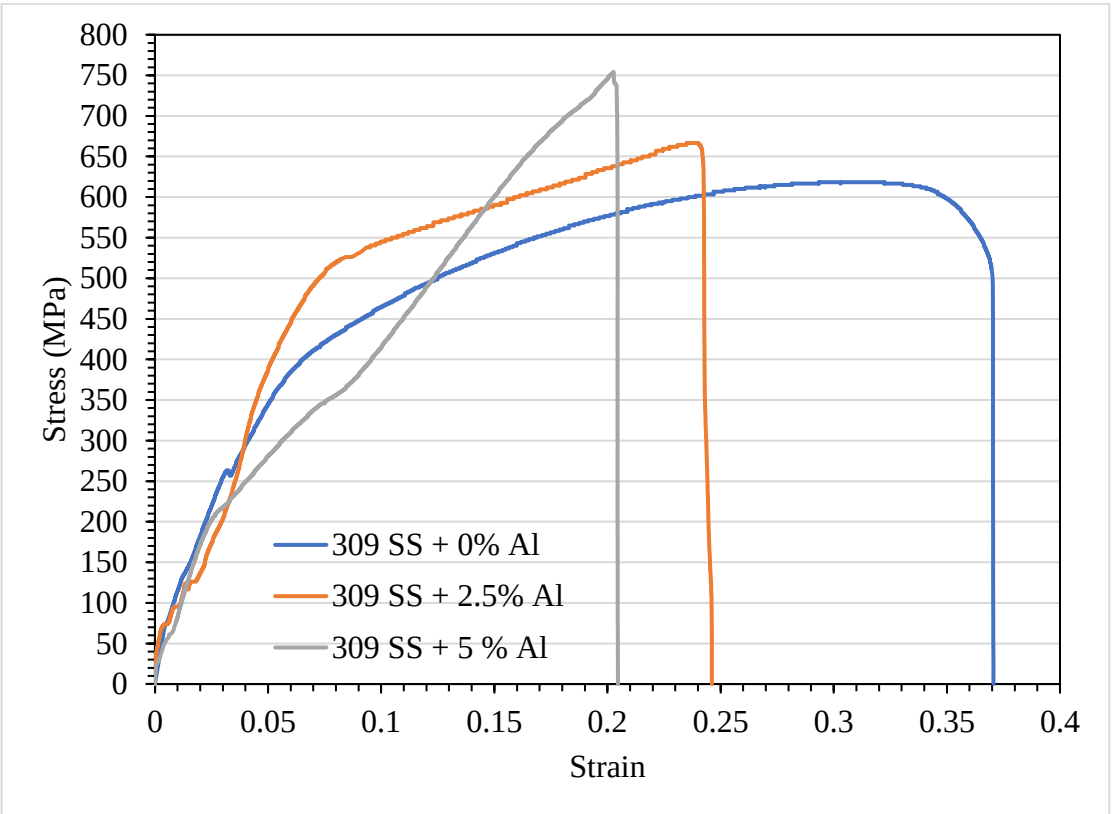

Figure (4.16) Stress-strain curves of vertical samples with and without the addition of aluminum .

The combined effect of aluminum addition with the direction of specimens on the ultimate tensile strength of the alloys is as shown in Figure (4.17). The tensile strength in both directions increased with increasing the aluminum additions. However, a clear difference can be seen between the two curves of the horizontal and vertical specimens due to the reasons mentioned above.

It is worth noting that tensile strength is just one of several mechanical properties that can be affected by adding Al to SS309. Other properties, such as yield strength, ductility, and fracture toughness, can also be influenced by changes in the microstructure and mechanical behavior of the alloy.

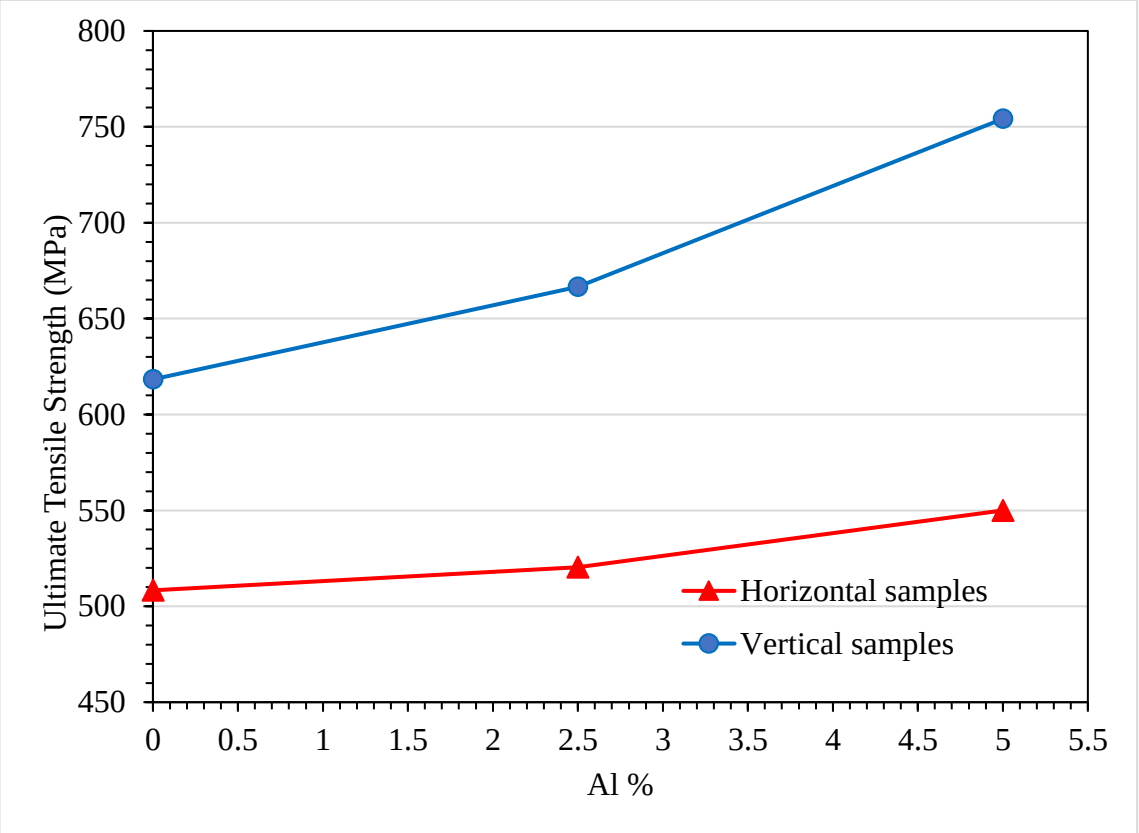

Figure (4.17) Tensile strength as a function of the addition of aluminum.

4.6 Wear Test

Wear testing is a crucial process used to evaluate the performance and durability of materials. It involves subjecting material samples to controlled loading, testing time, and specific environmental conditions to measure their wear resistance. The wear test Figures obtained provide valuable insights into the material's suitability for various applications.

(as shown in Figure 4.18) shows three examples of the change in the friction coefficient as a function of wear test time as obtained from the software of the testing machine. In all conditions, the friction coefficient increased rapidly at the beginning of the tests (Static friction area). After a short period, the friction coefficient reaches its highest level and starts the kinetic friction region. At this region, the curves become nearly horizontal with some fluctuation. However, the Figure shows that the levels are not equal and the friction coefficient decreased with increasing the content of aluminum in the alloy. This effect of the aluminum addition may be attributed to the changes in the microstructure and the local mechanical properties (microhardness) that took place due to the addition of aluminum (see sections 4.3 and 4.5).

(Figure 4.18) illustrates the difference in weight loss versus testing time for the additively manufactured SS309 with the effect of load value and rotation rate. In general, all the tested specimens show a almost between the weight loss and the testing time. However, very high differences can be seen between the slopes of these relations depending on the testing parameters. At the lower rotational rate (100 rpm) (i.e., lower linear distance), the specimens show very low weight loss (compared to the other specimens) even with increasing the applied load from 5 N to 10 N and then to 15 N. Increasing the rotational rate to 200 or 300 rpm increased the loss of weight especially when using the highest rotational rate accompanied with the highest applied load. This increase in loss of weight

is a logical result of the increase in the penetration of the testing tool through the surface layer of the tested material accompanied by the increase in the testing distance. On the other hand, as the applied pressure increased, the underlying layers and the top oxide layer they supported began to work harden.

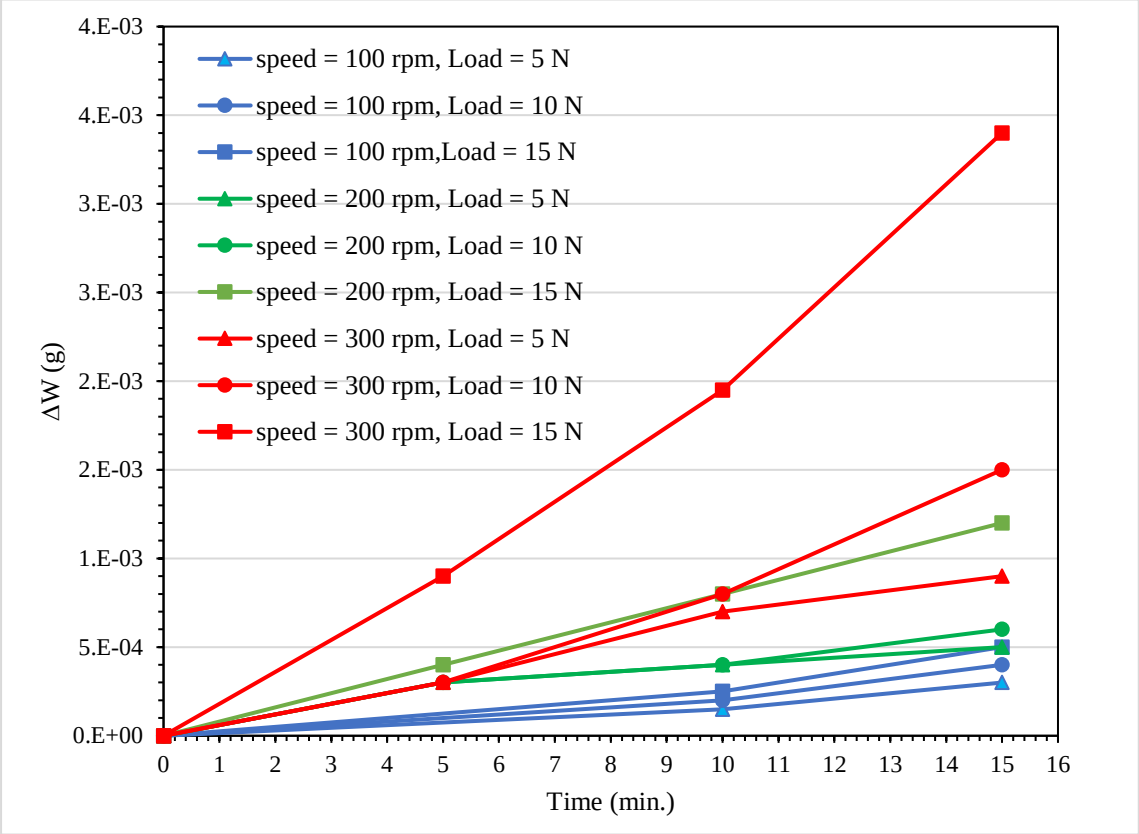

Figure (4.18) Effect of testing time, rotation rate, and loading on the weight loss during sliding wear test of additively manufactured stainless steel .

To show the effect of aluminum addition on the wear behavior of the SS309, several specimens were prepared. At this point, since the relation between the testing time and weight loss is linear, therefore, the test time was kept constant for these tests (at 15 min.). On the other hand, the two other parameters (applied load and rotation rate) were changed, and the relations between the applied load and the change in the weights were

graphed as shown in (Figure 4.19). The relationship is also linear for almost all aluminum percentages and rotational rates. However, the addition of aluminum dramatically reduced the weight losses especially when using the highest rotational rate with the highest applied load (300 rpm with 15 N). At these parameters, the addition of 5 % Al reduced the weight loss from 0.0034 g to 0.0012 g for the same testing time. This positive effect of the aluminum addition is a result of the change in the microstructure (see section 4.3), the hardness (see section 4.5), and the reduction of the friction coefficient (as shown in Figure 4.19).

The effect of heat treatment on the wear test was carried out with a constant load of 15 N and at a rotational rate of 300. Though, the aluminum percentage was changed to study its effect on the wear behavior before and after the heat treatment. As can be seen in (as shown in Figure 4.19), the heat treatment increased to some extent the weight loss of the SS309. On the other hand, the addition of 2.5% Al reduced this behavior change. By further increase in aluminum addition to 5 % Al the resulting alloy became more stable in terms of wear behavior and almost not affected by the heat treatment.

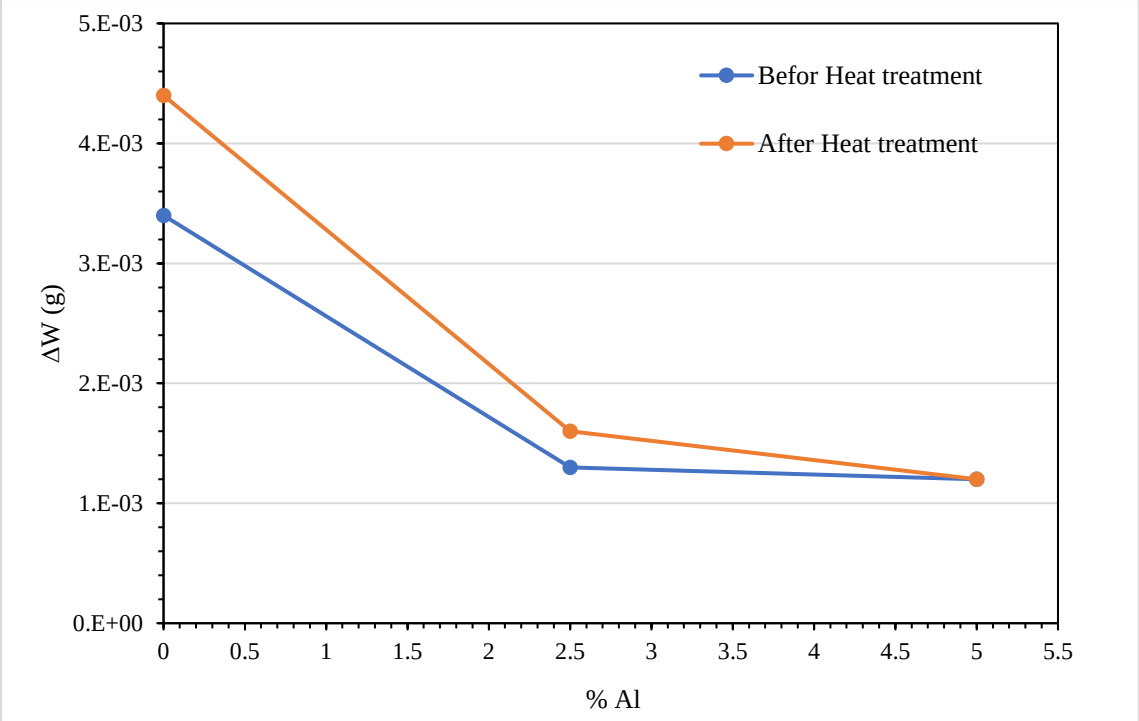

Figure (4.19) Effect of aluminum additions and heat treatment on the weight loss during sliding wear test of additively manufactured stainless steel (speed = 300 rpm, Load = 15 N).

4.7 Oxidation Test of Additively Manufactured SS309 with and without Aluminum Addition

The SS309 is well known for its ability to withstand oxidation at high temperatures [2] Therefore, it is important to investigate the effect of the addition of aluminum and the additive manufacturing process on the ability to resist oxidation. The oxidation test was done at two temperatures 800 and 1000 °C for 75 min. and the weight change was used as an indication of the oxidation resistance. (as shown in Figure 4.20) depicts changes in weight per unit surface area over time. The specimen without the addition of aluminum showed very high fluctuation in the weight gain between very high values and zero. The main reason behind this behavior is the instability of the built-up oxides on the surface of the stainless steel

at elevated temperatures. This instability resulted in the cracking and detaching of the oxide layer. And this cycle is repeated again and again by repeating the oxidation thermal cycle. By the addition of aluminum, more stable aluminum oxide can be produced and resulted in a stronger and more stable oxide layer. This effect can be seen in the behavior of the third alloy (with 5 % Al) in (as shown in Figure 4.20).

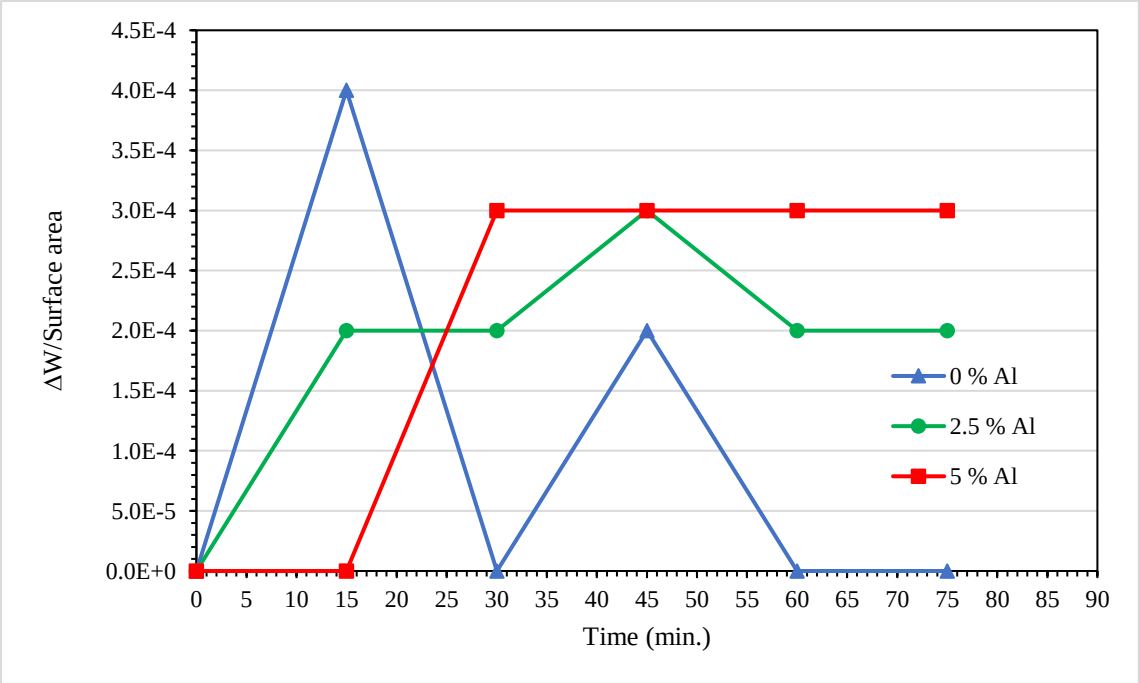

Figure (4.20) The effect of oxidation time on the specimens' weight change at 800 °C.

By increasing the test temperature to 1000 °C. The behavior mentioned above becomes clearer. As shown in (as shown in Figure 4.21), the SS309 specimens showed higher fluctuation in weight change than in earlier cases. In this test, this alloy lost some of its original weight instead of gaining weight by oxidation and this represents evidence of the instability and loss of oxide layer from the surface of this alloy at elevated temperature. On the other hand, the alloys with aluminum additions

remained to maintain stability even at this high temperature but with an increase in the weight gain compared to that for at 800 °C test.

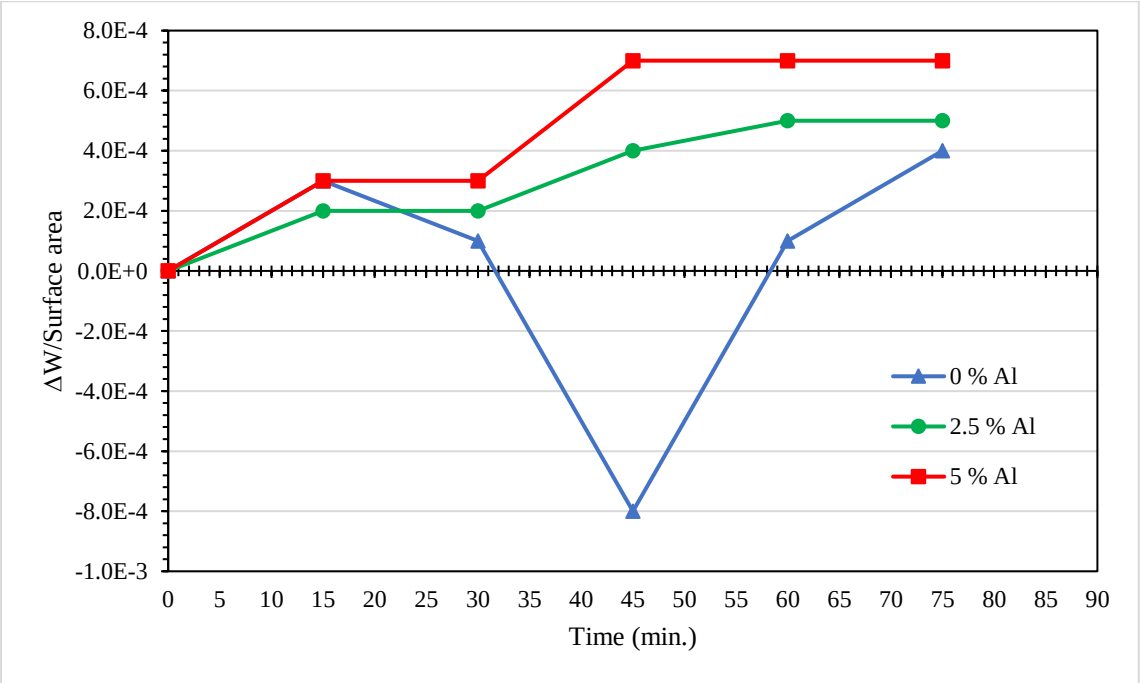

Figure (4.21) The effect of oxidation time on the specimens' weight change at 1000 °C.

The effect of aluminum additions not only could be seen in the weight gain but also the surface appearance of the tested samples. (as shown in Figure 4.22) shows the oxidized surfaces of the three alloys after they were tested at 1000 °C for 75 min. The surface of the first alloys (SS309) shows very high irregularity with thick oxide islands. On the other hand, the surface of the alloy with the 5 % Al addition shows a more uniform grey oxide layer similar to that seen on the aluminum alloys at lower temperatures.

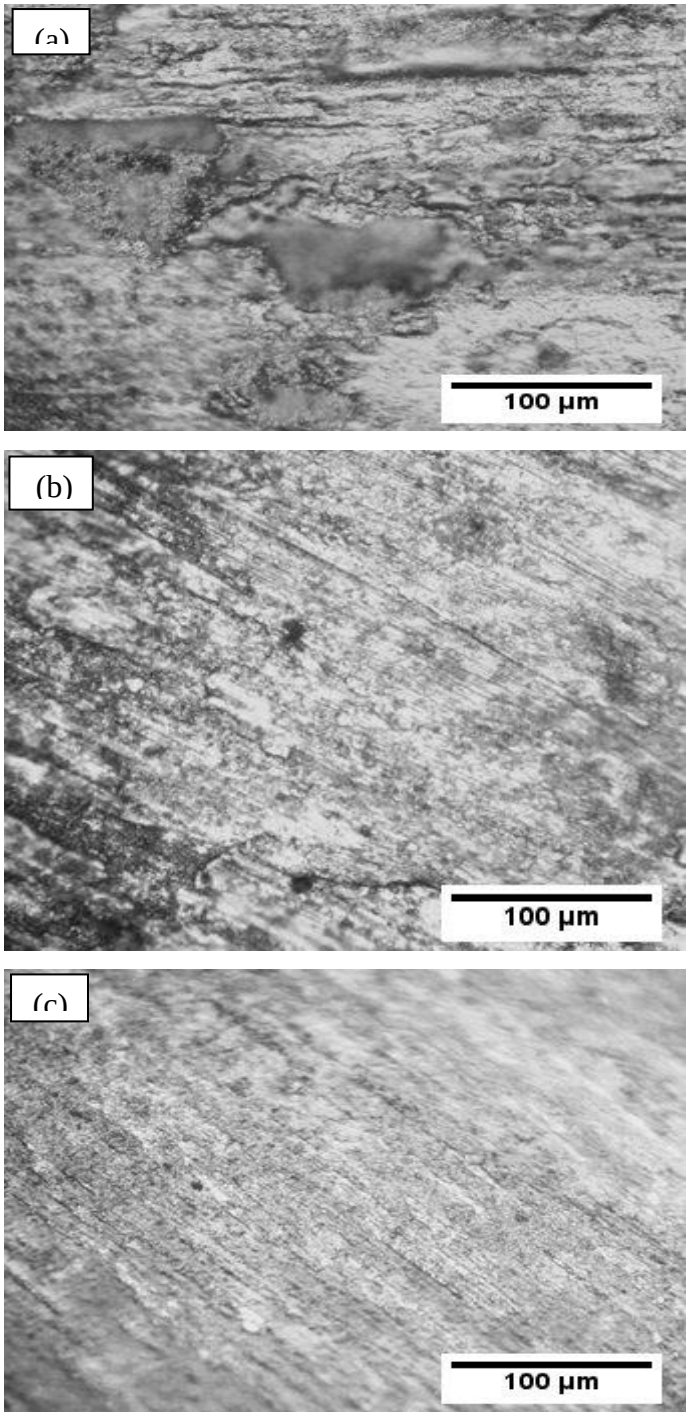

Figure (4.22): OM image for the oxidized surfaces (1000 °C) of the SS 309 prepared by WAAM with the addition of (a) 0, (b) 2.5, and (c) 5 wt. % Al .

4.8 Corrosion

4.8.1 Immersion Test

A set of corrosion evaluation tests have been used to specifically assess the corrosion behaviour likely to appear in this type of alloy when they are prepared by additive manufacturing. The tests were performed in two solutions 3 % NaCl (wt. %) and 3 % HCl (vol. %) in water.

(as shown in Figure (4.23) shows the effect of saline water on the weight loss of three samples of SS309L prepared by WAAM with (0,2.5, and 5 % Al) additions. The samples are immersed in a solution of 3 % wt. NaCl for more than 50 days. The three alloys show a rapid loss in weight during the initial stage of the test (about four days). However, the rate of weight loss starts to decline. Then it settles to one level for all alloys for the rest of the test time. These results are similar to that obtained by a study by (Davalos, et al. 2020) which indicated that the weights of stainless-steel samples were stable when immersed in a (NaCl) solution and at room temperature. This behaviour may be attributed to the fast growth of chromium oxide and aluminium oxide. However, the samples with aluminium additions show higher weight loss compared to the SS309 sample. Nonetheless, the gap between the weight loss of the alloys decreases by increasing the percentage of aluminium from 2.5 to 5 % due to the increase in the homogeneity of the microstructure (see section 4.3) which reduces the effect of galvanic corrosion.

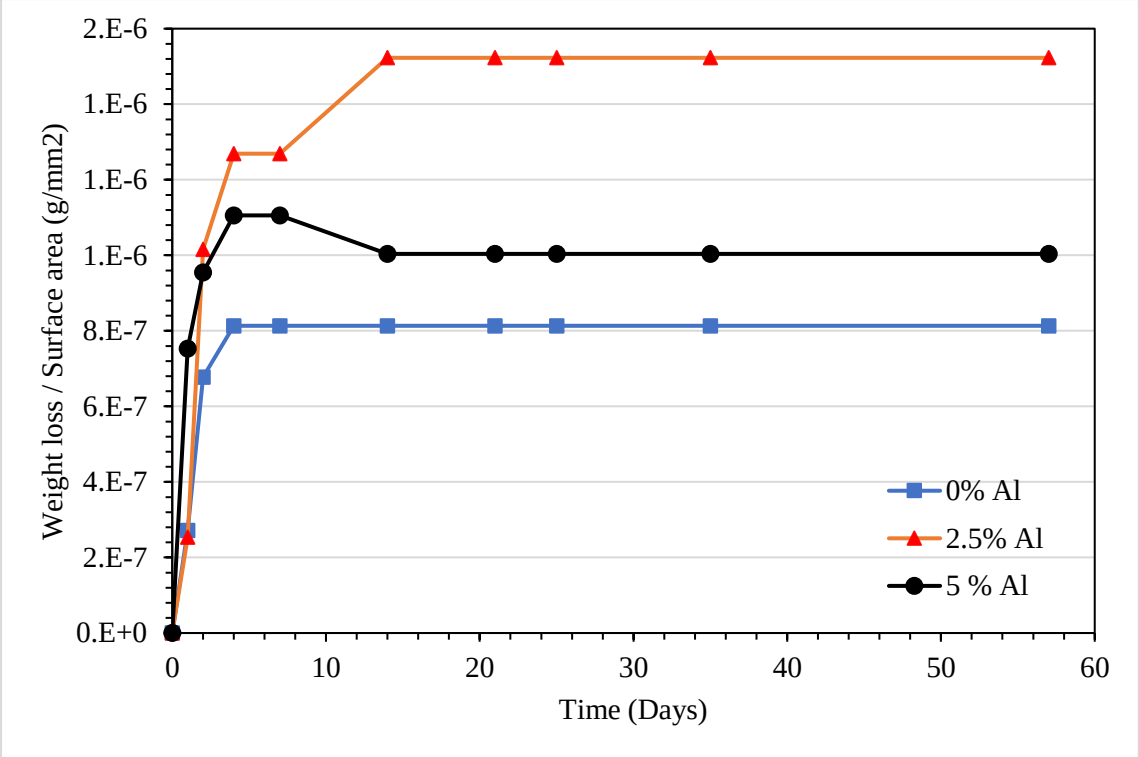

Figure (4.23) The effect of immersion time in 3 wt. % NaCl solution on the weight change per unite area of the SS309L samples prepared by WAAM

The immersion of the three alloys in a more hostile environment i.e. HCl solution at a concentration of 3% (vol.) increases the rapidity of sample weight loss as shown in Figure (4.24). In this test, the sample without aluminium addition also shows the lowest weight loss and its weight is very slightly affected after about 30 hrs. of immersion in the corrosive solution. This result came close to the study of (Li, and Bell., 2006), who immersed stainless steel in HCl solution at room temperature. However, the addition of aluminium increased the weight loss due to the high reactivity of aluminium in the corrosive environment. The increase in aluminium content reduced the weight loss for the same reasons above and due to the building of an oxide layer containing aluminium oxide.

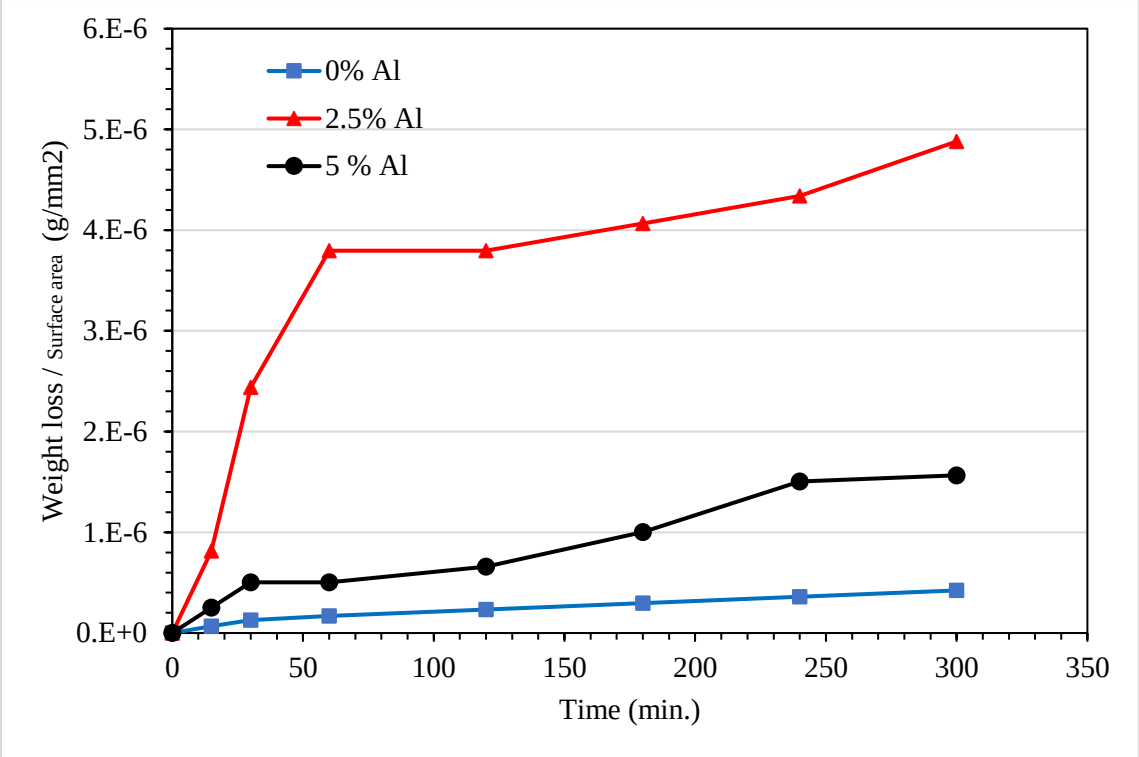

Figure (4.24) The effect of immersion time in 3% HCl solution on the weight change per unite area of the SS309L samples prepared by WAAM

4.8.2 The Polarization Test

For a more precise representation of the corrosion behavior of the prepared alloys, the polarization curves were drawn systematically for the three walls with three different chemical compositions before and after the heat treatment. A polarization curve, also known as a Tafel plot, is a graphical representation of the electrochemical behavior of a material in a specific electrochemical cell con Figure ration. It shows the relationship between the applied voltage (E) and the current (I) in an electrochemical system, typically when the material is subjected to anodic (corrosion) and cathodic (protection) reactions. The polarization curve provides important information about the corrosion behavior and electrochemical properties of a material.

The polarization curve for the base alloy (SS 309L) prepared by WAAM as shown in Figure 4.23). As can be seen the polarization curve consists of

two branches: the anodic branch and the cathodic branch. The anodic branch represents the behavior of the material when it corrodes (oxidizes), while the cathodic branch represents the behavior when protective reactions occur. On the anodic branch (upper branch), the current (I) increases as the applied potential (E) becomes more positive. This is the region where the material starts to corrode at an increasing rate. On the other hand, on the cathodic branch, the current increases and then decreases as the potential becomes more negative. This is the region where protective reactions, such as oxygen reduction or hydrogen evolution, occur, reducing the corrosion rate.

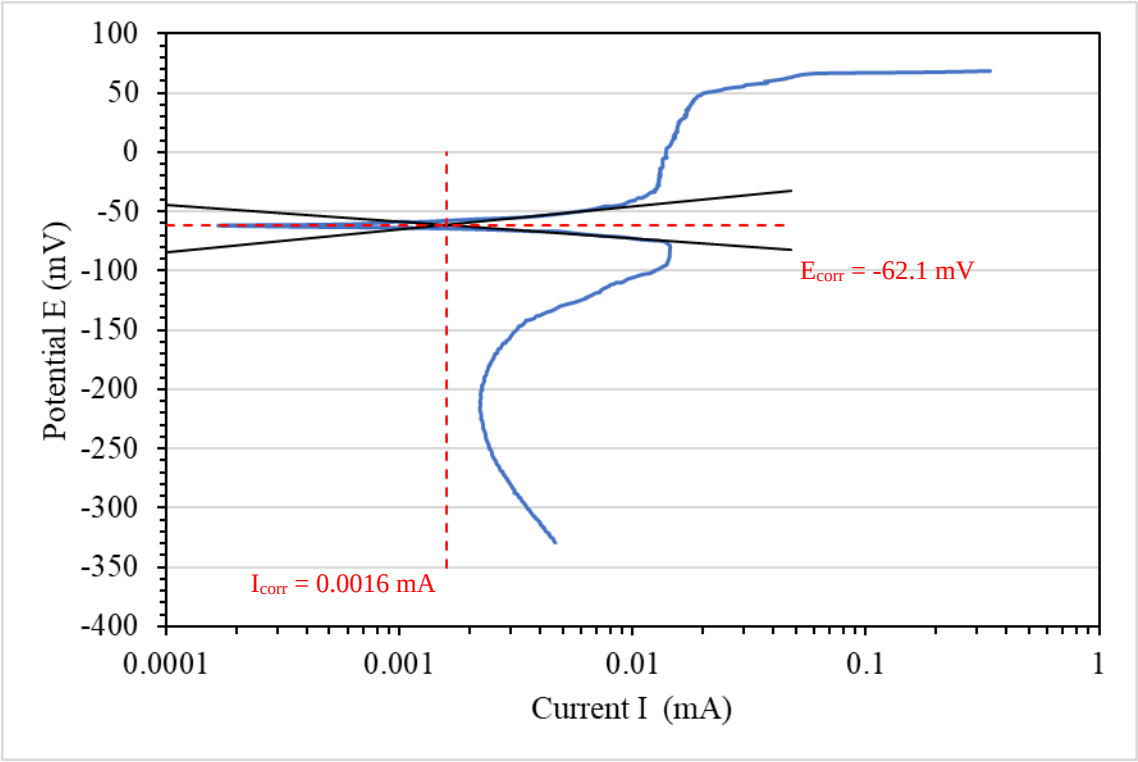

Figure (4.23) Polarization curves of the AM SS309L stainless steel in Saline water (NaCl) solution.

The corrosion potential is the voltage at which the material tends to corrode. It's an important parameter in assessing the material's susceptibility to corrosion. A more positive E_{corr} indicates better corrosion resistance. On the other hand, the corrosion current represents the rate at

which metal ions are released from the material due to corrosion. A lower I_{corr} value indicates better corrosion resistance. From as shown in Figure (4.24) the additively manufactured SS 309L shows an E_{corr} and I_{corr} of approximately -62.1 mV and 0.0016 mA respectively.

The addition of 2.5 % Al to the previously mentioned alloy (SS309L) resulted in a notable shift in the polarization curves (see Figure 4.24) , accompanied by changes in the corrosion current (I_{corr}) and corrosion potential (E_{corr}). Specifically, with the introduction of aluminum, the corrosion current decreased to 0.00135 mA, indicating an improvement in the material's corrosion resistance. Additionally, the corrosion potential shifted to a more positive value, measuring 58 mV. This shift suggests that the alloy became even more resistant to corrosion, as the material's tendency to corrode (as indicated by E_{corr}) became less pronounced, and the rate of metal ion release (as indicated by I_{corr}) decreased. These alterations in the polarization curves and corrosion parameters underscore the enhanced corrosion resistance conferred by the incorporation of aluminum into the alloy, making it more suitable for applications in corrosive environments.

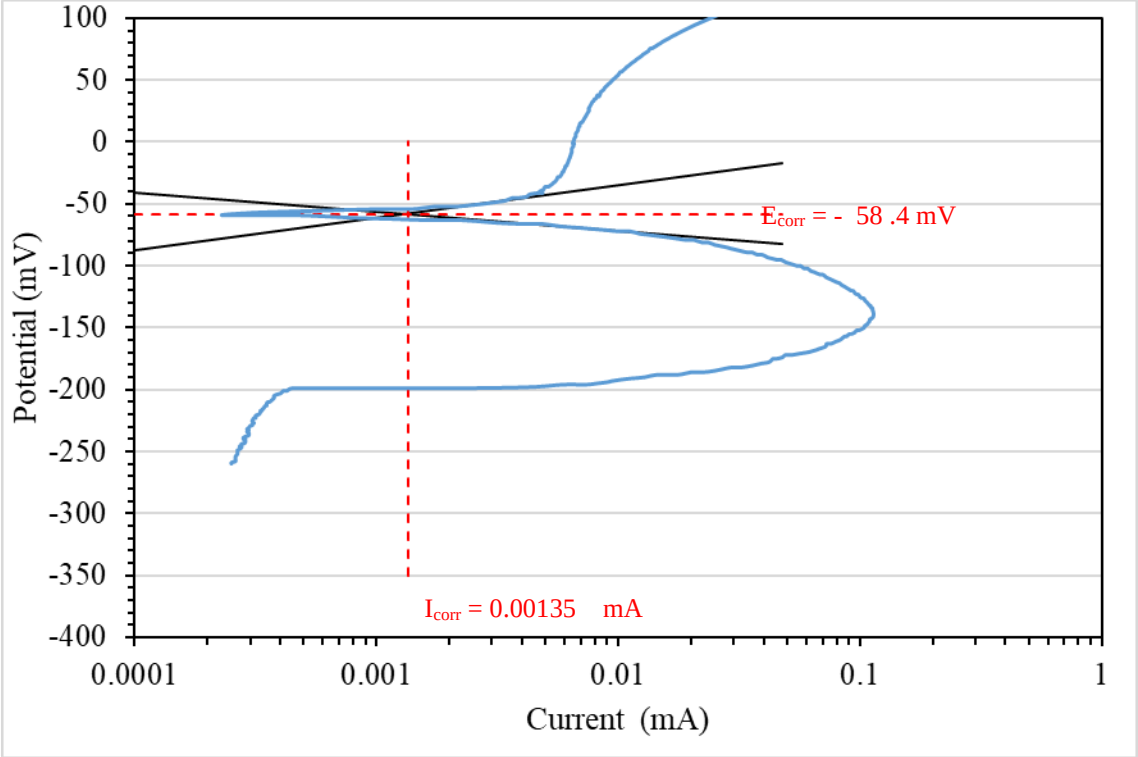

Figure (4.24) Polarization curves of the AM SS309L stainless steel with 2.5 % aluminum additions in Saline water (NaCl) solution.

Increasing the aluminum content to 5% in the aforementioned alloy had a substantial impact on its corrosion behavior, as evidenced by the polarization curve parameters (as shown in Figure 4.25). The corrosion current (I_{corr}) decreased significantly to a remarkably low value of 0.000215 mA, indicating a highly improved resistance to corrosion. Simultaneously, the corrosion potential (E_{corr}) shifted slightly to 57 mV, reinforcing the alloy's enhanced resistance to corrosion. This adjustment signifies that the alloy, with 5% aluminum, is exceptionally well-protected against both anodic and cathodic corrosion processes, making it exceptionally well-suited for use in highly corrosive environments where maintaining structural integrity and longevity are paramount concerns. The alloy's remarkable reduction in I_{corr}, coupled with the slight shift in E_{corr},

underscores the effectiveness of aluminum as a corrosion-resistant alloying element in this context.

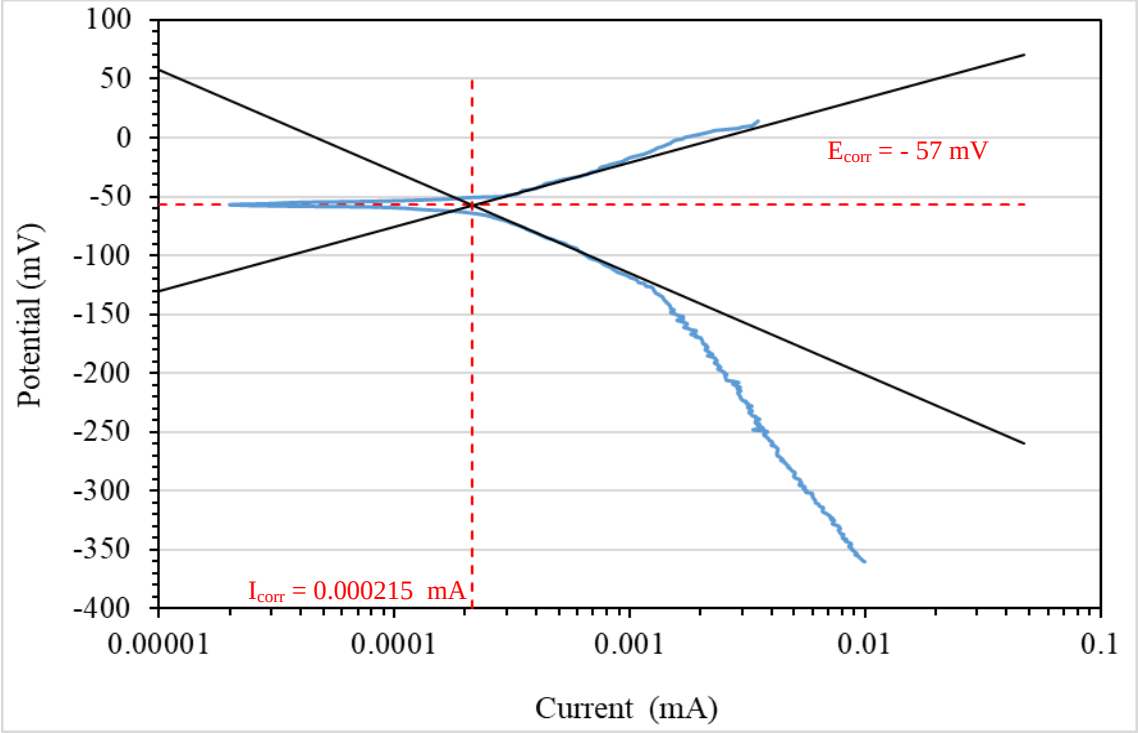

Figure (4.25) Polarization curves of the AM SS309L stainless steel with 5 % aluminum additions in Saline water (NaCl) solution.

CHAPTER FIVE

Conclusion and Future Work

CHAPTER FIVE

Conclusion and Future Work

5.1 Introduction

There are three samples of the in-wall form of the SS309 base alloy that was manufactured by CADDWDM. The CADDWDM process was used to deposit these walls with varying percentages of aluminum added (0, 2.5%, and 5% Al respectively).

These samples (walls) were examined from various, and their microstructures and mechanical characteristics were measured and compared.

5.2 Conclusions

The following conclusion may be drawn from the study's most important findings:

1-The selected parameters for the duple wire-arc additive manufacturing process in this study yield thin-walled components with few defects. The tests indicated that the components exhibited a high degree of thickness and had few intergranular or porosity cracks.

2. The deposited SS309 without Al featured two unique microstructural regions: coarse grains as a matrix with finer grains shown as islands in the structure.

3- The addition of Al significantly changed the microstructure of the deposited layer by encouraging the transition of columnar grains to more complex structure by the shifting of SS309 from austenitic to duplex stainless steel. On the other hand, the grain size steadily shrank and became more uniformly distributed as the percentage of aluminium increased (from 2.5% to 5% Al).

4- The addition of aluminium enhanced the micro-hardness of the deposited wall. The variation in microstructure between these three locations is thought to cause the hardness discrepancy. The discrepancies in hardness between these locations are nonetheless diminished by adding alumina particles until the hardness levels are almost identical. Furthermore.

5- The behaviour of the samples prepared by the additive manufacturing process was highly influenced by the addition of aluminium. The tensile strength of the samples increased whereas the ductility decreased significantly.

6- A notable difference could be seen in the tensile strength of the vertical and horizontal samples in the built walls.

7- The addition of aluminium to SS309 improved its surface properties such as wear and oxidation resistance

5.3 Future Work

Here are some recommendations that can be taken into account for upcoming work:

1- Study the effect of additions of nanoparticles on the microstructure and mechanical properties of the additively manufactured materials.
2- To crush the granule and stop columnar development, sandblasting or rolling can be employed immediately after the building of each layer.
3- Investigate the effect of different process parameters such as arc current, voltage, wire feed rate, and travel speed to optimize the process.
4- Use of other sources such as Laser to deliver the energy to the material during the AM process and compare the effect of heat source on the resulting parts.

5- Deposition of multi-material (two or more) using the double-wire arc additive manufacturing process and study the feasibility of in-situ alloying of some metals.

6- Monitor and control the thermal input during the double-wire arc additive manufacturing process by using thermocouples and thermal cameras to ensure the quality of the built parts .

References

[1] Alcisto, A.Enriquez, H.Garcia, S.Hinkson, T.Steelman, E.Silverman, P. Valdovino, H. Gigerenzer, J. Foyos, J. Ogren, J. Dorey, K. Karg, T. McDonald, and O.S. Es-Said, Tensile Properties and Microstructures of Laser-Formed Ti-6Al-4V, JMEP, 2011, 20(2), p 203–212

[2] Bajaj, A. Hariharan, A. Kini, P. Kürnsteiner, D. Raabe, E.A. Jägle, Mater. Sci., Steels in additive manufacturing: A review of their microstructure and properties. A 772 (2020) 138633.

[3] Tofail, E.P. Koumoulos, A. Bandyopadhyay, S. Bose, L. O'Donoghue, C.Charitidis, Additive manufacturing: scientific and technological challenges, market uptake and opportunities 21 (2018).

[4] G. Liu, X. Zhang, X. Chen, Y. He, L. Cheng, M. Huo, J. Yin, F. Hao, S. Chen, P. Wang, S. Yi, L. Wan, Z. Mao, Z. Chen, X. Wang, Z. Cao, J. Lu, Mater. Sci. Eng.R, Additive manufacturing of structural materials (2021) 100596.

[5] Zhiyuan Liu, Dandan Zhao, Pei Wang, Ming Yan, Can Yang, Zhangwei Chen, Jian Lu, Zhaoping Lu, Additive manufacturing of metals: Microstructure evolution and multistage control, 2021.

[6] J. Gonzalez-Gutierrez, S. Cano, S. Schuschnigg, C. Kukla, J. Sapkota, C. Holzer, Additive Manufacturing of Metallic and Ceramic Components by the Material Extrusion of Highly-Filled Polymers: A Review and Future Perspectives Materials 11 (2018) 840.

[7] C. Tenbrock, F.G. Fischer, K. Wissenbach, J.H. Schleifenbaum, P. Wagenblast, W. Meiners, J. Wagner, J. Mater. Process. Technol. Influence of keyhole and conduction mode melting for top-hat shaped beam profiles in laser powder bed fusion 278 (2020) 116514.

[8] P. Priya, B. Mercer, S. Huang, M. Aboukhatwa, L. Yuan, S. Chaudhuri, Mater. Towards prediction of microstructure during laser based additive manufacturing process of Co-Cr-Mo powder beds, Des. 196 (2020) 109117.

[9] B. Berman, Bus. Horizons, 3-D printing: the new industrial revolution, 55 (2012), pp. 155-162.

[10] D. Chen, S. Heyer, S. Ibbotson, K. Salonitis, J.G. Steingrímsson and S. Thiede, J. Clean. Prod., Direct digital manufacturing: definition, evolution, and sustainability implications, 107 (2015), pp. 615-625.

[11] S.H. Huang, P. Liu, A. Mokasdar and L. Hou, Int. J. Adv. Manuf. Technol., Additive manufacturing and its societal impact: a literature review, 67 (2013), pp. 1191-1203.

[12] I.J. Petrick and T.W. Simpson, 3D printing disrupts manufacturing: how economies of one create new rules of competition, 56 (6) (2013), pp. 12-16.

[13] V. Petrovic, J.V.H. Gonzalez, O.J. Ferrando, J.D. Gordillo, J.R.B. Puchades and L.P. Grinan, Additive layered manufacturing: sectors of industrial application shown through case studies, 49 (4) (2011), pp. 1061-1079.

[14] Simon Ford, Mlanie Despeisse, Additive manufacturing and sustainability: an exploratory study of the advantages and challenges, Journal of Cleaner Production 137 (2016) 1573e1587

[15] Mazher Mohammed, Daniel Wilson, Eli Gomez-Kervin, Aliaksei Petsiuk, Rachel Dick,Joshua M. Pearce, Sustainability and Feasibility Assessment of Distributed E-Waste Recycling using Additive Manufacturing in a Bi-Continental Context, 2021.

[16] Domenico A. Maisano, Elisa Verna, Paolo Minetola, Vincenzo Lunetto, Angioletta R. Catalano & Paolo C. Priarone, A structured comparison of decentralized additive manufacturing centers based on quality and sustainability, 121, pages993–1014 (2022).

[17] Junli Liu, Vuong Nguyen-Van, Biranchi Panda, Kate Fox, Anton du Plessis, and Phuong Tran, Additive Manufacturing of Sustainable Construction Materials and Form-finding Structures: A Review on Recent Progresses, 2022.

[18] ASTM, "Standard Terminology for Additive Manufacturing - General Principles - Terminology," in ISO/ASTM 52900, ed. West Conshohocken, PA, 2015.

[19] H. A. Youssef, H. A. El-Hofy, and M. H. Ahmed, Manufacturing Technology: Materials, Processes, and Equipment. International Edition: Taylor & Francis Group, CRC Press, 2012.

[20] N. Guo and M. C. Leu, "Additive Manufacturing: Technology, Applications and Research Needs," Frontiers of Mechanical Engineering, vol. 8, pp. 215-243, 2013.

[21]] I. Gibson, D. Rosen, and B. Stucker, Additive Manufacturing Technologies; 3D Printing, Rapid Prototyping, and Direct Digital Manufacturing. New York, USA: Springer, 2015.

[22] https://www.aperam.com/stainless/our-offer-by-family-grades/austenitic/

[23] Wong, K. V., & Hernandez, A. (2012). A review of additive manufacturing. International scholarly research notices, 2012.

[24] C. W. Hull, "Apparatus for Production of Three-Dimensional Objects by Stereolithography," Unites States Patent, 1986.

[23] Yusuf, S.M.; Cutler, S.; Gao, N. Review: The Impact of Metal Additive Manufacturing on the Aerospace Industry. Metals 2019, 9, 1286.

[24] F. Doreau, C. Chaput, and T. Chartier, "Stereolithography for Manufacturing Ceramic Parts," Advanced Engineering Materials, vol. 2, pp. 493-496, 2000.

[25] Zhang, S., Wang, Q., Yang, R., & Dong, C. (2021). Composition equivalents of stainless steels understood via gamma stabilizing efficiency. Scientific Reports, 11(1), 5423.

[26] C. K. Chua, K. F. Leong, and C. S. Lim, Rapid Prototyping: Principles and Applications, Second ed. Singapore: World Scientific Publishing Company, 2003.

[27] H.A.El-Hofy, Advanced Machining Processes; Nontraditional and Hybrid Machining Processes. International Edition: McGraw-Hill, 2005.

[28] H.A.El-Hofy, Advanced Machining Processes; Nontraditional and Hybrid Machining Processes. International Edition: McGraw-Hill, 2005.

[29] A. Boschetto and L. Bottini, "Accuracy Prediction in Fused Deposition Modeling," International Journal of Advanced Manufacturing Technology, vol. 73, pp. 913-928, 2014.

[30] J. R. Tumbleston, D. Shirvanyants, N. Ermoshkin, R. Janusziewicz, A. R. Johnson, D. Kelly, et al., "Continuous Liquid Interface Production of 3D Objects," Science, vol. 347, pp. 1349-1352, 2015.

[31] F. Ning, W. Cong, J. Qiu, J. Wei, and S. Wang, "Additive manufacturing of carbon fiber reinforced thermoplastic composites using fused deposition modeling," Composites Part B: Engineering, vol. 80, pp. 369-378, 2015.

[32] J. F. Rodriguez, J. P. Thomas, and J. E. Renaud, "Maximizing the Strength of Fused-Deposition ABS Plastic Parts " in International Solid Freeform Fabrication Symposium, USA, 1999.

[33] J. Mireles, D. Espalin, D. Roberson, B. Zinniel, F. Medina, and R. Wicker, "Fused Deposition Modeling of Metals," in International Solid Freeform Fabrication Symposium, USA, 2012, pp. 836-845.

[34] M. Yakout, M. A. Elbestawi, and S. C. Veldhuis, "On the characterization of stainless steel 316L parts produced by selective laser melting," International Journal of Advanced Manufacturing Technology, vol. Online First, pp. 1-22, 2017.

[35] M. Yakout and M. A. Elbestawi, "Additive Manufacturing of Composite Materials: An Overview," in The 6th International Conference on Virtual Machining Process Technology, Montréal, Canada, 2017.

[36] M. Yakout, A. Cadamuro, M. A. Elbestawi, and S. C. Veldhuis, "The selection of process parameters in additive manufacturing for aerospace alloys," International Journal of Advanced Manufacturing Technology, vol. 92, pp. 2081-2098, September 01 2017.

[37] J.-P. Kruth, P. Mercelis, L. Froyen, and M. Rombouts, "Binding Mechanisms in Selective Laser Sintering and Selective Laser Melting," in International Solid Freeform Fabrication Symposium, USA, 2004.

[38] J.-P. Kruth, M. C. Leu, and T. Nakagawa, "Progress in Additive Manufacturing and Rapid Prototyping," CIRP Annals - Manufacturing Technology, vol. 47, pp. 525-540, 1998.

[39] C. Over, W. Meiners, K. Wissenbach, M. Lindemann, and G. Hammann, "Selective Laser Melting: A New Approach for the Direct Manufacturing of Metal Parts and Tools," in International Conference on Laser Assisted Net Shape Engineering, Furth, Germany, 2001.

[40] R. J. Urbanic, S. M. Saqib, and K. Aggarwal, "Using Predictive Modeling and Classification Methods for Single and Overlapping Bead Laser Cladding to Understand Bead Geometry to Process Parameter Relationships," Journal of Manufacturing Science and Engineering, vol. 138, pp. 051012 (1-13), 2016.

[41] Yakout, M., Elbestawi, M. A., & Veldhuis, S. C. (2018). A review of metal additive manufacturing technologies. Solid State Phenomena, 278, 1-14.

[42] R. P. Mudge and N. R. Wald, "Laser Engineered Net Shaping Advances Additive Manufacturing and Repair," Welding Journal, vol. 86, pp. 44-48, 2007.

[43] L. Xue and M. Ul-Islam, "Laser Consolidation – A Novel One-Step Manufacturing Process for Making Net-Shape Functional Components," in Cost Effective Manufacture via Net-Shape Processing (RTO-MP-AVT-139), France, 2006, pp. (15) 1-14.

[44] H. Zhang, J. Xu, and G. Wang, "Fundamental Study on Plasma Deposition Manufacturing," in International Conference on Open Magnetic Systems for Plasma Confinement, Jeju Island, Korea, 2003.

[45] B. Baufeld, O. V. d. Biest, and R. Gault, "Additive Manufacturing of Ti-6Al-4V Components by Shaped Metal Deposition: Microstructure and Mechanical Properties," Materials & Design, vol. 31, pp. S106-S111, 2010.

[46] W. Gao, Y. Zhang, D. Ramanujan, K. Ramani, Y. Chen, C. B. Williams, et al., "The Status, Challenges, and Future of Additive Manufacturing in Engineering," Computer-Aided Design, 2015.

[47] D. Günther, B. Heymel, J. F. Günther, and I. Ederer, "Continuous 3D-Printing for Additive Manufacturing," Rapid Prototyping Journal, vol. 20, pp. 320-327, 2014.

[48] M. Lanzetta and E. Sachs, "Improved Surface Finish in 3D Printing Using Bimodal Powder Distribution," Rapid Prototyping Journal, vol. 9, pp. 157-166, 2003.

[49] M. Feygin, A. Shkolnik, M. N. Diamond, and E. Dvorsky, "Laminated Object Manufacturing System " USA Patent US5730817A, 1996.

[50] E. C. Santos, M. Shiomi, K. Osakada, and T. Laoui, "Rapid Manufacturing of Metal Components by Laser Forming," International Journal of Machine Tools & Manufacture vol. 46, pp. 1459-1468, 2006.

[51] Bikas H, Stavropoulos P, Chryssolouris G. Additive manufacturing methods and modelling approaches: a critical review. Int J Adv Manuf Technol 2016;83:389–405.

[52] Thapliyal, S. Challenges associated with the wire arc additive manufacturing (WAAM) of aluminum alloys. Mater. Res. Express 2019, 6, 112006.

[53] Frazier, W.E. Metal Additive Manufacturing: A Review. J. Mater. Eng. Perform. 2014, 23, 1917–1928.

[54] Syed, W.U.H.; Pinkerton, A.; Li, L. A comparative study of wire feeding and powder feeding in direct diode laser deposition for rapid prototyping. Appl. Surf. Sci. 2005, 247, 268–276.

[55] McAndrew, A.; Rosales, M.A.; Colegrove, P.; Hönnige, J.R.; Ho, A.; Fayolle, R.; Eyitayo, K.; Stan, I.; Sukrongpang, P.; Crochemore, A.; et al. Interpass rolling of Ti-6Al-4V wire + arc additively manufactured features for microstructural refinement. Additive Manufacturing 2018, 21, 340–349.

[56] Korzhyk, V.; Khaskin, V.; Voitenko, O.; Sydorets, V.; Dolianovskaia, O. Welding Technology in Additive Manufacturing Processes of 3D Objects. Mater. Sci. Forum 2017, 906, 121–130.

[57] Wu, B.; Pan, Z.; Ding, D.; Cuiuri, D.; Li, H.; Xu, J.; Norrish, J. A review of the wire arc additive manufacturing of metals: Properties, defects and quality improvement. J. Manuf. Process. 2018, 35, 127–139.

[58] Wu, W.; Xue, J.; Wang, L.; Zhang, Z.; Hu, Y.; Dong, C. Forming Process, Microstructure, and Mechanical Properties of Thin-Walled 316L Stainless Steel Using Speed-Cold-Welding Additive Manufacturing. Metals 2019, 9, 109.

[59] Feng,Y.;Zhan,B.;He,J.;Wang,K. The double wire feed and plasma arc additive manufacturing process for deposition in Cr-Ni stainless steel. J. Mater. Process. Technol. 2018, 259, 206–215.

[60] Hosseini, V.; Högström, M.; Hurtig, K.; Bermejo, M.A.V.; Stridh, L.-E.; Karlsson, L. Wire-arc additive manufacturing of a duplex stainless steel: Thermal cycle analysis and microstructure characterization. Weld. World 2019, 63, 975–987.

[61] Md. Rumman Ul Ahsan and Ali Newaz Mohammad Tanvir & Taylor Ross & Ahmed Elsawy & Min-Suk Oh & Duck Bong Kim," Fabrication of bimetallic additively manufactured structure (BAMS) of low carbon steel and 316L austenitic stainless steel with wire 1 arc additive manufacturing", 2019.

[62] Md. R.U. Ahsan, Xuesong Fan, Gi-Jeong Seo, Changwook Ji, Mark Noakes, Andrzej Nycz, Peter K. Liaw, Duck Bong Kim," Microstructures and mechanical behavior of the bimetallic additively-manufactured structure (BAMS) of austenitic stainless steel and Inconel 625", 2020

[63] Klocke, F., Brecher, C., Heinen, D., Rosen, C. J., & Breitbach, T. (2010). Flexible scanner-based laser surface treatment. Physics Procedia, 5, 467-475.

[64] Saitta, L., Arcadio, F., Celano, G., Cennamo, N., Zeni, L., Tosto, C., & Cicala, G. (2023). Design and manufacturing of a surface plasmon resonance sensor based on inkjet 3D printing for simultaneous measurements of refractive index and temperature. The International Journal of Advanced Manufacturing Technology, 124(7-8), 2261-2278.

[65] Kawale, S. S., Jang, I., Farandos, N. M., & Kelsall, G. H. (2022). Inkjet 3D-printing of functional layers of solid oxide electrochemical reactors: a review. Reaction Chemistry & Engineering, 7(8), 1692-1712.

[66] Lim, H. (2010). A review of spun bond process. Journal of Textile and Apparel, Technology and Management, 6(3), 1-13.

[67] Gu, D. D., Meiners, W., Wissenbach, K., & Poprawe, R. (2012). Laser additive manufacturing of metallic components: materials, processes and mechanisms. International materials reviews, 57(3), 133-164.

[68] Sames, W. J., List, F. A., Pannala, S., Dehoff, R. R., & Babu, S. S. (2016). The metallurgy and processing science of metal additive manufacturing. International materials reviews, 61(5), 315-360.

[69] Gardner, L. (2023, January). Metal additive manufacturing in structural engineering–review, advances, opportunities and outlook. In Structures (Vol. 47, pp. 2178-2193). Elsevier.

[70] Singh, S., Ramakrishna, S., & Singh, R. (2017). Material issues in additive manufacturing: A review. Journal of Manufacturing Processes, 25, 185-200.

[71] Yin, F., Hu, S., Xu, R., Han, X., Qian, D., Wei, W., ... & aao, K. (2020). Strain rate sensitivity of the ultrastrong gradient nanocrystalline

316L stainless steel and its rate-dependent modeling at nanoscale. International Journal of Plasticity, 129, 102696.

[72] Chaudhari, R., Parikh, N., Khanna, S., Vora, J., & Patel, V. (2022). Effect of multi-walled structure on microstructure and mechanical properties of 1.25 Cr-1.0 Mo steel fabricated by GMAW-based WAAM using metal-cored wire. Journal of Materials Research and Technology, 21, 3386-3396.

[73] Gray III, G. T., Livescu, V., Rigg, P. A., Trujillo, C. P., Cady, C. M., Chen, S. R., ... & Fensin, S. J. (2017). Structure/property (constitutive and spallation response) of additively manufactured 316L stainless steel. Acta Materialia, 138, 140-149.

[74] Zhang, Y., & Yang, J. (2019). CALPHAD-based alloy design of cast austenitic heat-resistant steels with enhanced strength at 1000° C. Calphad, 67, 101679.

[75] Gu, C., Liu, R., Wang, C., Sun, Y., & Zhang, S. (2020). Effect of aluminum on microstructure and high-temperature oxidation resistance of austenitic heat-resistant steel. Metals, 10(2), 176.

[76] Santa-aho, S., Sorsa, A., Honkanen, M., & Vippola, M. (2020). Detailed Barkhausen noise and microscopy characterization of Jominy end-quench test sample of CF53 steel. Journal of Materials Science, 55(11), 4896-4909.

[77] Eftink, B. P., Weaver, J. S., Valdez, J. A., Livescu, V., Chen, D., Wang, Y., ... & Gray III, G. T. (2020). Proton irradiation and characterization of additively manufactured 304L stainless steels. Journal of Nuclear Materials, 531, 152007.

[78] Ahsan, M. R., Tanvir, A. N. M., Seo, G. J., Bates, B., Hawkins, W., Lee, C., ... & Kim, D. B. (2020). Heat-treatment effects on a bimetallic additively-manufactured structure (BAMS) of the low-carbon steel and austenitic-stainless steel. Additive Manufacturing, 32, 101036.

[79] Ghanavati, R., & Naffakh-Moosavy, H. (2021). Additive manufacturing of functionally graded metallic materials: A review of experimental and numerical studies. Journal of Materials Research and Technology, 13, 1628-1664.

[80] Gu, J., Ding, J., Williams, S. W., Gu, H., Bai, J., Zhai, Y., & Ma, P. (2016). The strengthening effect of inter-layer cold working and post-deposition heat treatment on the additively manufactured Al–6.3 Cu alloy. Materials Science and Engineering: A, 651, 18-26.

[81] Dak, G., & Pandey, C. (2020). A critical review on dissimilar welds joint between martensitic and austenitic steel for power plant application. Journal of Manufacturing Processes, 58, 377-406.

[82] Astafurov, S., & Astafurova, E. (2021). Phase composition of austenitic stainless steels in additive manufacturing: A review. Metals, 11(7), 1052.

[83] Rodrigues, T. A., Escobar, J. D., Shen, J., Duarte, V. R., Ribamar, G. G., Avila, J. A., ... & Oliveira, J. P. (2021). Effect of heat treatments on 316 stainless steel parts fabricated by wire and arc additive manufacturing: Microstructure and synchrotron X-ray diffraction analysis. Additive Manufacturing, 48, 102428.

الخلاصة

آلة ترسيب الأسلاك المزدوجة ذات التصميم بمساعدة الكمبيوتر (CADDWDM) هناك ثلاث عينات داخلية من السبائك الأساسية SS309 المصنعة بواسطة CADDWDM تم استخدام عملية CADDWDM لترسيب هذه الجدران بنسب مختلفة من الألومنيوم المضاف (0.2.5% و 5% من AL) على التوالي .(تم فحص هذه العينات (الجدران) بمختلف أنواعها، وقياس ومقارنة بنيتها المجهرية وخواصها الميكانيكية. تنتج المعلمات المحددة لعملية تصنيع المواد المضافة ذات القوس المزدوج في هذه الدراسة مكونات ذات جدران رقيقة مع القليل من العيوب. أشارت الاختبارات إلى أن المكونات أظهرت درجة عالية من السماكة وبها عدد قليل من الشقوق أو المسامية بين الحبوب

من ناحية أخرى، انخفض حجم الحبوب بشكل مطرد وأصبح أكثر توزيعا بشكل موحد مع زيادة محتوى الألومنيوم (من 2.5٪ إلى 5٪ AL). أدت إضافة الألومنيوم إلى تعزيز الصلابة الدقيقة للجدار المترسب. ويعتقد أن الاختلاف في البنية المجهرية بين هذه المواقع الثلاثة هو سبب اختلاف الصلابة. ومع ذلك، يتم تقليل التناقضات في الصلابة بين هذه المواقع عن طريق إضافة جزيئات الألومينا حتى تصبح مستويات الصلابة متطابقة تقريبًا. زادت قوة الشد للعينات بينما انخفضت الليونة بشكل ملحوظ. أدت إضافة الألومنيوم إلى SS309 إلى تحسين خصائص سطحه مثل مقاومة التآكل والأكسدة. آلة ترسيب الأسلاك المزدوجة ذات التصميم بمساعدة الكمبيوتر .(CADDWDM) هناك ثلاث عينات داخلية من السبائك الأساسية SS309 المصنعة بواسطة .CADDWDM تم استخدام عملية CADDWDM لترسيب هذه الجدران بنسب مختلفة من الألومنيوم المضاف (0.2.5% و 5% من AL) على التوالي . تم فحص هذه العينات (الجدران) بمختلف أنواعها، وقياس ومقارنة بنيتها المجهرية وخواصها الميكانيكية. تنتج المعلمات المحددة لعملية تصنيع المواد المضافة ذات القوس المزدوج في هذه الدراسة مكونات ذات جدران رقيقة مع القليل من العيوب. أشارت الاختبارات إلى أن المكونات أظهرت درجة عالية من السماكة وبها عدد قليل من الشقوق أو المسامية بين الحبوب. يتميز SS309 المترسب بدون Al بمنطقتين فريدتين من البنية المجهرية: الحبوب الخشنة كمصفوفة مع الحبوب الدقيقة الموضحة كجزر في البنية.

أدت إضافة Al إلى تغيير كبير في البنية المجهرية للطبقة المودعة من خلال تعزيز انتقال الحبوب العمودية إلى البنية الأكثر تعقيدًا عن طريق تحويل SS309 من الفولاذ المقاوم للصدأ الأوستيني إلى الفولاذ المقاوم للصدأ المزدوج. من ناحية أخرى، انخفض حجم الحبوب بشكل مطرد وأصبح أكثر توزيعا بشكل موحد مع زيادة محتوى الألومنيوم (من 2.5٪ إلى 5٪ AL). أدت إضافة الألومنيوم إلى تعزيز

الصلابة الدقيقة للجدار المترسب. تم تحويل البنية المجهرية من بنية أحادية الطور (Austinit) إلى بنية ثنائية الطور (Austinit+Ferrite)، ويعتقد أن الاختلاف في البنية المجهرية بين هذه المواقع الثلاثة هو سبب اختلاف الصلابة. ومع ذلك، يتم تقليل التناقضات في الصلابة بين هذه المواقع عن طريق إضافة جزيئات الألومينا حتى تصبح مستويات الصلابة متطابقة تقريبًا. زادت قوة الشد للعينات. أدت إضافة الألومنيوم إلى SS309 إلى تحسين خصائص سطحه مثل مقاومة التآكل والأكسدة , زادت نسبة الصلابة قبل المعالجة الحرارية حيث كانت نسبة الصلابة في الجدار الأول بدون إضافة الألومنيوم 237 وعند إضافة الألومنيوم بمعدل 5% أصبحت نسبة الصلابة 277 وبعد المعالجات الحرارية زادت نسبة الصلابة في الجدار الأول كان 221، وبعد إضافة الألمنيوم في الجدار الثالث أصبح معدل الصلابة 268.

أدت إضافة سبيكة Al إلى SS309L إلى زيادة قوة الشد النهائية، على سبيل المثال، كانت قوة الشد النهائية حوالي 610 ميجا باسكال للعينات الرأسية دون أي إضافة للألمنيوم. إلا أنها أصبحت حوالي 754 ميجا باسكال لـ SS309L مع إضافة 5% Al.

وزارة التعليم العالي والبحث العلمي
جـــــــــــامعة بـــابـــــــل
كـــــليـــــــة هندسة المـــــــواد
قســـــــــم هندسة المعـــــــادن

تحضير وتوصيف الفولاذ المقاوم SS309L للصدأ المصنع بتقنية الإضافة باستخدام سبيكة المنيوم

رسالة

مقدمة الى قسم هندسة المعادن في كلية هندسة المواد/جامعة بابل وهي جزء من متطلبات نيل درجةالماجستيرفيعلومهندسةالمواد/المعادن

من قبل

رانيا علي حمودي عبد الكريم
بكالوريوس هندسة المواد (2018)

بإشراف

الأستاذ المساعد الدكتور باسم محيسن الزبيدي

1445هـ **2023 م**